Testing an astronomically-based decadal-scale empirical harmonic climate model versus the IPCC (2007) general circulation climate models

Nicola Scafetta [1]

[1]*ACRIM (Active Cavity Radiometer Solar Irradiance Monitor Lab) & Duke University, Durham, NC 27708, USA.*

Abstract

We compare the performance of a recently proposed empirical climate model based on astronomical harmonics against all CMIP3 available general circulation climate models (GCM) used by the IPCC (2007) to interpret the 20th century global surface temperature. The proposed astronomical empirical climate model assumes that the climate is resonating with, or synchronized to a set of natural harmonics that, in previous works (Scafetta, 2010b, 2011b), have been associated to the solar system planetary motion, which is mostly determined by Jupiter and Saturn. We show that the GCMs fail to reproduce the major decadal and multidecadal oscillations found in the global surface temperature record from 1850 to 2011. On the contrary, the proposed harmonic model (which herein uses cycles with 9.1, 10-10.5, 20-21,60-62 year periods) is found to well reconstruct the observed climate oscillations from 1850 to 2011, and it is able to forecast the climate oscillations from 1950 to 2011 using the data covering the period 1850-1950, and vice versa. The 9.1-year cycle is shown to be likely related to a decadal Soli/Lunar tidal oscillation, while the 10-10.5, 20-21 and 60-62 year cycles are synchronous to solar and heliospheric planetary oscillations. We show that the IPCC GCM's claim that all warming observed from 1970 to 2000 has been anthropogenically induced is erroneous because of the GCM failure in reconstructing the quasi 20-year and 60-year climatic cycles. Finally, we show how the presence of these large natural cycles can be used to correct the IPCC projected anthropogenic warming trend for the 21st century. By combining this corrected trend with the natural cycles, we show that the temperature may not significantly increase during the next 30 years mostly because of the negative phase of the 60-year cycle. If multisecular natural cycles (which according to some authors have significantly contributed to the observed 1700-2010 warming and may contribute to an additional natural cooling by 2100) are ignored, the same IPCC projected anthropogenic emissions would imply a global warming by about 0.3-1.2 ^oC by 2100, contrary to the IPCC 1.0-3.6 ^oC projected warming. The results of this paper reinforce previous claims that the relevant physical mechanisms that explain the detected climatic cycles are still missing in the current GCMs and that climate variations at the multidecadal scales are astronomically induced and, in first approximation, can be forecast.

Keywords: solar variability, planetary motion, climate change, climate models

1. Introduction

Herein, we test the performance of a recently proposed astronomical-based empirical harmonic climate model (Scafetta, 2010b, 2011b) against all general circulation climate models (GCMs) adopted by the IPCC (2007) to interpret climate change during the last century. A large Supplement file with all GCM simulations herein studied plus additional information is added to this manuscript. A reader is invited to look at the figures depicting the single GCM runs there reported to have a feeling about the performance of these models.

The astronomical harmonic model assumes that the climate system is resonating with or is synchronized to a set of natural frequencies of the solar system. The synchronicity between solar system oscillations and climate cycles has been extensively discussed and argued in Scafetta (2010a, 2010b, 2011b), and in the numerous references cited in those papers. We used the velocity of the Sun relative to the barycenter of the solar system and a record of historical mid-latitude aurora events. It was observed that there is a good synchrony of frequency and phase between multiple astronomical cycles with periods between 5 to 100 years and equivalent cycles found in the climate system. We refer to those works for details and statistical tests. The major hypothesized mechanism is that the planets, in particular Jupiter and Saturn, induce solar or heliospheric oscillations that induce equivalent oscillations in the electromagnetic properties of the upper atmosphere. The latter induces similar cycles in the cloud cover and in the terrestrial albedo forcing the climate to oscillate in the same way. The soli/lunar tidal cyclical dynamics also appears to play an important role in climate change at specific frequencies.

This work focuses only on the major decadal and multidecadal oscillations of the climate system, as observed in the global surface temperature data since AD 1850. A more detailed discussion about the interpretation of the secular climate warming trending since AD 1600 can be found in Scafetta and West (2007) and in Scafetta (2009) and in numerous other references there cited. About the millenarian cycle since the Middle Age a discussion is present in Scafetta (2010a) where the relative contribution of solar, volcano and anthropogenic forcing is also addressed, and in the numerous references cited in the above three papers. Also correlation studies between the secular trend of the temperature and the geomagnetic aa-index, the sunspot number and the solar cycle length address the above issue and are quite numerous: for example (Hoyt and Schatten, 1997; Sonnemann, 1998; Thejll and Lassen, 2000). Thus, a reader interested in better understanding the secular climate trending topic is invited to read those papers. In particular, about the 0.8^oC warming trending observed since 1900 numerous empirical studies based on the comparison between the past climate secular and multisecular patterns and equivalent solar activity patterns have concluded that at least 50-70% of the observed 20th century warming could be associated to the increase of solar activity observed since the Maunder minimum of the 17th century: for example see (Scafetta and West, 2007; Scafetta, 2009; Loehle and Scafetta, 2011; Soon, 2009; Soon et al., 2011; Kirkby, 2007; Hoyt and Schatten, 1997; Le Mouël et al., 2008; Thejll and Lassen, 2000; Weihong and Bo, 2010; Eichler et al., 2009). Moreover, Humlum et al. (2011) noted that the natural multi-secular/milennial climate cycles observed during the late Holocene climate change clearly suggest that the secular 20th century warming could be mostly due to these longer natural cycles, which are also expected to cool the climate during the 21th century. A similar conclusion has been reached by another study focusing on the multi-secular and millennial cycles observed in the temperature in the central-eastern Tibetan Plateau during the past 2485 years (Liu et al., 2011). For the benefit of the reader, in section 7 in the Supplement file the results reported in two of the above papers are very briefly presented to graphically support the above claims.

It is important to note that the above empirical results contrast greatly with the GCM estimates adopted by the IPCC claiming that more than 90% of the warming observed since 1900 has been anthropogenically induced (compare figures 9.5a and 9.5b in the IPCC report which are reproduced in section 4 in the Supplement File). In the above papers it has been often argued that the current GCMs miss important climate mechanisms such as, for example, a modulation of the cloud system via a solar induced modulation of the cosmic ray incoming flux, which would greatly amplify the climate sensitivity to solar changes by modulating the terrestrial albedo (Scafetta, 2011b; Kirkby, 2007; Svensmark, 1998, 2007; Shaviv, 2008).

In addition to a well-known decadal climate cycle commonly associated to the Schawbe solar cycle by numerous authors (Hoyt and Schatten, 1997), several studies have emphasized that the climate system is characterized by a quasi bi-decadal (from 18 yr to 22 yr) oscillation and by a quasi 60-year oscillation (Stockton et al., 1983; Currie, 1984; Cook, 1997; Agnihotri and Dutta, 2003; Klyashtorin et al., 2009; Sinha et al., 2005; Yadava and Ramesh, 2007; Jevrejeva et al., 2008; Knudsen et al., 2011; Davis and Bohling, 2001; Scafetta, 2010b; Weihong and Bo, 2010; Mazzarella and Scafetta, 2011; Scafetta, 2011b). For example, quasi 20-year and 60-year large cycles are clearly detected in all global surface temperature instrumental records of both hemispheres since 1850 as well as in numerous astronomical records. There is a phase synchronization between these terrestrial and astronomical cycles. As argued in Scafetta (2010b), the observed quasi bidecadal climate cycle may also be around a 21-year periodicity because of the presence of the 22-year solar Hale magnetic cycle, and there may also be an additional influence of the 18.6-year soli/lunar nodal cycle. However, for the purpose of the present paper, we can ignore these corrections which may require other cycles at 18.6 and 22 years. In the same way, we ignore other possible slight cycle corrections due to the interference/resonance with other planetary tidal cycles and with the 11-year and 22-year solar cycles, which are left to another study.

About the 60-year cycle it is easy to observe that the global surface temperature experienced major maxima in 1880-1881, 1940-1941 and 2000-2001. These periods occurred during the Jupiter/Saturn great conjunctions when the two planets were quite close to the Sun and the Earth. This events occur every three J/S synodic cycles. Other local temperature maxima occurred during the other J/S conjunctions, which occur every about 20 years: see figures 10 and 11 in Scafetta (2010b), where this correspondence is shown in details through multiple filtering of the data. Moreover, the tides produced by Jupiter and Saturn in the heliosphere and in the Sun have a period of about $0.5/(1/11.86 - 1/29.45) \approx 10$ years plus the 11.86-year Jupiter orbital tidal cycles. The two tides beat generating an additional cycle at about $1/(2/19.86 - 1/11.86) = 61$ years (Scafetta, 2011b). Indeed, a quasi 60-year climatic oscillations have likely an astronomical origin because the same cycles are found in numerous secular and millennial aurora and other solar related records (Charvátová et al., 1988; Komitov, 2009; Ogurtsov et al., 2002; Patterson et al., 2004; Yu et al., 1983; Scafetta, 2010a,b; Mazzarella and Scafetta, 2011; Scafetta, 2011b).

A 60-year cycle is even referenced in ancient Sanskrit texts among the observed monsoon rainfall cycles (Iyengar, 2009), a fact confirmed by modern monsoon studies (Agnihotri and Dutta, 2003). It is also observed in the sea level rise since 1700 (Jevrejeva et al., 2008) and in numerous ocean and terrestrial records for centuries (Klyashtorin et al., 2009). A natural 60-year climatic cycle associated to planetary astronomical cycles may also explain the origin of 60-year cyclical calendars adopted in traditional Chinese, Tamil and Tibetan civilizations (Aslaksen, 1999). Indeed, all major ancient civilizations knew about the 20-year and 60-year astronomical cycles associated to Jupiter and Saturn (Temple, 1998).

In general, power spectrum evaluations have shown that frequency peaks with periods of about

9.1, 10-10.5, 20-22 and 60-63 years are the most significant ones and are common between astronomical and climatic records (Scafetta, 2010b, 2011b). Evidently, if climate is described by a set of harmonics, it can be in first approximation reconstructed and forecast by using a planetary harmonic constituent analysis methodology similar to the one that was first proposed by Lord Kelvin (Thomson, 1881; Scafetta, 2011b) to accurately reconstruct and predict tidal dynamics. The harmonic constituent model is just a superposition of several harmonic terms of the type

$$F(t) = A_0 + \sum_{i=1}^{N} A_i \cos(\omega_i t + \phi_i).$$ (1)

whose frequencies ω_i are deduced from the astronomical theories and the amplitude A_i and phase ϕ_i of each harmonic constituent are empirically determined using regression on the available data, and then the model is used to make forecasts. Several harmonics are required: for example, most locations in the United States use computerized forms of Kelvin's tide-predicting machine with 35-40 harmonic constituents for predicting local tidal amplitudes (Ehret, 2008), so a reader should not be alarmed if many harmonic constituents may be needed to accurately reconstruct the climate system.

Herein we show that a similar harmonic empirical methodology can, in first approximation, reconstruct and forecast global climate changes at least on a decadal and multidecadal scales, and that this methodology works much better than the current GCMs adopted by the IPCC in 2007. In fact, we will show that the IPCC GCMs fail to reproduce the observed climatic oscillations at multiple temporal scales. Thus, the computer models adopted by the IPCC in 2007 are found to be missing the important physical mechanisms responsible for the major observed climatic oscillations. An important consequence of this finding is that these GCMs have seriously misinterpreted the reality by significantly overestimating the anthropogenic contribution, as also other authors have recently claimed (Douglass et al., 2007; Lindzen and Choi, 2011; Spencer and Braswell, 2011). Consequently, the IPCC projections for the 21st century should not be trusted.

2. The IPCC GCMs do not reproduce the global surface temperature decadal and multi-decadal cycles

Figure 1 depicts the monthly global surface temperature anomaly (from the base period 1961-90) of the Climatic Research Unit (HadCRUT3) (Broham et al., 2006) from 1850 to 2011 against an advanced general circulation model average simulation (Hansen et al., 2007), which has been slightly shifted downward for visual convenience. The chosen units are the degree Celsius in agreement with the climate change literature referring to temperature anomalies. The GISS ModelE is one of the major GCMs adopted by the IPCC (IPCC, 2007). Here we study all available climate model simulations for the 20th century collected by Program for Climate Model Diagnosis and Intercomparison (PCMDI) mostly during the years 2005 and 2006, and this archived data constitutes phase 3 of the Coupled Model Intercomparison Project (CMIP3). These GCMs use the observed radiative forcings (simulations "tas:20c3m") adopted by the IPCC (2007). All GCM simulations are depicted and analyzed in Section 2 of the Supplement file added to this paper. These GCM simulations cover a period that may begin during the second half of the 19th century and end during the 21th century. The following calculations are based on the maximum overlapping period between each model simulation and the 1850-2011 temperature period. The
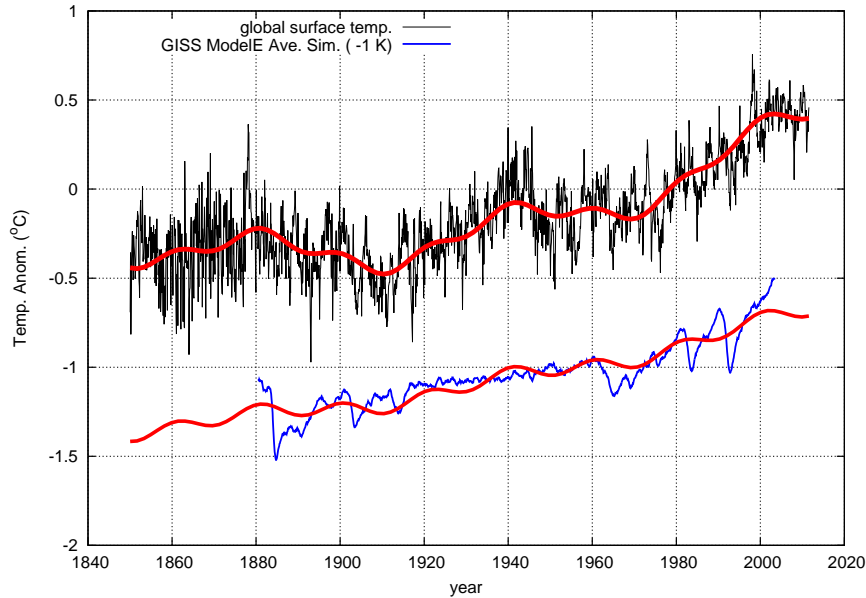
4

Figure 1: Global surface temperature (top (http://www.cru.uea.ac.uk/cru/data/temperature/) and GISS ModelE average simulation (bottom). The records are fit with Eq 5. Note also the large volcano eruption signatures that appear clearly overestimated in the GCM's simulation.

CMIP3 GCM simulations analyzed here can be downloaded from Climate Explorer web-site: see the Supplement file for details.

A simple visual inspection suggests that the temperature presents a quasi 60-year cyclical modulation oscillating around an upward trend (Scafetta, 2010b; Loehle and Scafetta, 2011). In fact, we have the following 30-year trending patterns: 1850-1880, warming; 1880-1910, cooling; 1910-1940, warming; 1940-1970, cooling; 1970-2000, warming; and it is almost steady or presents a slight cooling since 2001 (2001-2011.5 rate = -0.46 ±0.3 $^oC/century$). Other global temperature reconstructions, such as the GISSTEM (Hansen et al., 2007) and the GHCN-Mv3 by NOAA, present similar patterns (see Section 1 in the Supplement file). Note that GISSTEM/1200 presents a slight warming since 2001 (2001-2011.5 rate = +0.47 ±0.3 $^oC/century$), which appears to be due to the GISS poorer temperature sampling during the last decade of the Antarctic and Arctic regions that were artificially filled with a questionable 1200 km smoothing methodology (Tisdale, 2010). However, when a 250 km smooth methodology is applied, as in GISSTEM/250, the record shows a slight cooling during the same period (2001-2011.5 rate = -0.16 ±0.3 $^oC/century$). HadCRUT data has much better coverage of the Arctic and Southern Oceans that GISSTEM and, therefore, it is likely more accurate. Note that CRU has recently produced an update of their SST ocean record, HadSST3, (Kennedy et al., 2011), but it stops in 2006 and was not merged yet with the land record. This new corrected record presents an even clearer

5

60-year modulation than the HadSST2 record because in it the slight cooling from 1940 to 1970 is clearer (Mazzarella and Scafetta, 2011).

Indeed, the 60-year cyclicity with peaks in 1940 and 2000 appears quite more clearly in numerous regional surface temperature reconstructions that show a smaller secular warming trending. For example, in the United States (D'Aleo, 2011), in the Arctic region (Soon, 2009), in several single stations in Europe and other places (Le Mouël et al., 2008) and in China (Soon et al., 2011). In any case, a 60-year cyclical modulation is present for both the Norther and Southern Hemisphere and for both Land and Ocean regions (Scafetta, 2010b) even if it may be partially hidden by the upward warming trending. The 60-year modulation appears well correlated to a recently proposed solar activity reconstruction (Loehle and Scafetta, 2011).

The 60-year cyclical modulation of the temperature from 1850 to 2011 is further shown in Figure 2 where the autocorrelation functions of the global surface temperature and of the GISS ModelE average simulation are compared. The autocorrelation function is defined as:

$$r(\tau) = \frac{\sum_{t=1}^{N-\tau}(T_t - \bar{T})(T_{t+\tau} - \bar{T})}{\sqrt{[\sum_{t=1}^{N-\tau}(T_t - \bar{T})^2 \sum_{t=\tau}^{N}(T_t - \bar{T})^2]}}, \tag{2}$$

where $\bar{T}$ is the average of the N-data long temperature record and τ is the time-lag. The autocorrelation function of the global surface temperature (Fig. 2A) and of the same record detrended of its quadratic trend (Fig. 2B) reveals the presence of a clear cyclical pattern with minima at about 30-year lag and 90-year lag, and maxima at about 0-year lag and 60-year lag. This pattern indicates the presence of a quasi 60-year cyclical modulation in the record. Moreover, because both figures show the same pattern it is demonstrated that the quadratic trend does not artificially creates the 60-year cyclicity. On the contrary, the GISS ModelE average simulation produces a very different autocorrelation pattern lacking any cyclical modulation. Figure 2C shows the autocorrelation function of the two records detrended also of their 60-year cyclical fit, and the climatic record appears to be characterized by a quasi 20-year smaller cycle, as deduced by the small but visible quasi regular 20-year waves, at least up to a time-lag of 70 years after which other faster oscillations with a decadal scale dominate the pattern. On the contrary, the autocorrelation function of the GCM misses both the decadal and bi-decadal oscillations and again shows a strong 80-year lag peak, absent in the temperature. The latter peak is due to the quasi 80-year lag between the two computer large volcano eruption signatures of Krakatoa (1883) and Agung (1963-64), and to the quasi 80-year lag between the volcano signatures of Santa Maria (1902) and El Chichón (1982). Because this 80-year lag autocorrelation peak is not evident in the autocorrelation function of the global temperature we can conjecture that the GISS ModelE is significantly overestimating the volcano signature, in addition to not reproducing the natural decadal and multidecadal temperature cycles: this claim is further supported in Section 5 of the Supplement file.

A similar qualitative conclusion applies also to all other GCMs used by the IPCC, as shown in Section 2 of the Supplement file. The single GCM runs as well as their average reconstructions appear quite different from each other: some of them are quite flat until 1970, others are simply monotonically increasing. Volcano signals often appear overestimated. Finally, although these GCM simulations present some kind of red-noise variability supposed to simulate the multi-annual, decadal and multi-decadal natural variability, a simple visual comparison among the simulations and the temperature record gives a clear impression that the simulated variability has nothing to do with the observed temperature dynamics. In conclusion, a simple visual analysis
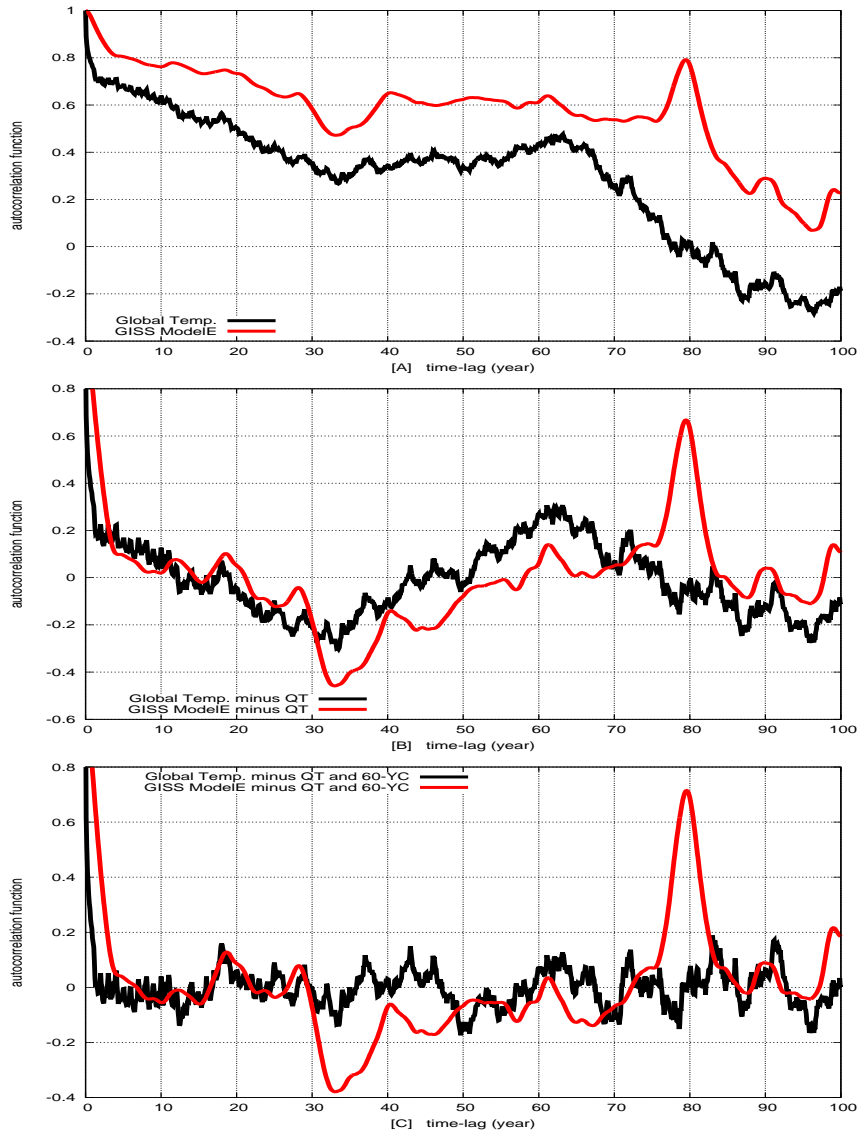
Figure 2: Autocorrelation function (Eq. 2) of the global surface temperature and of the GISS ModelE average simulation: [A] Original data; [B] data detrended of their quadratic fit; [C] The 60-year modulation is further detrended. Note the 60-year cyclical modulation of the autocorrelation of the temperature with minima at 30-year and 90-year lags and maxima at 0-year and 60-year lags, which is not reproduced by the GCM simulation. Moreover, the computer simulation presents an autocorrelation peak at 80-year lag related to a pattern produced by volcano eruptions, which is absent in the temperature. See Section 5 in the supplement file for further evidences about the GISS ModelE serious overestimation of the volcano signal in the global surface temperature record.

of the records suggests that the temperature is characterized 10-year, 20-year and 60-year oscillations that are simply not reproduced by the GCMs. This is also implicitly indicated by the very smooth and monotonically increasing pattern of their average reconstruction depicted in the IPCC figure SPM.5 (see Section 4 in the Supplement file).

Figures 3A and 3B shows two power spectra estimates of the temperature records based on the Maximum Entropy Method (MEM) and the Lomb periodogram (Press et al., 2007). Four major peaks are found at periods of about 9.1, 10-10.5, 20-21 and 60-62 years: other common peaks are found but not discussed here. Both techniques produce the same spectra. To verify whether the detected major cycles are physically relevant and not produced by some unspecified noise or by the specific sequences, mathematical algorithms and physical assumptions used to produce the HadCRUT record, we have compared the same double power spectrum analysis applied to the three available global surface temperature records (HadCRUT3, GISSTEM/250 and GHCN-Mv3) during their common overlapping time period (1880-2011): see also section 1 in the Supplement file. As shown in the figures the temperature sequences present almost identical power spectra with major common peaks at about 9.1, 10-10.5, 20 and 60 years. Note that in Scafetta (2010b), the relevant frequency peaks of the temperature were determined by comparing the power spectra of HadCRUT temperature records referring to different regions of the Earth such as those referring to the Northern and Southern hemispheres, and to the Land and the Ocean. So, independent major global surface temperature records present the same major periodicities: a fact that further argues for the physical global character of the detected spectral peaks.

Note that a methodology based on a spectral comparison of independent records is likely more physically appropriate than using purely statistical methodologies based on Monte Carlo randomization of the data, that may likely interfere with weak dynamical cycles. Note also that a major advantage of MEM is that it produces much sharper peaks that allow a more detailed analysis of the *low-frequency band* of the spectrum. Section 5 in the Supplement file contains a detailed explanation about the number of poles M needed to let MEM to resolve the very-low frequency range of the spectrum: see also Courtillot et al. (1977).

Because the temperature record presents major frequency peaks at about 20-year and 60-year periodicities plus an apparently accelerating upward trend, it is legitimate to extract these multidecadal patterns by fitting the temperature record (monthly sampled) from 1850 to 2011 with the 20 and 60-year cycles plus a quadratic polynomial trend. Thus, we use a function $f(t) + p(t)$ where the harmonic component is given by

$$f(t) = C_1 \cos\left[\frac{2\pi(t - T_1)}{60}\right] + C_2 \cos\left[\frac{2\pi(t - T_2)}{20}\right], \tag{3}$$

and the upward quadratic trending is given by

$$p(t) = P_2 * (t - 1850)^2 + P_1 * (t - 1850) + P_0 . \tag{4}$$

The regression values for the harmonic component are: $C_1 = 0.10 \pm 0.01\ {}^oC$ and $C_2 = 0.040 \pm 0.005\ {}^oC$, and the two dates are $T_1 = 2000.8 \pm 0.5\ AD$ and $T_2 = 2000.8 \pm 0.5\ AD$. For the quadratic component we find: $P_0 = -0.30 \pm 0.2\ {}^oC$, $P_1 = -0.0035 \pm 0.0005\ {}^oC/yr$ and $P_2 = 0.000049 \pm 0.000002\ {}^oC/yr^2$. Note that the two cosine phases are free parameters and the regression model gives the same phases for both harmonics, which suggests that they are related. Indeed, this common phase date approximately coincides with the closest (to the sun) conjunction between
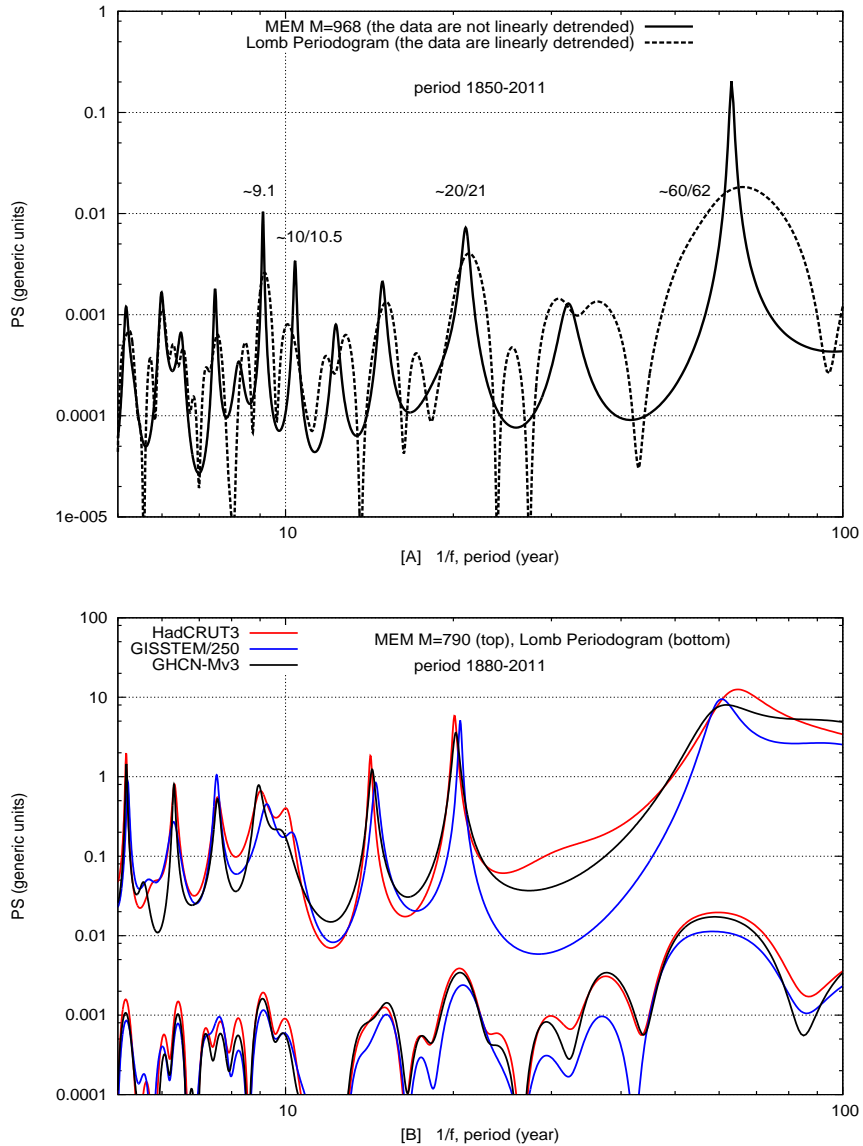
8

Figure 3: [A] Maximum Entropy Method (MEM) with M=N/2 (solid) and the Lomb Periodogram (dash) of the Had-CRUT3 global surface temperature monthly sampled from 1850 to 2011 (see Section 3 of the Supplement file for details and explanations). The two techniques produce the same peaks, but MEM produces much sharper peaks. The major four peaks are highlighted in the figure. [B] As above for the HadCRUT, GISSTEM/250 and GHCN-Mv3 global surface temperature records during the period 1880-2011: see section 1 in the Supplement file. Note that the spectra are quite similar, but for GISSTEM the cycles are somehow slightly smoother and smallers than for the other two sequences, as the bottom curves show. The result shows that all GCMs significantly fail in reproducing the 20-year and 60-year cycle amplitudes observed in the temperature record by an average factor of 3.

9

Jupiter and Saturn, which occurred (relative to the Sun) on June/23/2000 ($\approx$ 2000.5), as better shown in Scafetta (2010b).

It is important to stress that the above quadratic function $p(t)$ is just a convenient geometrical representation of the observed warming accelerating trend during the last 160 years, not outside the fitting interval. Another possible choice, which uses two linear approximations during the periods 1850-1950 and 1950-2011, has also be proposed (Loehle and Scafetta, 2011). However, our quadratic fitting trending cannot be used for forecasting purpose, and it is not a component of the astronomical harmonic model. Section 4 will address the forecast problem in details.

It is possible to test how well the IPCC GCM simulations reproduce the 20 and 60-year temperature cycles plus the upward trend from 1850 to 2011 by fitting their simulations with the following equation

$$ m(t) = a * 0.10 \cos \left[\frac{2\pi(t - 2000.8)}{60} \right] + b * 0.040 \cos \left[\frac{2\pi(t - 2000.8)}{20} \right] + c * p(t) + d \,, \qquad (5) $$

where a, b, c and d are regression coefficients. Values of a, b and c statistically compatible with the number 1 indicate that the model well reproduces the observed temperature 20 and 60-year cycles, and the observed upward temperature trend from 1850 to 2011. On the contrary, values of a, b and c statistically incompatible with 1 indicate that the model does not reproduce the observed temperature patterns.

The regression values for all GCM simulations are reported in Table 1. Figure 4 shows the values of the regression coefficients a, b and c for the 26 climate model ensemble-mean records and all fail to well reconstruct both the 20 and the 60-year oscillations found in the climate record. In fact, the values of the regression coefficients a and b are always well below the optimum value of 1, and for some model these values are even negative. The average among the 26 models is $a = 0.30 \pm 0.22$ and $b = 0.35 \pm 0.42$, which are statistically different from 1. This result would not change if all available single GCM runs are analyzed separately, as extensively shown in Section 2 of the Supplement file.

About the capability of the GCMs of reproducing the upward temperature trend from 1850 to 2011, which is estimated by the regression coefficient c, we find a wide range of results. The average is $c = 1.11 \pm 0.50$, which is centered close to the optimum value 1. This result explains why the multi-model global surface average simulation depicted in the IPCC figures 9.5 and SPM.5 apparently reproduces the 0.8 ^oC warming observed since 1900. However, the results about the regression coefficient c vary greatly from model to model: a fact that indicates that these GCMs usually also fail to properly reproduce the observed upward warming trend from 1850 to 2011.

Table 1 and the tables in Section 2 in the Supplement file also report the estimated reduced χ^2 values between the measured GCM coefficients a_m, b_m and c_m (index "m" for model) and the values of the same coefficients a_T, b_T and c_T (index "T" for temperature) estimated for the temperature. The reduced χ^2 (chi square) values for three degree of freedom (that is three independent variables) are calculated as

$$ \chi^2 = \frac{1}{3} \left[\frac{(a_m - a_T)^2}{\Delta a_m^2 + \Delta a_T^2} + \frac{(b_m - b_T)^2}{\Delta b_m^2 + \Delta b_T^2} + \frac{(c_m - c_T)^2}{\Delta c_m^2 + \Delta c_T^2} \right], \qquad (6) $$

where the Δ values indicate the measured regression errors. We found $\chi^2 \gg 1$ for all models: a fact that proves that all GCMs fail to simultaneously reproduce the 20-year, 60-year and the
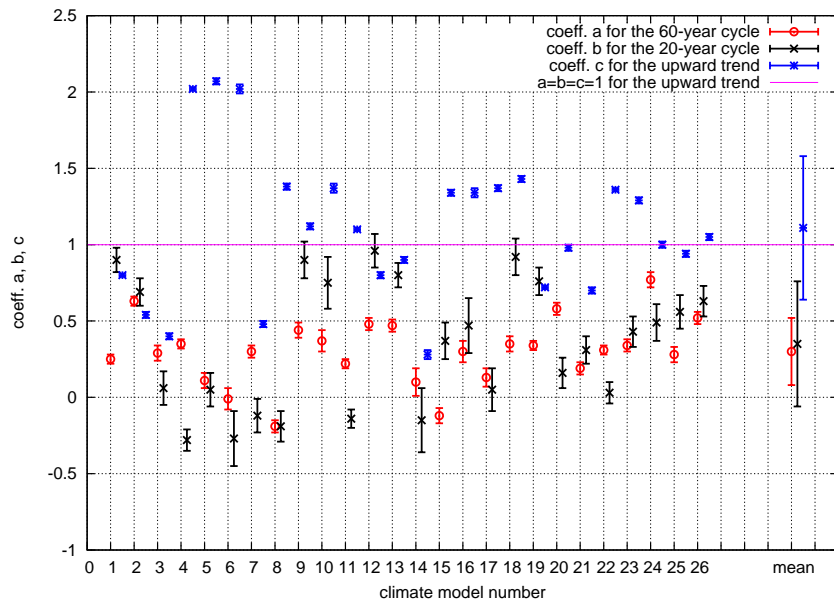
10

Figure 4: Values of the regression coefficients *a*, *b* and *c* relative to the amplitude of the 60 and 20-year cycles, and the upward trend obtained by regression fit of the 26 GCM simulations of the 20th century used by the IPCC. See Table 1 and the Section 2 in the Supplement file for details.

upward trend observed in the temperature with a probability higher than 99.9%. This χ^2 measure based on the multidecadal patterns is quite important because climate changes on a multidecadal scale are usually properly referred to as *climate changes*, and a climate model should at least get these temperature variations right to have any practical economical medium-range planning utility such as street construction planning, agricultural and industrial location planning, prioritization of scientific energy production research versus large scale applications of current very expensive green energy technologies, etc.

It is also possible to include in the discussion the two detected decadal cycles as

$$g(t) = C_3 \cos\left[\frac{2\pi(t - T_3)}{10.44}\right] + C_4 \cos\left[\frac{2\pi(t - T_4)}{9.07}\right]. \tag{7}$$

A detailed discussion about the choice of the two above periods and their physical meaning is better addressed in Section 4. Fitting the temperature for the period 1850-2011 gives: $C_3 = 0.03 \pm 0.01\ {}^oC$, $T_3 = 2002.7 \pm 0.5\ AD$, $C_4 = 0.05 \pm 0.01\ {}^oC$, $T_4 = 1997.7 \pm 0.3\ AD$. It is possible to test how well the IPCC GCMs reconstruct these two decadal cycles by fitting their simulations with the following equation

$$n(t) = m(t) + s * 0.03 \cos\left[\frac{2\pi(t - 2002.7)}{10.44}\right] + l * 0.05 \cos\left[\frac{2\pi(t - 1997.7)}{9.07}\right], \tag{8}$$

where s and l are regression coefficients. Values of s and l statistically compatible with the number 1 indicate that the model well reproduces the two observed decadal temperature cycles, respectively. On the contrary, values of s and l statistically incompatible with 1 indicate that the model does not reproduce the observed temperature cycles. The results referring the average model run, as defined above, are reported in Table 2, where it is evident that the GCMs fail to reproduce these two decadal cycles as well. The average values among the 26 models is: $s = 0.06 \pm 0.40$ and $l = 0.34 \pm 0.37$, which are statistically different from 1. In many cases the regression coefficients are even negative. The table also includes the reduced χ^2 (chi square) values for five degree of freedom by extending Eq. 6 to include the other two decadal cycles. Again, we found $\chi^2 \gg 1$ for all models.

Finally, we can estimate how well the astronomical model made of the sum of the four harmonics plus the quadratic trend (that is: $f(t) + g(t) + p(t)$) reconstructs the 1850-2011 temperature record relative to the GCM simulations. For this purpose we evaluate the root mean square (RMS) residual values between the 4-year average smooth curves of each GCM average simulation and the 4-year average smooth of the temperature curve, and we do the same between the astronomical model and the 4-year average smooth temperature curve. We use a 4-year average smooth because the model is not supposed to reconstruct the fast sub-decadal fluctuations. The RMS residual values are reported in Table 2. The RMS residual value relative to the harmonic model is 0.051 ${}^oC$, while for the GCMs we get RMS residual values from 2 to 5 times larger. This result further indicates that the geometrical model is significantly more accurate than the GCMs in reconstructing the global surface temperature from 1850 to 2011.

The above finding reinforces the conclusion of Scafetta (2010b) that the IPCC (2007) GCMs do not reproduce the observed major decadal and multidecadal dynamical patterns observed in the global surface temperature record. This conclusion does not change if the single GCM runs are studied.

12

3. Reconstruction of the global surface temperature oscillations: 1880-2011

A regression model may always produce results in a reasonable agreement within the same time interval used for its calibration. Thus, showing that an empirical model can reconstruct the same data used for determining its free regression parameters would be not surprising, in general. However, if the same model is shown to be capable of forecasting the patterns of the data outside the temporal interval used for its statistical calibration, then the model likely has a physical meaning. In fact, in the later case the regression model would be using constructors that are not simply independent generic mathematical functions, but are functions that capture the dynamics of the system under study. Only a mathematical model that is shown to be able to both reconstruct and forecast (or predict) the observations is physically relevant according the scientific method.

The climate reconstruction efficiency of an empirical climate model based on a set of astronomical cycles with the periods herein analyzed has been tested and verified in Scafetta (2010b), Loehle and Scafetta (2011) and Scafetta (2011b). Herein, we simply summarize some results for the benefit of the reader and for introducing the following section.

In figures 10 and 11 in Scafetta (2010b) it is shown that the 20-year and 60-year oscillations of the speed of the Sun relative to the barycenter of the solar system are in a very good phase synchronization with the correspondent 20 and 60-year climate oscillations. Moreover, detailed spectra analysis has revealed that the climate system shares numerous other frequencies with the astronomical record.

In figures 3 and 5 in Loehle and Scafetta (2011) it is shown that an harmonic model based on 20-year and 60-year cycles and free phases calibrated on the global surface temperature data for the period 1850-1950 is able to properly reconstruct the 20-year and 60-year modulation of the temperature observed since 1950. This includes a small peak around 1960, the cooling from 1940 to 1970, the warming from 1970 to 2000 and a slight stable/cooling trending since 2000. It was also found a quasi linear residual with a warming trending of about $0.66 \pm 0.16\,^oC/century$ that was interpreted as due to a net anthropogenic warming trending.

In Scafetta (2011b), it was found that the historical mid-latitude aurora record, mostly from central and southern Europe, presents the same major decadal and multidecadal oscillations of the astronomical records and of the global surface temperature herein studied. It has been shown that a harmonic model with aurora/astronomical cycles with periods of 9.1, 10.5, 20, 30 and 60 years calibrated during the period 1850-1950 is able to carefully reconstruct the decadal and multidecadal oscillations of the temperature record since 1950. Moreover, the same harmonic model calibrated during the period 1950-2010 is able to carefully reconstruct the decadal and multidecadal oscillations of the temperature record from 1850 to 1950. The argument about the 1850-1950-fit versus 1950-2010-fit is crucial for showing the forecasting capability of the proposed harmonic model. This property is what distinguishes a mere curve fitting exercise from a valid empirical dynamical model of a physical system. This is a major requirement of the scientific method Scafetta (2011b). A preliminary physical model based on a forcing of the cloud system has been proposed to explain the synchrony between the climate system and the astronomical oscillations.

The above results have supported the thesis that climate is forced by astronomical oscillations and can be partially reconstructed and forecasted by using the same cycles, but for an efficient forecast there is the need of additional information. This is done in the next section.

4. Corrected anthropogenic projected warming trending and forecast of the global surface temperature: period 2000-2100

Even assuming that the detected decadal and multidecadal cycles will continue in the future, to properly forecast climate variation for the next decades, additional information is necessary: 1) the amplitudes and the phases of possible multisecular and millennial cycles; 2) the net anthropogenic contribution to the climate warming according to realistic emission scenarios.

The first issue is left to another paper because it requires a detailed study of the paleoclimatic temperature proxy reconstructions which are relatively different from each other. These cycles are those responsible for the cooling periods during the Maunder and Dalton solar minima as well as for the Medieval Warm Period and the Little Ice Age. So, we leave out these cycles here. Considering that we may be at the very top of these longer cycles, ignoring their contribution may be reasonable only if our forecast is limited to the first decades of the 21st century. However, a rough preliminary estimate would suggests that these longer cycles may contribute globally to an additional cooling of about 0.1-0.2 ^oC by 2100 because the millenarian cycle presents an approximate min-max amplitude of about 0.5-0.7 ^oC (Ljungqvist, 2010) and the top of these longer cycles would occur somewhere during the 21st century (Humlum et al., 2011; Liu et al., 2011). Secular and millennial longer natural cycles could have contributed about 0.2-0.3 ^oC warming from 1850 to 2010 (Scafetta and West, 2007; Eichler et al., 2009: Scafetta, 2009, 2010a).

The second issue is herein explicitly addressed by using an appropriate argument that adopts the same GHG emission scenarios utilized by the IPCC, but correct their climatic effect. In fact, the combination of the 20-year and 60-year cycles, as evaluated in Eq. 3, should have contributed for about 0.3 ^oC of the 0.5 ^oC warming observed from 1970 to 2000. During this period the IPCC (2007) have claimed, by using the GCMs studied herein, that the natural forcing (solar plus volcano) would have caused a cooling up to 0.1-0.2 ^oC (see figure 9.5b in the IPCC report, which is herein reproduced with added comments in Figure S3A in the the Section 4 in the Supplement file). As it is evident in the IPCC figure 9.5a (also shown in the Supplement file), the IPCC GCM results imply that from 1970 to 2000 the net anthropogenic forcing contributed a net warming of the observed 0.5 ^oC plus, at most, another 0.2 ^oC, which had to offset the alleged natural volcano cooling of up to -0.2 ^oC. A 0.7 ^oC anthropogenic warming trend in this 30-year period corresponds to an average anthropogenic warming rate of about $2.3^oC/century$ since 1970. This value is a realistic estimate of the average GCM performance because the average GCM projected anthropogenic net warming rate is 2.3 ± 0.6 $^oC/century$ from 2000 to 2050 according to several GHG emission scenarios (see figure SPM.5 in the IPCC report, which is herein reproduced with added comments in Figure S4B in the Supplement file).

On the contrary, if about 0.3 ^oC of the warming observed from 1970 to 2000 has been naturally induced by the 60-year natural modulation during its warming phase, at least 43-50% of the alleged 0.6-0.7 ^oC anthropogenic warming has been naturally induced, and the 2.3 $^oC/century$ net anthropogenic trending should be reduced at least to 1.3 $^oC/century$.

However, the GCM alleged 0.1-0.2 ^oC cooling from 1970 to 2000 induced by volcano activity may be a gross overestimation of the reality. In fact, as revealed in Figure 2, the GCM climate simulation presents a strong volcano signature peak at 80-year time lag that is totally absent in the temperature record, even after filtering. This would imply that the volcano signature should be quite smaller and shorter than what the GCMs estimate, as empirical studies have shown (Lockwood, 2008; Thomson et al., 2009). Section 5 of the Supplement file shows that the GISS ModelE appears to greatly overestimate the long-time signature associated to volcano activity

against the same signature as estimated by empirical studies.

Moreover, the observed 0.5 ^oC warming from 1970 to 2000, which the IPCC models associate to anthropogenic GHG plus aerosol emissions and to other anthropogenic effects, may also be partially due to poorly corrected urban heat island (UHI) and land use changes (LUC) effects, as argued in detailed statistical studies (McKitrick and Michaels, 2007; McKitrick, 2010). As extensively discussed in those papers, it may be reasonable that the $\sim$ 0.5 ^oC warming reported since 1950-1970 in the available temperature records has been overestimated up to 0.1-0.2 ^oC because of poorly corrected UHI and LUC effects. Indeed, the land warming since 1980 has been almost twice the ocean warming, which may be not fully explained by the different heat capacity between land and ocean. Moreover, during the last decades the agencies that provide the global surface temperature records have changed several times the methodologies adopted to attempt to correct UHI and LUC spurious warming effects and, over time, have produced quite different records (D'Aleo, 2011). Curiously, the earlier reconstructions show a smaller global warming and a more evident 60-year cyclical modulation from 1940 to 2000 than the most recent ones.

Finally, there may be an additional natural warming due to multisecular and millennial cycles as explained in the Introduction. In fact, the solar activity increased during the last four centuries (Scafetta, 2009), and the observed global surface warming during the 20th century is very likely also part of a natural and persistent recovery from the Little Ice Age of AD 1300-1900 (Scafetta and West, 2007; Scafetta, 2009; Loehle and Scafetta, 2011; Soon, 2009; Soon et al., 2011; Kirkby, 2007; Hoyt and Schatten, 1997; Le Mouël et al., 2008; Thejll and Lassen, 2000; Weihong and Bo, 2010; Eichler et al., 2009; Humlum et al., 2011; Liu et al., 2011): see also section 7 in the Supplement file.

Thus, the above estimated 1.30 $^oC/century$ anthropogenic warming trending is likely an upper limit estimate. As a lower limit we can reasonably assume the 0.66 ± 0.16 $^oC/century$, as estimated in Loehle and Scafetta (2011), which would be compatible with the claim that only 0.2 ^oC warming (instead of 0.7 ^oC) of the observed 0.5 ^oC warming since 1970 could be anthropogenically induced. This result would be consistent with the fact that according empirical studies (Lockwood, 2008; Thomson et al., 2009) the cooling long-range effects of the volcano eruptions almost vanished in 2000 (see Section 5 in the Supplement file) and that the secular natural trend could still be increasing. So, from 2000 to 2050 we claim that the same IPCC (2007) anthropogenic emission projections could only induce a warming trend approximately described by the curve

$$q(t) = (0.009 \pm 0.004)(t - 2000). \tag{9}$$

There are also two major quasi decadal oscillations with periods of about 9.1 yr and 10-10.5 yr: see Figure 3. The 9.1-year cycle may be due to a Soli/Lunar tidal cycle (Scafetta, 2010b, 2011b) . In fact, the lunar apsidal line rotation period is 8.85 years while the Soli/Lunar nodal cycle period is 18.6 years. Note that there are two nodes and the configuration Sun-Moon-Earth and Sun-Earth-Moon are equivalent for the tides: thus, the resulting tidal cycles should have a period of about 18.6/2=9.3 yr. The two cycles at 8.85-year and 9.3-year should beat, and produce a fast cycle with an average period of $2/(1/8.85 + 1/9.93) = 9.07$ yr that could be modulated by a slow cycle with period of $2/(1/8.85 - 1/9.93) = 182.9$ yr. There may also be an additional influence of the half Saros eclipse cycle that is about 9 years and 5.5 days. In conclusion, the quasi 9.1-year cycle appears to be related to a Soli/Lunar tidal cycle dynamics. The 10-10.5-year cycle has been interpreted as related to an average cycle between the $0.5/(1/11.862 - 1/29.457) = 9.93$ yr Jupiter/Saturn half-synodic tidal cycle and the 11-year solar cycle (we would have a beat cycle

with period of $2/(1/9.93 + 1/11) = 10.44$ yr). Moreover, a quasi 9.91-year and 10.52-year cycles have been found in the natural gravitational resonances of the solar system (Bucha et al., 1985; Grandpiere, 1996; Scafetta, 2011b).

It is possible to include these two cycles in the harmonic model using the additional harmonic function Eq. (7) and our final model based on 4-frequency harmonics plus two independent trending functions is made as

$$h(t) = f(t) + g(t) + \begin{cases} p(t) & \text{if } 1850 < t < 2000 \\ p(2000) + q(t) & \text{if } 2000 < t < 2100 \end{cases} \qquad (10)$$

To test the forecasting capability of the $g(t)$ harmonics, the $f(t) + g(t) + p(t)$ model is calibrated in two complementary periods. Note that $g(t)$ is sufficiently orthogonal to $f(t) + p(t)$, so we keep $f(t) + p(t)$ unchanged for not adding too many free regression parameters. Fitting the period 1850-1950 gives: $C_3 = 0.03 \pm 0.01 \, ^oC$, $T_3 = 2003 \pm 0.5 \, AD$, $C_4 = 0.05 \pm 0.01 \, ^oC$, $T_4 = 1997.5 \pm 0.3 \, AD$. Fitting the period 1950-2011 gives: $C_3 = 0.04 \pm 0.01 \, ^oC$, $T_3 = 2002.1 \pm 0.5 \, AD$, $C_4 = 0.05 \pm 0.01 \, ^oC$, $T_4 = 1998.1 \pm 0.3 \, AD$. Fitting the period 1850-2011 gives: $C_3 = 0.03 \pm 0.01 \, ^oC$, $T_3 = 2002.7 \pm 0.5 \, AD$, $C_4 = 0.05 \pm 0.01 \, ^oC$, $T_4 = 1997.7 \pm 0.3 \, AD$. If the decadal period 10.44 yr is substituted with a 10 yr period for 1850-2011, we get: $C_3 = 0.02 \pm 0.01 \, ^oC$, $T_3 = 2000.4 \pm 0.5 \, AD$, $C_4 = 0.04 \pm 0.01 \, ^oC$, $T_4 = 1997.7 \pm 0.3 \, AD$.

We observe that all correspondent amplitudes and phases coincide within the error of measure, which implies that the model has forecasting capability. Moreover, the phase related to the 9.1-year cycle presents a maximum around 1997-1998. We observe that this period is in good phase with the Soli/Lunar nodal dates at the equinoxes, when the Soli/Lunar spring tidal maxima are located in proximity of the equator, and the extremes in the tidal variance occurs (Sidorenkov, 2005). In fact, each year there are usually two solar eclipses and two lunar eclipses, but the month changes every year and the cycle repeats every about 9 years with the moon occupying the opposite node. Thus, eclipses occur, within a two week interval, close to the equinoxes (around March 20/21 and September 22/23) every almost 9 years. Section 6 in the Supplement file reports the dates of the solar and lunar eclipses occurred from 1988 to 2010 and compares these dates with the detected 9-year temperature cycle. Two lunar eclipses occurred on 24/Mar/1997 and 16/Sep/1997, the latter eclipse also occurred at the lunar perigee (that is, when the Moon is in its closest position to the Earth) so that the line of the lunar apsides too was oriented along the Earth-Sun direction (so that the two cycles could interfere constructively). Two solar eclipses took place almost 9-years later at almost the same dates, 22/Sep/2006 (at the lunar apogee) and 19/Mar/2007 (at the lunar perigee). This date matching suggests that the 9.1-year cycle is likely related to a Soli/Lunar tidal cycle. Indeed, this cycle is quite visible in the ocean oscillations (Scafetta, 2010b, 2011b) and ocean indexes such as the Atlantic Multidecadal Oscillation (AMO) and the Pacific Decadal Oscillation (PDO).

The timing of the 10-10.5-year cycle maximum (2000-2003), corresponds relatively well with the total solar irradiance maximum in 2002 (Scafetta and Willson, 2009) and the Jupiter/Saturn conjunction around 2000.5 (so that the two cycles could interfere constructively). This suggests that this decadal cycle has a solar/astronomical origin.

The above information is combined in Figures 5A and 5B that depict: the monthly sampled global surface temperature since 1850; a 4-year moving average estimates of the same; the proposed model given in Eq. 10 with two and four cycles, respectively. Finally, for comparison, we plot the IPCC projected warming using the average GCM projection estimates, which is given by a linear trending warming of $2.3 \pm 0.6 \, ^oC/century$ from 2000 to 2050 while since 2050 the

projections spread a little bit more according to alternative emission scenarios (see figure S4B in Section 4 in the Supplement file). The two figures are complementary by highlighting both a low resolution forecast that extends to 2100, which can be more directly compared with the IPCC projections, and a higher resolution forecast for the next decades that may be more important for an immediate economical planning, as explained above.

Figure 5 clearly shows the good performance of the proposed model (Eq. 10) in reconstructing the dacadal and multidecadal oscillations of the global surface temperature since 1850. The model has forecasting capability also at the decadal scale because the two curves calibrated using the independent periods 1850-1950 and 1950-2011 are synchronous to each other also at the decadal scale and are synchronous with the temperature modulation revealed by the 4-year smooth curve: the statistical divergence between the harmonic model reconstruction and the data have a standard deviation of $\sigma = 0.15\ ^oC$, which is due to the large and fast ENSO related oscillations, while the divergence with the grey 4-year smooth curve of the temperature has a standard deviation of $\sigma = 0.05\ ^oC$, as Table 2 reports.

Figure 5 shows that the IPCC warming projection since 2000 (at a rate of $2.3 + 0.6\ ^oC/century$ plus a vertical error of $\pm0.1\ ^oC$) does not agree with the observed temperature pattern since about 2005-2006. On the contrary, the empirical model we propose, Eq. 10, appears to reasonably forecast the observed trending of the global surface temperature since 2000, which appears to have been almost steady: the error bars are calculated by taking into account both the statistical error of the model ($\sim \pm0.1\ ^oC$) (because, at the moment, the harmonic model includes only the decadal and multidecadal scales and, evidently, it is not supposed to reconstruct the fast ENSO related oscillations) plus the projected anthropogenic net warming with a linear rate within the interval $0.5-1.3\ ^oC/century$, as discussed above. According our model, by 2050 the climate may warm by about $0.1-0.5\ ^oC$, which is significant less than the average $1.2 \pm 0.4\ ^oC$ projected by the IPCC. If multisecular natural cycles (which according to several authors have significantly contributed to the observed 1700-2000 warming and very likely will contribute to a cooling since the 21st century) are ignored, the temperature may warm by about $0.3-1.2\ ^oC$ by 2100 contrary to the $1.0-3.6\ ^oC$ warming projected by the IPCC (2007) according to its various emission scenarios.

The divergence of the temperature data from the IPCC projections and their persistent convergence with the astronomical harmonic model can be calculated by evaluating a time continuous discrepancy $\chi^2(t)$ (*chi-squared*) function defined as

$$\chi^2(t) = \frac{(Tem(t) - Mod(t))^2}{(\Delta Mod(t))^2},\qquad(11)$$

where $Tem(t)$ is the 4-year smooth average temperature curve depicted in the figure, which highlights the decadal oscillation, $Mod(t)$ is used first for indicating the IPCC GCM average projection curve and second for indicating the harmonic model average forecast curve as depicted in the figure, and $\Delta Mod(t)$ is used to indicate the time dependent uncertainty first of the IPCC projection and second of the harmonic model, respectively, which are depicted in the two shadow regions in Figure 5. In the above equation the implicit error associated to the 4-year smooth average temperature curve is considered negligible (it has an order of magnitude of $0.01\ ^oC$) compared to the uncertainty of the models $\Delta Mod(t)$, which has an order of magnitude of $0.1\ ^oC$ and above, so we can ignore it in the denominator of Eq. 11. Values of $\chi^2(t) < 1$ indicate a sufficient *agreement* between the data and the model at the particular time t, while values of $\chi^2(t) > 1$ indicate *disagreement*. Figure 6 depicts Eq. 11 and clearly shows that the astronomical harmonic model forecast is quite accurate as the time progress since 2000. Indeed, the performance of our
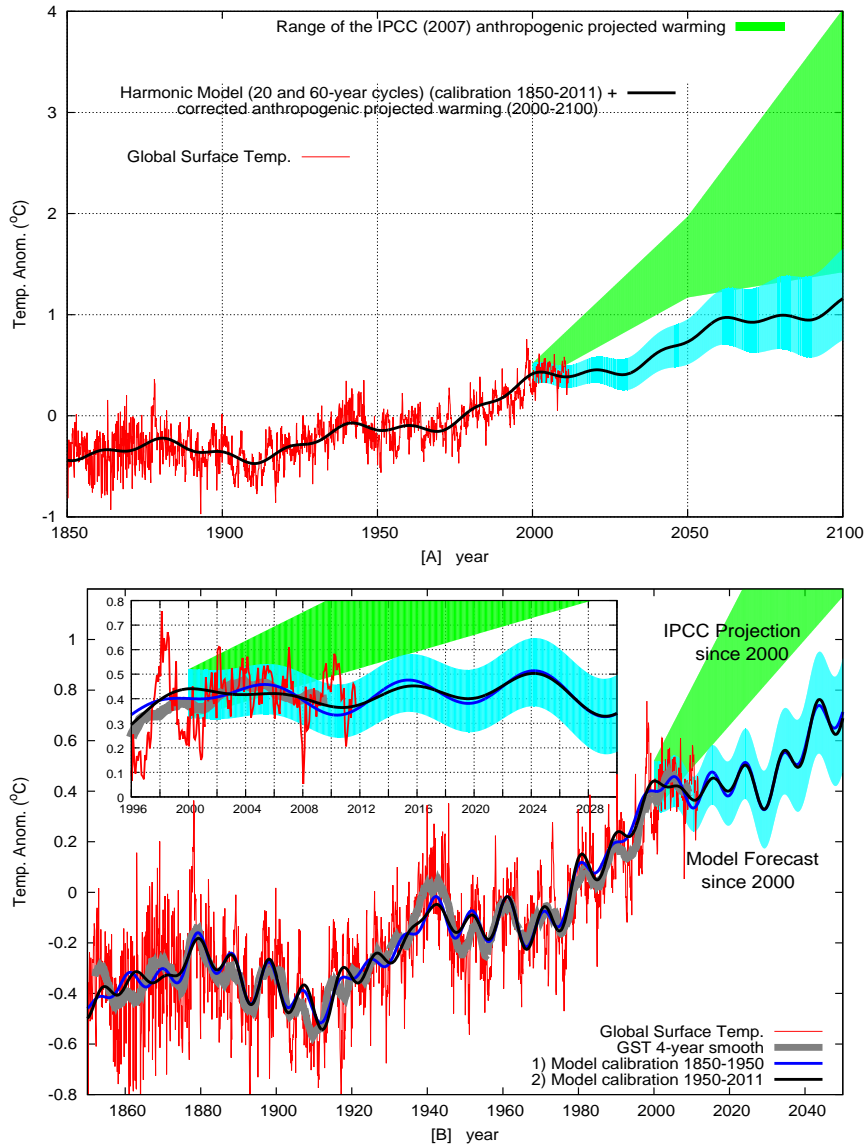
Figure 5: [A] The monthly sampled global surface temperature from 1950 to 2050 (red); the proposed empirical model (Eq. 10) made of the discussed 2 cycles (20 and 60 yr) plus the quadratic trend until 2000 that is substituted with the corrected anthropogenic net projected warming as explained in the text (black); the IPCC 2007 projections (green). [B] The monthly sampled global surface temperature from 1950 to 2050 (red); a 4-year moving average estimates of the same (smooth wide gray curve); the proposed empirical model (Eq. 10) made of the discussed 4 cycles (9.07, 10.44, 20 and 60 yr) plus the quadratic trend until 2000 that is substituted with the anthropogenic net estimated contribution given by a linear trend with a rate within the interval 0.5-1.3 $^oC/century$ as discussed in the text (black and blue small curves); finally, by comparison the IPCC projected warming using the average GCM projection with a trend of 2.3±0.6 $^oC/century$ from 2000 to 2050. Note than the two harmonic model curves use the two decadal harmonics at 9.07-year and 10.44-year periods calibrated on the temperature data during two complementary time periods, 1850-1950 and 1950-2011 respectively. As evident in the figure, the decadal oscillations reconstructed by the two alternative models are very well synchronized between them and with the oscillations revealed in the grey 4-year smooth temperature gray curve. This result suggests that the astronomical harmonic model has forecast capability. The insert figure is reproduced in a full page figure in the supplement file.
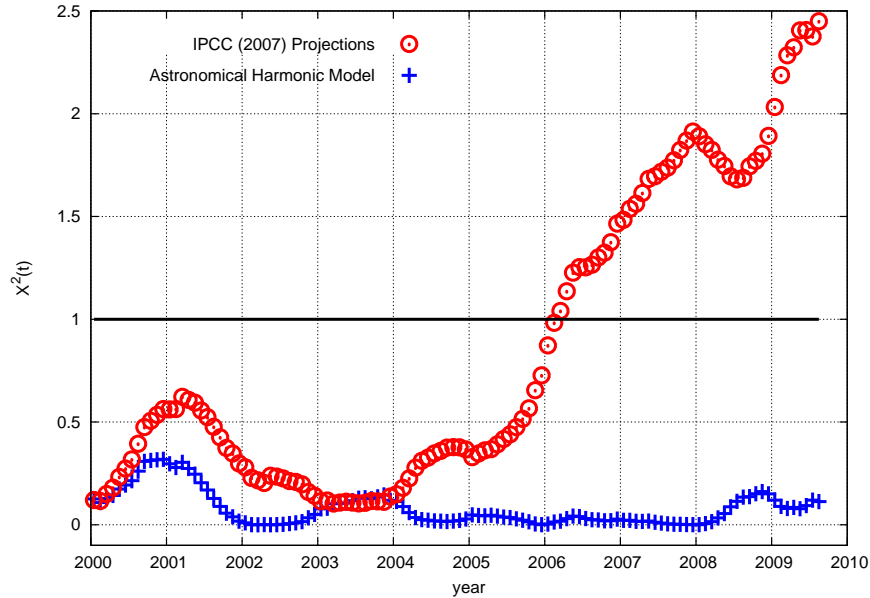
Figure 6: The curves are produced with Eq. 11 and give a time dependent estimate of how well the astronomical harmonic model (crosses) and the IPCC projections (circles) forecast the temperature data (4-year smooth average temperature gray curve in Figure 5) since 2000. The IPCC projections significantly diverge from the temperature data since 2004-2006. The astronomical harmonic model is shown to forecast the data quite well and it is quite stable in time. The variable χ^2 needs to be less than 1 for statistical compatibility.

geometrical model is always superior than the IPCC projections. The IPCC (2007) projections significantly diverge from the data since 2004-2006.

5. Discussion and Conclusion

The scientific method requires that a physical model fulfils two conditions: it has to reconstruct *and* predict (or forecast) physical observations. Herein, we have found that the GCMs used by the IPCC (2007) seriously fail to properly reconstruct even the large multidecadal oscillations found in the global surface temperature which have a climatic meaning. Consequently, the IPCC projections for the 21st century cannot be trusted. On the contrary, the astronomical empirical harmonic model proposed in Scafetta (2010b, 2011b) has been shown to be capable of reconstructing and, more importantly, forecasting the decadal and multidecadal oscillations found in the global surface temperature with a sufficiently good accuracy. Figures 5 and 6 shows that in 1950 it could have been possible to accurately forecast the decadal and multidecadal oscillations observed in the climate since 1950, which includes a steady/cooling trend from 2000 to 2011. Four major cycles have been detected and used herein with period of 9.1 yr (which appears to be

linked to a Soli/Lunar tidal cycle), and of 10-10.5, 20-21 and 60-61 yr (which appears to be in phase with the gravitational cycles of Jupiter and Saturn that can also modulate the solar cycles at the equivalent time-scales). However, other astronomical cycles may be involved in the process.

This result argues in favor of a celestial origin of the climate oscillations and whose mechanisms were not included in the climate models adopted by the IPCC in 2007. The harmonic interpretation of climate change also appears more reasonable than recent attempts of reproducing with GCMs some limited climate pattern such as the observed slight cooling from 1998 to 2008 by claiming that it is a red-noise-like internal fluctuation of the climatic system (Meehl et al., 2011) or by carefully playing with the very large uncertainty in the climate sensitivity to CO_2 changes and in the aerosol forcing (Kaufmann et al., 2011). In fact, a quasi 60-year cycle in the climate system has been observed for centuries and millennia in several independent records, as explained in the Introduction.

By not properly reconstructing the 20-year and 60-year natural cycles we found that the IPCC GCMs have seriously overestimated also the magnitude of the anthropogenic contribution to the recent global warming. Indeed, other independent studies have found serious incompatibilities between the IPCC climate models and the actual observations and reached the same conclusion. For example, Douglass et al. (2007) showed that there is a large discrepancy between observed tropospheric temperature trends and the IPCC climate model predictions from Jan 1979 to Dec 2004: GCM ensemble mean simulations show that the increased CO_2 concentration should have produced an increase in the tropical warming trend with altitude, but balloon and satellite observations do not show any increase (Singer, 2011). Spencer and Braswell (2011) have showed that there is a large discrepancy between the satellite observations and the behavior of the IPCC climate models on how the Earth loses energy as the surface temperature changes. Both studies imply that the modeled climate sensitivity to CO_2 is largely overestimated by the IPCC models. Our findings would be consistent with the above results too and would imply a climate sensitivity to CO_2 doubling much lower than the IPCC's proposal of 1.5-4.5 ^oC. Lindzen and Choi (2011) has argued for a climate sensitivity to a CO_2 doubling of 0.5 ^oC - 1.3 ^oC by using variations in Earth's radiant energy balance as measured by satellites. We claim that the reason of the discrepancy between the model outcomes and the data is due to the fact that the current GCMs are missing major astronomical forcings related to the harmonies of the solar system and the physical/climatic mechanisms related to them (Scafetta, 2011b).

Probably several solar and terrestrial mechanisms are involved in the process (Scafetta, 2009, 2010b, 2011b). It is reasonable that with their gravitational and magnetic fields, the planets can directly or indirectly modulate the solar activity, the heliosphere, the solar wind and, ultimately, the terrestrial magnetosphere and ionosphere. In fact, planetary tides, as well as solar motion induced by planetary gravity may increase solar nuclear fusion rate (Grandpiere, 1996; Wolff and Patrone, 2010). Moreover, Charvátová et al. (1988), Komitov (2009), Mazzarella and Scafetta (2011) and Scafetta (2011b) showed that the historical multi-secular aurora record and some cosmogenic beryllium records presents a large quasi 60-year cycle which would suggest that the astronomical cycles regulated by Jupiter and Saturn are the primary indirect cause of the oscillations in the terrestrial ionosphere. Ogurtsov et al. (2002) have found that several multi secular solar reconstructions do present a quasi 60-year cycle together with longer cycles. Loehle and Scafetta (2011) have argued that a quasi 60-year cycle may be present in the total solar irradiance (TSI) since 1850, although the exact reconstruction of TSI is not currently possible. Indeed, TSI direct satellite measurements since 1978 have produced alternative composites such as the ACRIM (Willson and Mordvinov, 2003), which may present a pattern that would be compatible with a 60-year cycle. In fact, the ACRIM TSI satellite composite presents an increase from

1980 to 2002 and a decrease afterward. On the contrary, the PMOD TSI composite adopted by the IPCC Fröhlich (2006) does not present any patter resembling a 60-year modulations but a slightly decrease since 1980. However, the way how the PMOD science team has adjusted the TSI satellite records to obtain its composite may be erroneous (Scafetta and Willson, 2009; Scafetta, 2011a).

Indeed, Scafetta (2011b) found that several mid-latitude aurora cycles (quasi 9.1, 10-10.5, 20-21 and 60-62 yr cycles) correspond to the climate cycles herein detected. We believe that the oscillations found in the historical mid-latitude aurora record are quite important because reveal the existence of equivalent oscillations in the electric properties of the atmosphere, which can regulate the cloud system (Svensmark, 1998; Carslaw et al., 2002; Svensmark, 2007; Tinsley et al., 2007; Kirkby, 2007; Enghoff et al., 2011; Kirkby et al., 2011). In addition, the variations in solar activity also modulate the incoming cosmic ray flux that may lead to a cloud modulation. The letter too would modulate the terrestrial albedo with the same frequencies found in the solar system. As shown in Scafetta (2011b) just a 1-2% modulation of the albedo would be sufficient to reproduce the climatic signal at the surface, which is an amplitude compatible with the observations. Oscillations in the albedo would cause correspondent oscillations in the climate mostly through warming/cooling cycles induced in the ocean surface. For example, a 60-year modulation has been observed in the frequency of major hurricanes on the Atlantic ocean that has been associated to a 60-year cycle in the strength of the Atlantic Thermohaline Circulation (THC), which would also imply a similar oscillation in the Great Ocean Conveyor Belt (Gray and Klotzbach, 2011). Moreover, herein we have found further evidences that the 9.1-year cycle is linked to the Soli/Lunar tidal dynamics. Ultimately, the climate amplifies the effect of harmonic forcing through several internal feedback mechanisms, which ultimately tend to synchronize all climate oscillations with the solar-lunar-planetary astronomical oscillations through collective synchronization mechanisms (Pikovsky et al., 2001; Strogatz, 2009; Scafetta, 2010b).

For the above reasons, it is very unlikely that the observed climatic oscillations are due only to an internal variability of the climate system that evolves independently of astronomical forcings, as proposed by some authors (Latif et al., 2006; Meehl et al., 2011). Indeed, the GCMs do not really reconstruct the actual observed oscillations at all temporal scales, nor they have ever been able to properly forecast them. It is evident that simply showing that a model is able to produce some kind of red-noise-like variability (as shown in the numerous GCM simulations depicted in the figures in the Supplement file) is not enough to claim that the model has really modeled the observed dynamics of the climate.

For the imminent future, the global climate may remain approximately steady until 2030-2040, as it has been observed from the 1940s to the 1970s because the 60-year climate cycle has entered into its cooling phase around 2000-2003, and this cooling will oppose the adverse effects of a realistic anthropogenic global warming, as shown in Figure 5. By using the same IPCC projected anthropogenic emissions our partial empirical harmonic model forecast forecast a global warming by about 0.31.2 ^{o}C by 2100, contrary to the IPCC 1.03.6 ^{o}C projected warming. The climate may also further cool if additional natural secular and millennial cycles enter into their cooling phases. In fact, the current warm period may be part of a quasi millennial natural cycle, which is currently at its top as it was during the roman and medieval times, as can be deduced from climate records (Schulz and Paul, 2002; Ljungqvist, 2010) and solar records covering the last millennia (Bard et al., 2000; Ogurtsov et al., 2002). Preliminary attempts to address this issue have been made by numerous authors as discussed in the Introduction such as, for example, by Humlum et al. (2011), while a more detailed discussion is left to another paper.

References

Agnihotri, R. and K. Dutta, 2003. Centennial scale variations in monsoonal rainfall (Indian, east equatorial and Chinese monsoons): Manifestations of solar variability. Current Science 85, 459-463.

Aslaksen, H., 1999. The mathematics of the Chinese calendar. National University of Singapore. http://www.math.nus.edu.sg/aslaksen/calendar/chinese.shtml

Bard, E., G. Raisbeck, F. Yiou and J. JOUZEL, 2000. Solar irradiance during the last 1200 years based on cosmogenic nuclides. Tellus 52B, 985992.

Brohan, P., J. J. Kennedy, I. Harris, S. F. B. Tett and P. D. Jones, 2006. Uncertainty estimates in regional and global observed temperature changes: a new dataset from 1850. J. Geophys. Res. 111, D12106.

Bucha, V., I. Jakubcová, and M. Pick, 1985. Resonance frequencies in the Suns motion. Studia Geophysica et Geodetica 29, 107111.

Carslaw K. S., Harrison R. G. and Kirkby J., 2002. Cosmic Rays, Clouds, and Climate. Science 298, 1732-1737.

Charvátová I., J. Střeštík and L. Křivský, 1988. The periodicity of aurorae in the years 1001-1900. Stud. Geophys. Geod. 32, 70-77.

Cook E. R., D. M. Meko, C. W. Stockton, 1997. A New Assessment of Possible Solar and Lunar Forcing of the Bidecadal Drought Rhythm in the Western United States. J. Climate 10, 13431356.

Currie R. G., 1984. Evidence for 18.6 year lunar nodal drought in western North America during the past millennium. J. Geophys. Res. 89, 1295-1308.

Courtillot, V., J. L. Le Mouël, and P. N. Mayaud (1977). Maximum Entropy Spectral Analysis of the Geomagnetic Activity Index aa Over a 107-Year Interval, J. Geophys. Res., 82(19), 2641-2649.

D'Aleo J., 2011. A critical look at the surface temperature records. In Evidence-based Climate science, edited by D. Easterbrook, Chapter 3, 91-73. (Elsevier, Amsterdam).

Davis J.C., and Bohling G., 2001. The Search for Patterns in Ice-Core Temperature Curves: in Gerhard, Lee C., William E. Harrison, and Bernold M. Hanson, eds., Geological Perspectives of Global Climate Change, 213-230.

Douglass D.H., Christy J.R., Pearson B.D. and Singer S.F., (2007). A comparison of tropical temperature trends with model predictions. Int. J. Climatol. DOI: 10.1002/joc.1651

Ehret T., 2008. Old Brass Brains - Mechanical Prediction of Tides. ACSM Bulletin, 41-44.

Eichler, A., Olivier, S., Henderson, K., Laube, A., Beer, J., Papina, T., Gäggeler, H.W., Schwikowski, M., 2009. Temperature response in the Altai region lags solar forcing. Geophys. Res. Lett. 36, L01808 10.1029/2008GL035930.

Enghoff M. B., Pedersen J. O. P., Uggerhj U. I., Paling S. M., Svensmark H., 2011. Aerosol nucleation induced by a high energy particle beam, Geophys Res Lett. 38, L09805.

Fröhlich C., 2006. Solar irradiance variability since 1978: revision of the PMOD composite during solar cycle 21. Space Sci. Rev., 125, 5365.

Grandpiere A., 1996. On the origin of the solar cycle periodicity, Astrophysics and Space Science 243, 393-400.

Gray W.M., and P. J. Klotzbach, 2011. Have increases in CO_2 contributed to the recent large upswing in Atlantic basin major hurricanes since 1995? In Evidence-based Climate Science, edited by D. Easterbrook, Chapter 9, 223-249. (Elsevier, Amsterdam).

Hansen, J. et al. 2007. Climate simulations for 1880-2003 with GISS modelE, Climate Dynam. 29, 661-696.

Hoyt, D. V., and K. H. Schatten, 1997. *The Role of the Sun in the Climate Change*. Oxford Univ. Press, New York.

Humlum, O., Solheim, J.-K. and Stordahl, K. 2011. Identifying natural contributions to late Holocene climate change. Global and Planetary Change 79, 145-156.

IPCC: Solomon, S. et al. (eds) in *Climate Change 2007: The Physical Science Basis.Contribution of Working Group I to the Fourth Assessment Report of the Intergovernmental Panel on Climate Change*, (Cambridge University Press, Cambridge, 2007).

Iyengar, R. N., 2009. Monsoon rainfall cycles as depicted in ancient Sanskrit texts. Current science 97, 444-447.

Jevrejeva, S., J. C. Moore, A. Grinsted, and P. Woodworth, L., 2008. Recent global sea level acceleration started over 200 years ago? Geophys. Res. Lett. 35, L08715.

Kaufmann R.K., Kauppi H., Mann M.L., and Stock J.H., 2011. Reconciling anthropogenic climate change with observed temperature 1998-2008. PNAS 108, 11790-11793. doi: 10.1073/pnas.1102467108.

Kennedy J.J., Rayner N.A., Smith R.O., Saunby M., Parker D.E., (2011). Reassessing biases and other uncertainties in sea-surface temperature observations since 1850: biases and homogenisation. J. Geophys. Res. 116: D14103 & D14104.

Kirkby, J., 2007. Cosmic Rays and Climate. Surveys in Geophys. 28, 333-375.

Kirkby J. et al., 2011. Role of sulphuric acid, ammonia and galactic cosmic rays in atmospheric aerosol nucleation. Nature 476, 429-433.

Klyashtorin, L.B., V. Borisov, and A. Lyubushin, 2009. Cyclic changes of climate and major commercial stocks of the Barents Sea. Mar. Biol. Res. 5, 4-17.

Komitov, B., 2009. The Sun-climate relationship II: The cosmogenic beryllium and the middle latitude aurora. Bulgarian Astronomical Journal 12, 7590.

Knudsen, M. F., Seidenkrantz M-S., Jacobsen B. H. and Kuijpers A., 2011. Tracking the Atlantic Multidecadal Oscillation through the last 8,000 years. Nature Communications 2, 178.

Latif M., Collins M., Pohlmann H. and Keenlyside N., 2006. A Review of Predictability Studies of Atlantic Sector Climate on Decadal Time Scales. J. Climate 19, 5971-5987.

Ljungqvist F.C., 2010. A new reconstruction of temperature variability in the extra-tropical Northern Hemisphere during the last two millennia. Geografiska Annaler Series A 92, 339-351.

Lindzen R.S. and Choi Y-S., 2011. On the Observational Determination of Climate Sensitivity and Its Implications, Asia-Pacific J. Atmos. Sci., 47(4), 377-390.

Liu Y., Cai Q.F., Song H.M., ZhiSheng A.N., LINDERHOLM H.W., 2011. Amplitudes, rates, periodicities and causes of temperature variations in the past 2485 years and future trends over the central-eastern Tibetan Plateau. Chinese Sci. Bull. 56, 2986-2994.

Loehle C. and Scafetta N., 2011. Climate Change Attribution Using Empirical Decomposition of Climatic Data. The Open Atmospheric Science J. 5, 74-86.

Lockwood, M., 2008. Analysis of the contributions to global mean air surface temperature rise. Proc. R. Soc. A 464, 1-17.

Mazzarella A. and N. Scafetta, 2011. Evidences for a quasi 60-year North Atlantic Oscillation since 1700 and its meaning for global climate change, Theor. Appl. Climatol. DOI 10.1007/s00704-011-0499-4

McKitrick, R. and P. Michaels, 2007. Quantifying the influence of anthropogenic surface processes and inhomogeneities on gridded global climate data. J. of Geophysical Research 112, D24S09.

McKitrick, R., 2010. Atmospheric circulations do not explain the temperature-industrialization correlation. Statistics, Politics and Policy 1, 1.

Meehl G.A., J.M. Arblaster, J.T. Fasullo, A. Hu, and K.E. Trenberth, 2011. Model-based evidence of deep-ocean heat uptake during surface-temperature hiatus periods. Nature Climate Change 1, 360-364.

Le Mouël J-L., Courtillot V., E. Blanter, and M. Shnirman, 2008. Evidence for a solar signature in 20th-century temperature data from the USA and Europe. Geoscience 340, 421-430.

Ogurtsov, M.G., Y.A. Nagovitsyn, G.E. Kocharov, and H. Jungner, 2002. Long-period cycles of the Suns activity recorded in direct solar data and proxies. Solar Phys. 211, 371-394.

Patterson, R. T., A. Prokoph and A. Chang, 2004. Late Holocene sedimentary response to solar and cosmic ray activity influenced climate variability in the NE Pacific. Sedimentary Geology 172, 6784.

Pikovsky A., M. Rosemblum and J. Kurths, 2001. Synchronization: A Universal Concept in Nonlinear Sciences. Cambridge University Press.

Press W. H., S. A. Teukolsky, W. T. Vetterling and B. P. Flannery. Numerical Recipes, Third Edition. (Cambridge University Press, 2007).

Scafetta, N., and B. J. West, 2007. Phenomenological reconstructions of the solar signature in the Northern Hemisphere surface temperature records since 1600. J. Geophys. Res. 112, D24S03.

Scafetta, N., 2009. Empirical analysis of the solar contribution to global mean air surface temperature change. J. Atm. and Solar-Terr. Phys. 71, 1916-1923.

Scafetta, N., and R.C. Willson, 2009. ACRIM-gap and TSI trend issue resolved using a surface magnetic flux TSI proxy model. Geophys. Res. Lett., 36, L05701.

Scafetta N., 2010a. Climate Change and Its causes, A Discussion about Some Key Issues. La Chimica e l'Industria 1, 70-75. The English translation is published by Science and Public Policy Institute. http://scienceandpublicpolicy.org/originals/climate_change_causes.html

Scafetta, N., 2010b. Empirical evidence for a celestial origin of the climate oscillations and its implications. J. of Atmospheric and Solar-Terrestrial Physics 72, 951970.

Scafetta N., 2011a. Total Solar Irradiance Satellite Composites and their Phenomenological Effect on Climate. In Evidence-based Climate science, edited by D. Easterbrook, Chapter 12, 289-316. (Elsevier, Amsterdam).

Scafetta N., 2011b. A shared frequency set between the historical mid-latitude aurora records and the global surface temperature. J. of Atmospheric and Solar-Terrestrial Physics 74, 145-163. DOI: 10.1016/j.jastp.2011.10.013

Schulz M., and Paul A., 2002. Holocene Climate Variability on Centennial-to-Millennial Time Scales: 1. Climate Records from the North-Atlantic Realm, 41-54. in Wefer, G. Berger, W., Behre, K-E., Jansen, E. eds, *Climate Development and History of the North Atlantic Realm.* (Springer-Verlag Berlin Heidelberg).

Shaviv, N.J., 2008. Using the oceans as a calorimeter to quantify the solar radiative forcing. J. Geophys. Res. 113, A11101 10.1029/2007JA012989

Singer S.F., 2011. Lack of consistency between modeled and observed temperature trends. Energy & Environment, 22(4), 375-406.

Sinha, A. et al., 2005. Variability of Southwest Indian summer monsoon precipitation during the Bølling-Allerød. Geology 33, 813816.

23

Sidorenkov N., 2005. Long-term changes in the variance of the earth orientation parameters and of the excitation functions. Proceedings of the "Journées Systèmes de Référence Spatio-Temporels 2005" Warsaw, 19-21 September 2005.

Soon W., 2009. Solar Arctic-mediated climate variation on multidecadal to centennial timescales: empirical evidence, mechanistic explanation, and testable consequences. Physical Geography, 30, 144-184.

Soon W., K. Dutta, D.R. Legates, V. Velasco, W. Zhang, 2011. Variation in surface air temperature of China during the 20th century. J. of Atmospheric and Solar-Terrestrial Physics 73(16), 2331-2344.

Spencer, R.W. and Braswell, W.D., 2011. On the Misdiagnosis of Surface Temperature Feedbacks from Variations in Earth's Radiant Energy Balance. Remote Sens. 3, 1603-1613.

Sonnemann G., 1998. Comment on "Does the correlation between solar cycle length and Northern Hemisphere and temperatures rule out any significant global warming from greenhouse gases?" By Peter Laut and Jasper Grundmann. J. of Atmospheric and Solar Terrestrial Physics 60, 1625-1630.

Stockton C. W., J. M. Mitchell, and D. M. Meko, 1983. A reappraisal of the 22-year drought cycle. Solar-Terrestrial Influences on Weather and Climate, B. M. McCormac, Ed., Colorado Associated University Press, 507515.

Strogatz S. H., 2009. Exploring complex networks, Nature 410, 268-276.

Svensmark H., 1998. Influence of Cosmic Rays on Earth's Climate. Physical Review Letters 81(22), 50275030.

Svensmark, H., 2007. Cosmoclimatology: A New Theory Emerges. Astronomy & Geophysics 48, 1.18-1.24.

Temple, R. K. G., 1998. The Sirius Mystery. Destiny Books. in ˋAppendix III: Why Sixty years?" http://www.bibliotecapleyades.net/universo/siriusmystery/siriusmystery.htm

Thejll P., and K. Lassen, 2000. Solar forcing of the Northern hemisphere land air temperature: New data. Journal of Atmospheric and Solar-Terrestrial Physics, 62, 1207-1213.

Thompson, D. W. J., J. M. Wallace, P. D. Jones and J. J. Kennedy, 2009. Identifying signatures of natural climate variability in time series of global-mean surface temperature: Methodology and Insights. J. Climate 22, 6120-6141.

Thomson, W. (Lord Kelvin), 1881. The tide gauge, tidal harmonic analyzer, and tide predictor. Proceedings of the Institution of Civil Engineers 65, 3-24.

Tinsley, B. A., 2008. The global atmospheric electric circuit and its effects on cloud microphysics. Rep. Prog. Phys. 71, 066801.

Tisdale B., (2010). GISS deletes arctic and southern ocean sea surface temperature data. http://wattsupwiththat.com/2010/05/31/giss-deletes-arctic-and-southern-ocean-sea-surface-temperature-data/

Weihong Q., and L. Bo, 2010. Periodic oscillations in millennial global-mean temperature and their causes. Chinese Science Bulletin 35, 4052-4057.

Willson, R.C., and A.V. Mordvinov, 2003. Secular total solar irradiance trend during solar cycles 21-23, Geophys. Res. Lett., 30, 1199-1282.

Wolff C. L. and P. N. Patrone, 2010. A New Way that Planets Can Affect the Sun. Solar Physics 266, 227-246.

Yadava, M. G. and R. Ramesh, 2007. Significant longer-term periodicities in the proxy record of the Indian monsoon rainfall. New Astronomy 12, 544555.

Yu, Z., S. Chang, M. Kumazawa, M. Furumoto, A. Yamamoto, 1983. Presence of periodicity in meteorite falls. National Institute of Polar Research, Memoirs, Special issue 30, 362-366.

24

#	model	a (60-year)	b (20-year)	c (trend)	d (bias)	χ^2 (abc)
	temp	1.03 ± 0.05	0.99 ± 0.12	1.01 ± 0.02	0.00 ± 0.01	0.21
1	GISS ModelE	0.25 ± 0.03	0.90 ± 0.08	0.80 ± 0.01	0.08 ± 0.01	89
2	BCC CM1	0.63 ± 0.03	0.69 ± 0.09	0.54 ± 0.02	0.08 ± 0.01	109
3	BCCR BCM2.0	0.29 ± 0.05	0.06 ± 0.11	0.40 ± 0.02	0.08 ± 0.01	202
4	CGCM3.1 (T47)	0.35 ± 0.03	-0.28 ± 0.07	2.02 ± 0.01	0.40 ± 0.01	753
5	CGCM3.1 (T63)	0.11 ± 0.05	0.05 ± 0.11	2.07 ± 0.02	0.40 ± 0.01	536
6	CNRM CM3	-0.01 ± 0.07	-0.27 ± 0.18	2.02 ± 0.03	0.39 ± 0.01	322
7	CSIRO MK3.0	0.30 ± 0.04	-0.12 ± 0.11	0.48 ± 0.02	0.08 ± 0.01	176
8	CSIRO MK3.5	-0.19 ± 0.04	-0.19 ± 0.10	1.38 ± 0.02	0.25 ± 0.01	197
9	GFDL CM2.0	0.44 ± 0.05	0.90 ± 0.12	1.12 ± 0.02	0.21 ± 0.01	28
10	GFDL CM2.1	0.37 ± 0.07	0.75 ± 0.17	1.37 ± 0.03	0.26 ± 0.01	53
11	GISS AOM	0.22 ± 0.03	-0.14 ± 0.06	1.10 ± 0.01	0.22 ± 0.01	93
12	GISS EH	0.48 ± 0.04	0.96 ± 0.11	0.80 ± 0.02	0.14 ± 0.01	43
13	GISS ER	0.47 ± 0.04	0.80 ± 0.08	0.90 ± 0.02	0.11 ± 0.01	31
14	FGOALS g1.0	0.10 ± 0.09	-0.15 ± 0.21	0.28 ± 0.03	0.06 ± 0.01	171
15	INVG ECHAM4	-0.12 ± 0.05	0.37 ± 0.12	1.34 ± 0.02	0.24 ± 0.01	138
16	INM CM3.0	0.30 ± 0.07	0.47 ± 0.18	1.34 ± 0.03	0.24 ± 0.01	54
17	IPSL CM4	0.13 ± 0.06	0.05 ± 0.14	1.37 ± 0.02	0.26 ± 0.01	107
18	MIROC3.2 Hires	0.35 ± 0.05	0.92 ± 0.12	1.43 ± 0.02	0.19 ± 0.01	104
19	MIROC3.2 Medres	0.34 ± 0.03	0.76 ± 0.09	0.72 ± 0.01	0.14 ± 0.01	104
20	ECHO G	0.58 ± 0.04	0.16 ± 0.10	0.98 ± 0.02	0.18 ± 0.01	26
21	ECHAM5/MPI-OM	0.19 ± 0.04	0.31 ± 0.09	0.70 ± 0.02	-0.02 ± 0.01	104
22	MRI CGCM 2.3.2	0.31 ± 0.03	0.03 ± 0.07	1.36 ± 0.01	0.27 ± 0.01	149
23	CCSM3.0	0.34 ± 0.04	0.43 ± 0.10	1.29 ± 0.02	0.24 ± 0.01	76
24	PCM	0.77 ± 0.05	0.49 ± 0.12	1.00 ± 0.02	0.16 ± 0.01	7
25	UKMO HADCM3	0.28 ± 0.05	0.56 ± 0.11	0.94 ± 0.02	0.18 ± 0.01	42
26	UKMO HADGEM1	0.52 ± 0.04	0.63 ± 0.10	1.05 ± 0.02	0.20 ± 0.01	24
	average	0.30 ± 0.22	0.35 ± 0.41	1.11 ± 0.47	0.19 ± 0.11	143.8

Table 1: Values of the regression parameters of Eq. 5 obtained by fitting the 25 IPCC [2007] climate GCM ensemble-mean estimates. #1 refers to the ensemble average of the GISS ModelE depicted in Figure 1a; #2-#26 refers to the 25 IPCC GCMs. Pictures and analysis concerning all 95 records including each single GCM run are shown in Section 2 in the Supplement File that accompanies this paper. The optimum value of these regression parameters should be $a = b = c = 1$ as presented in the first raw that refers to the regression coefficients of the same model used to fit the temperature record. The last column refers to a reduced χ^2 test based on three coefficients a, b and c: see Eq. 6. This determines the statistical compatibility of the regression coefficient measured for the GCM models and those observed in the temperature. It is always measured a reduced $\chi^2 \gg 1$ for three degrees of freedom, which indicates that the statistical compatibility of the GCMs with the observed 60-year, 20-year temperature cycles plus the secular trending is less than 0.1%. These GCM regression values are depicted in Figure 4: the regression coefficients for each available GCM simulation are reported in the Supplement file. The χ^2 test in the first line refers to the compatibility of the proposed model in Eq. 3 relative to the ideal case of $a = b = c = 1$ that gives a reduced $\chi^2 = 0.21$ which imply that the statistical compatibility of Eq. 3 with the temperature cycles plus the secular trending is about 90%. The fit has been implemented using the nonlinear least-squares (NLLS)Marquardt-Levenberg algorithm.

#	model	s (10.44-year)	l (9.1-year)	χ^2 (abcsl)	RMS (^0C)
0	temperature	1.06 ± 0.16	0.99 ± 0.10	0.15	0.051
1	GISS ModelE	0.30 ± 0.11	0.40 ± 0.07	61	0.107
2	BCC CM1	0.53 ± 0.11	0.49 ± 0.07	70	0.105
3	BCCR BCM2.0	-0.11 ± 0.15	0.06 ± 0.09	137	0.158
4	CGCM3.1 (T47)	-0.47 ± 0.09	0.06 ± 0.06	479	0.212
5	CGCM3.1 (T63)	0.39 ± 0.15	-0.11 ± 0.09	337	0.220
6	CNRM CM3	0.22 ± 0.24	-0.07 ± 0.14	202	0.229
7	CSIRO MK3.0	-0.54 ± 0.14	-0.01 ± 0.09	128	0.169
8	CSIRO MK3.5	-0.53 ± 0.13	0.44 ± 0.08	134	0.156
9	GFDL CM2.0	-0.26 ± 0.16	0.62 ± 0.10	25	0.113
10	GFDL CM2.1	0.13 ± 0.23	0.98 ± 0.14	34	0.170
11	GISS AOM	0.19 ± 0.09	0.10 ± 0.05	73	0.101
12	GISS EH	0.27 ± 0.14	0.66 ± 0.09	30	0.106
13	GISS ER	0.29 ± 0.11	0.48 ± 0.07	25	0.094
14	FGOALS g1.0	-0.69 ± 0.29	0.23 ± 0.17	111	0.252
15	INVG ECHAM4	-0.35 ± 0.16	-0.23 ± 0.10	105	0.132
16	INM CM3.0	-0.15 ± 0.24	1.01 ± 0.14	36	0.150
17	IPSL CM4	0.49 ± 0.19	0.48 ± 0.11	68	0.137
18	MIROC3.2 Hires	0.17 ± 0.16	0.43 ± 0.09	69	0.122
19	MIROC3.2 Medres	0.24 ± 0.11	0.47 ± 0.07	69	0.106
20	ECHO G	0.52 ± 0.13	0.54 ± 0.08	20	0.097
21	ECHAM5/MPI-OM	0.15 ± 0.12	-0.09 ± 0.07	82	0.126
22	MRI CGCM 2.3.2	0.04 ± 0.10	0.25 ± 0.06	103	0.114
23	CCSM3.0	0.12 ± 0.13	0.91 ± 0.08	50	0.110
24	PCM	1.01 ± 0.16	0.70 ± 0.09	5	0.093
25	UKMO HADCM3	0.07 ± 0.15	-0.34 ± 0.09	49	0.123
26	UKMO HADGEM1	-0.46 ± 0.14	0.32 ± 0.08	30	0.107
	average	0.06 ± 0.40	0.34 ± 0.37	97.39	0.139

Table 2: Values of the regression parameters *s* and *l* of Eq. 8 obtained by fitting the 26 IPCC [2007] climate GCM ensemble-mean estimates. The fit has been implemented using the nonlinear least-squares (NLLS)Marquardt-Levenberg algorithm. Note that the two regression coefficients are quite different from the optimum values $s = l = 1$, as found for the temperature. The column referring to the reduced χ^2 test is based on all five regression coefficients (a, b, c, s and l) by extending Eq. 6. Again it is always observed a $\chi^2 \gg 1$, which indicates incompatibility between the GCM and the temperature patterns. The last column indicates the RMS residual values between the 4-year average smooth curves of each GCM simulation and the 4-year average smooth curve of the temperature: the value associated to the first raw (*temperature*) RMS=0.051 ^oC) refers to the RMS of the astronomical harmonic model that suggests that the latter is statistically 2-5 times more accurate than the GCM simulations in reconstructing the temperature record.

Testing an astronomically-based decadal-scale empirical harmonic climate model versus the IPCC (2007) general circulation climate models
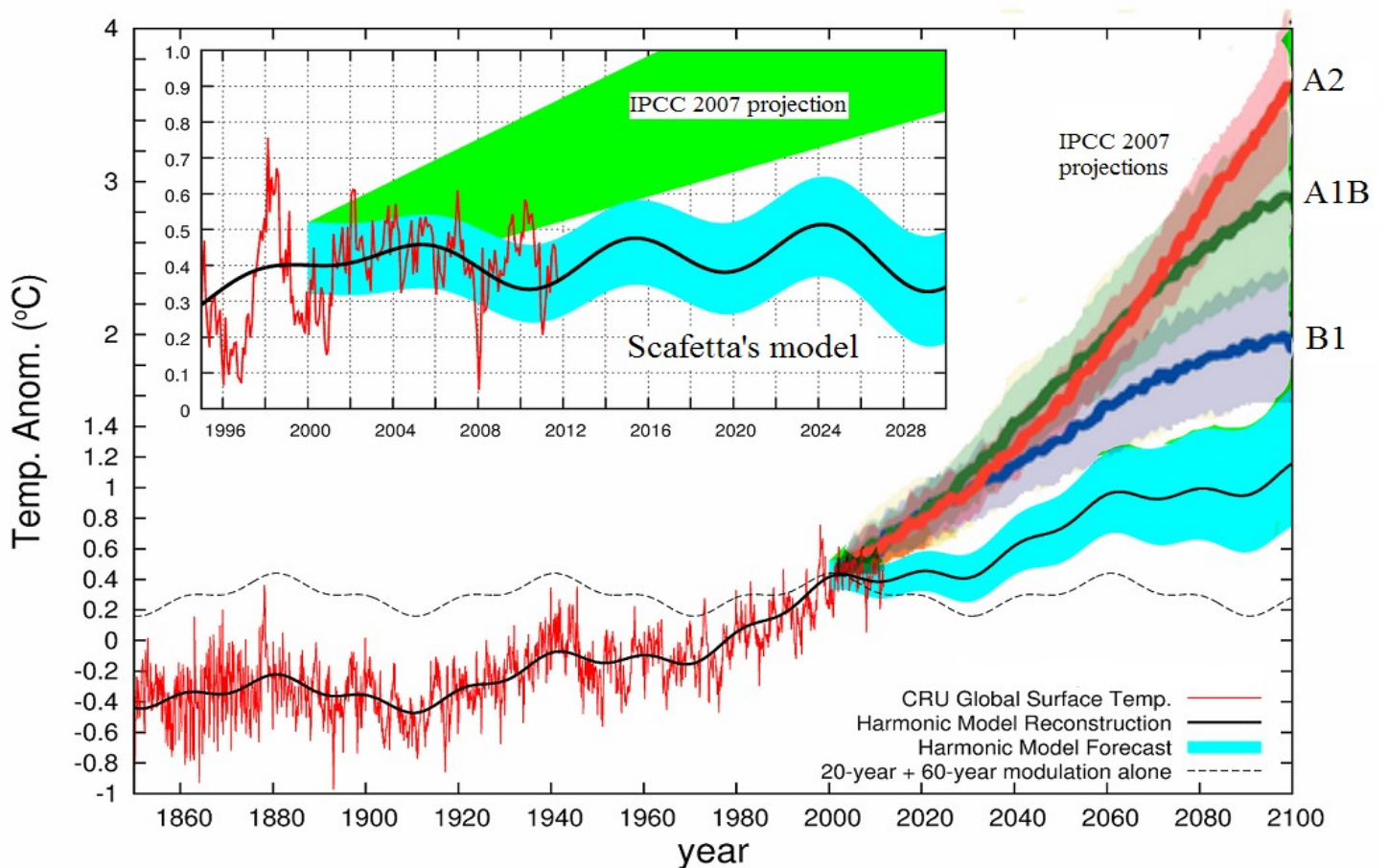
Nicola Scafetta

ACRIM (Active Cavity Radiometer Solar Irradiance Monitor Lab) & *Duke University, Durham, NC 27708, USA.*
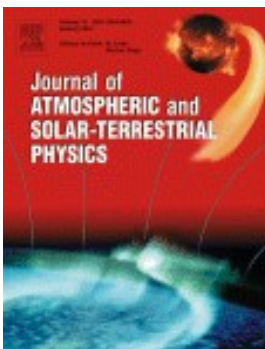
Supplement file for

"Testing an astronomically-based decadal-scale empirical harmonic climate model vs. the IPCC (2007) general circulation climate models"

Nicola Scafetta

Section 1: page 2.
Power spectrum comparison:HadCRUT3, GISSTEM/250, GHCN-Mv3

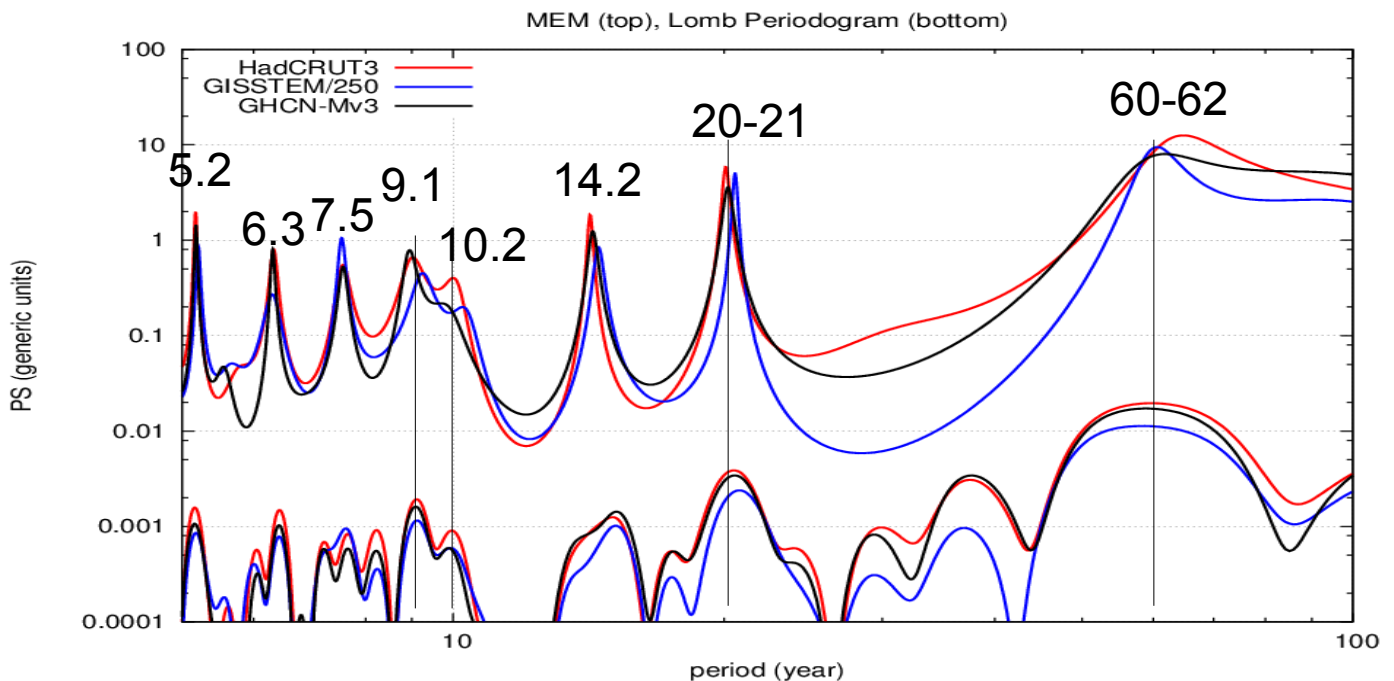Data from : http://climexp.knmi.nl/selectfield_obs.cgi?someone@somewhere

Figure S1. [A] The figure shows a comparison between the three available global surface temperature signals: HadCRUT3, GISSTEM with 250km smooth and NOAA GHCN-Mv3 since 1880. The power spectra records look similar. The detected frequency peaks match those found for the speed of the Sun relative to the solar system barycenter: look at Table 2 in Scafetta (2011b). [B] The power spectra are evaluated with the MEM with 790 poles (top) (see Section 3 for explanation) and with the Lomb periodogram (bottom). The power spectra look similar and present similar main peaks. These include the four peaks discussed in the text, as shown in the figure. The 20 and 60-year cycles are the major one, the decadal cycle is also large because made of two cycles. (The linear upward trending is detrended before the PS analysis)

Section 2: page 3-28
Testing the IPCC climate models

Here we analyze all available model output simulations relative to the global average surface temperature (tas) prepared for IPCC Fourth Assessment climate of the 20th Century experiment (20C3M), which use all known (natural plus anthropogenic) climatic forcings. The simulations obtained with 25 GCM models are collected by the Program for Climate Model Diagnosis and Intercomparison (PCMDI), the JSC/CLIVAR Working Group on Coupled Modelling (WGCM) and their Coupled Model Intercomparison Project (CMIP) and Climate Simulation Panel for organizing the model data analysis activity, and the IPCC WG1 TSU for technical support. All simulations can be downloaded from Climate Explorer at:

http://climexp.knmi.nl/selectfield_co2.cgi?

Documentations about the models can be found at:

http://www-pcmdi.llnl.gov/ipcc/model_documentation/ipcc_model_documentation.php

We fit the computer simulations with Eq. 5 in the main paper to find the relative amplitude factor "a", "b" and "c" of the 60 and 20-year cyclical modulations of the global surface temperature and of the upward trend, respectively, as reproduced by the computer simulation. A value of the regression factor close to 1 indicates that the model simulation well reproduces the correspondent pattern modulation of the temperature. The result of the analysis relative to 26 different computer model simulation is depicted in the tables and the regression coefficients for the mean model run are reported in Table 1 and in Figure 4 in the main paper.

Each figure depicts several curves vertically displaced for visual convenience: in red the global surface temperature (the green curve is Eq. 3 + Eq. 4 in the paper); in blue the mean of the individual runs of a given GCM (in the case only one run is available it would coincide with the mean); the curves below the blue curve correspond to the individual runs numbered as in the original files as #0, #1, #2 etc.

The tables below each figure report the regression coefficients "a", "b", "c" and "d" with the corresponding error. The last column of each table report the reduced χ^2 test, values close to 1 would indicate that the model well agrees with the 60-year cycle, 20-year cycle and upward trend observed in the temperature.

Note that the χ^2 values are always much larger than 1 and that the average values for the regression coefficients are "a = 0.30 +/- 0.22" and "b = 0.035 +/- 0.41", which indicates that the models do not reproduce the 60 and 20-year temperature cyclical modulation. In many cases a simple visual comparison suggests significant discrepancies between the global surface temperature patterns and the model output.
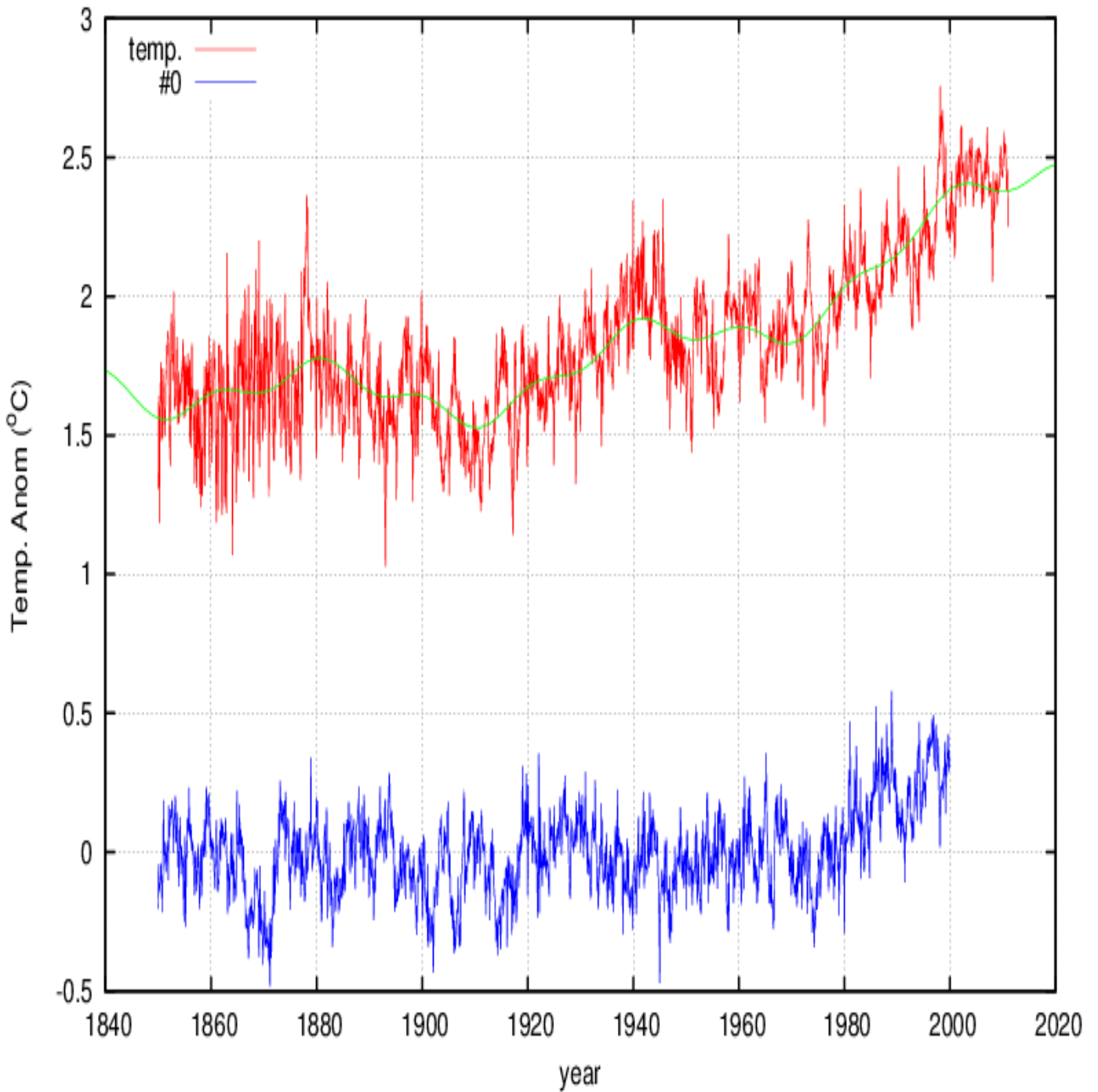
2) itas bcc cm1 20c3m
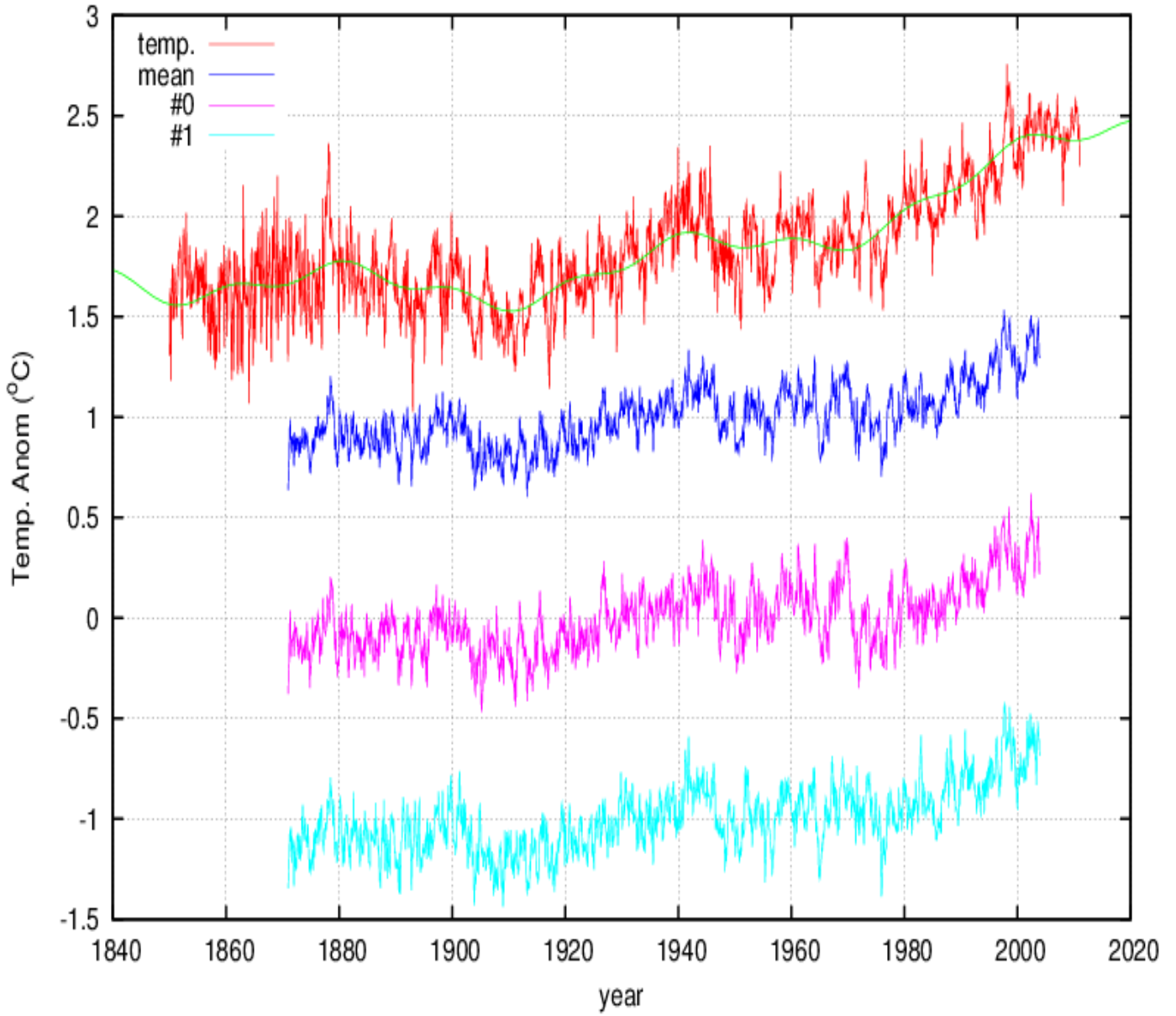
Institution: Beijing Climate Center, China

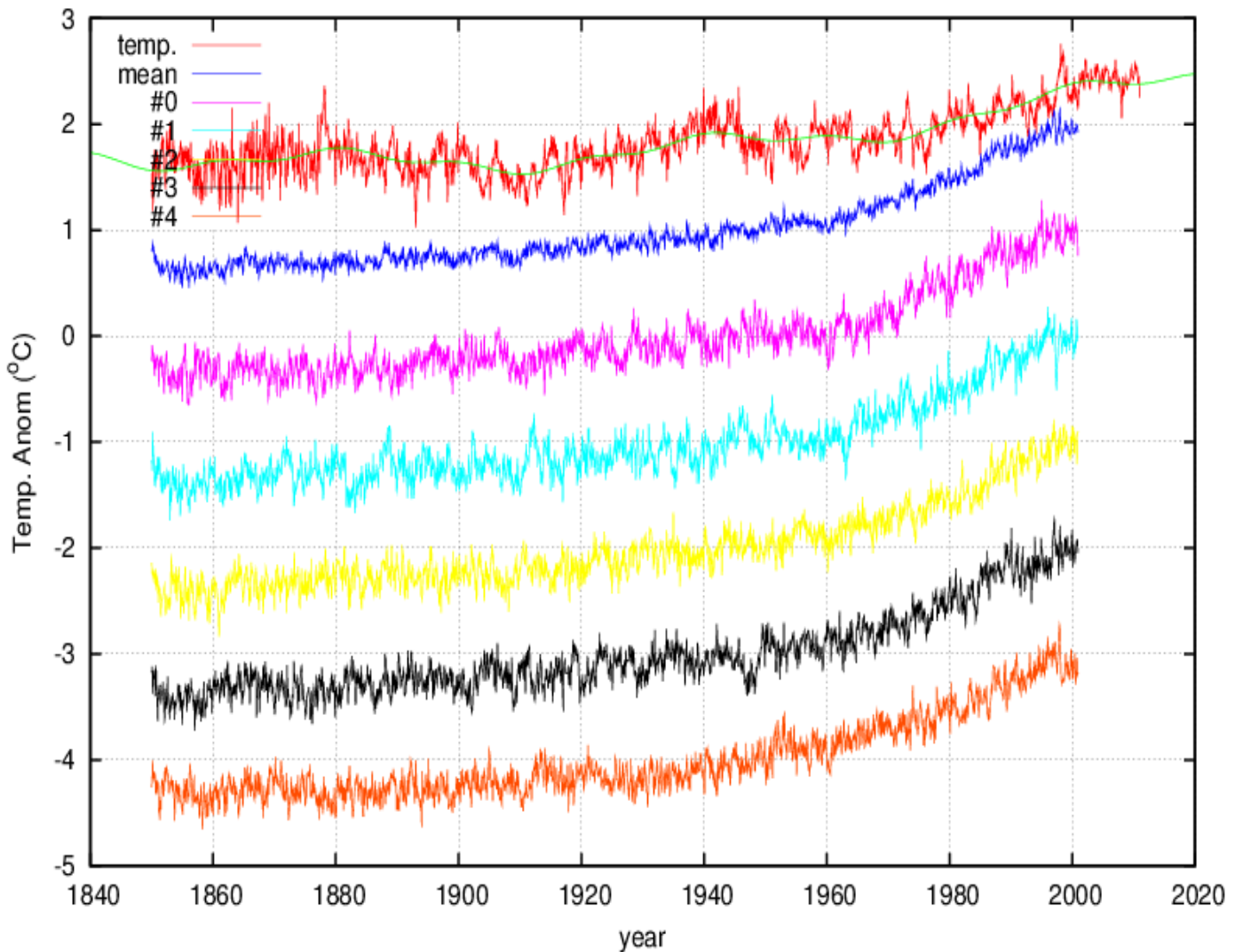| model	n.	a	err	b	err	c	err	d	err	X^2
BCC CM1	mean	0.63	0.03	0.69	0.09	0.54	0.02	0.08	0.004	109
BCC CM1	0	0.66	0.04	0.68	0.11	0.52	0.02	0.08	0.004	112
BCC CM1	1	0.59	0.04	0.70	0.10	0.55	0.02	0.09	0.004	105

3) itas bccr bcm2 0 20c3m

Institution: Bjerknes Center for Climate Research, Norway
Note that the simulation is practically flat until 1970.
The simulated decadal oscillations appear artificial and unrelated to the actual observation.

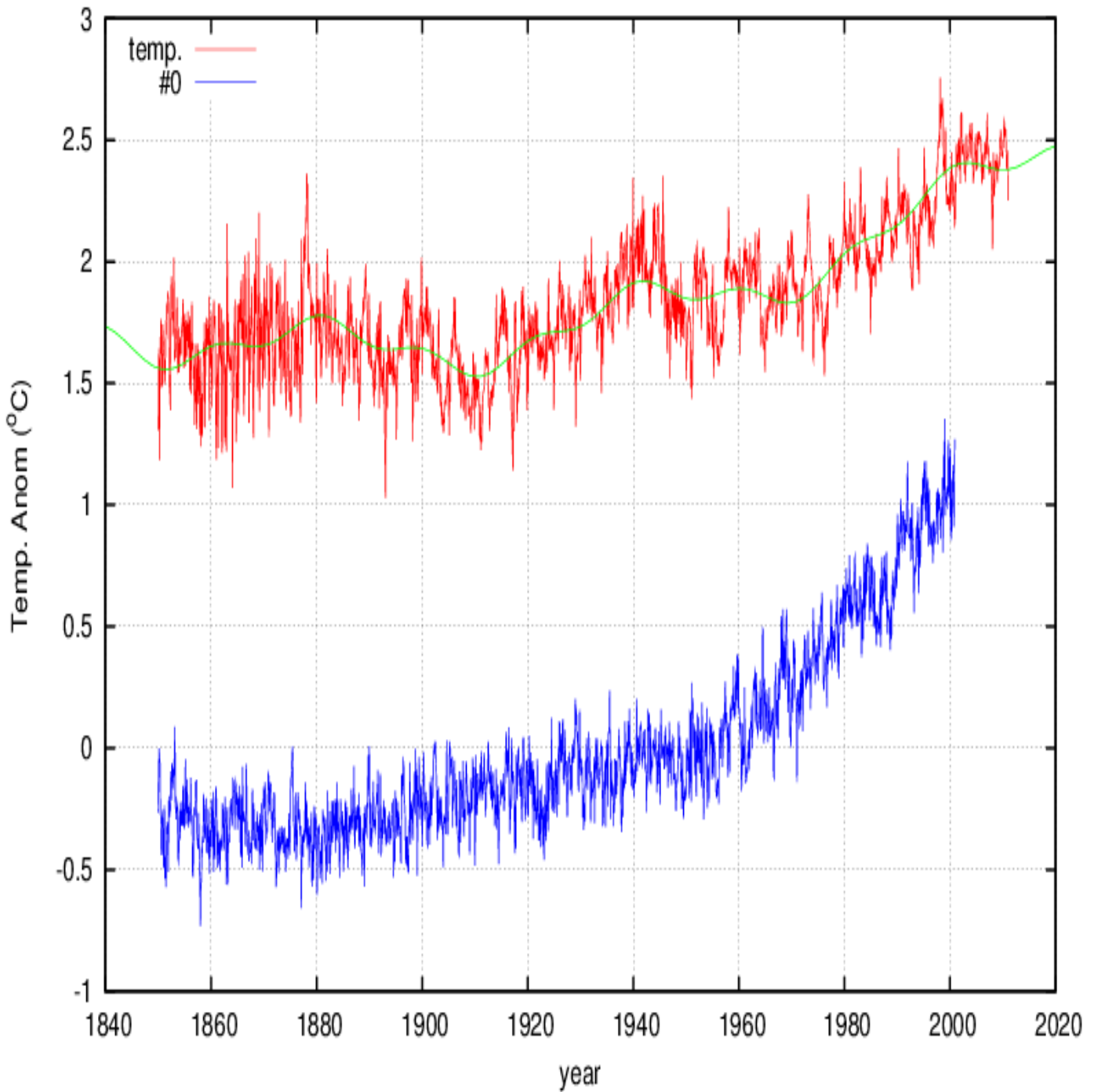| model	n.	a	err	b	err	c	err	d	err	X^2
BCCR BCM2.0	0	0.29	0.05	0.06	0.11	0.40	0.02	0.08	0.005	202

4) itas cccma cgcm3 1 20c3m

Institution: Canadian Centre for Climate Modelling & Analysis, Canada
Note that the simulations increase quite monotonically without any multidecadal dynamics.

| model	n.	a	err	b	err	c	err	d	err	X^2
CGCM3.1 (T47)	mean	0.35	0.03	-0.28	0.07	2.02	0.01	0.40	0.003	753
CGCM3.1 (T47)	0	0.33	0.05	0.16	0.12	2.00	0.02	0.40	0.005	449
CGCM3.1 (T47)	1	0.47	0.05	-0.85	0.12	2.00	0.02	0.40	0.005	468
CGCM3.1 (T47)	2	0.54	0.05	-0.22	0.12	2.00	0.02	0.40	0.005	441
CGCM3.1 (T47)	3	0.33	0.05	-0.05	0.12	2.00	0.02	0.40	0.005	454
CGCM3.1 (T47)	4	0.06	0.05	-0.45	0.12	1.97	0.02	0.39	0.005	471

5) cccma cgcm3 1 t63 20c3m

Institution: Canadian Centre for Climate Modelling & Analysis, Canada
Note that the simulations increase quite monotonically without any multidecadal dynamics.

| model	n.	a	err	b	err	c	err	d	err	X^2
CGCM3.1 (T63)	0	0.11	0.05	0.05	0.11	2.07	0.02	0.40	0.005	536

6) itas cnrm cm3 20c3m
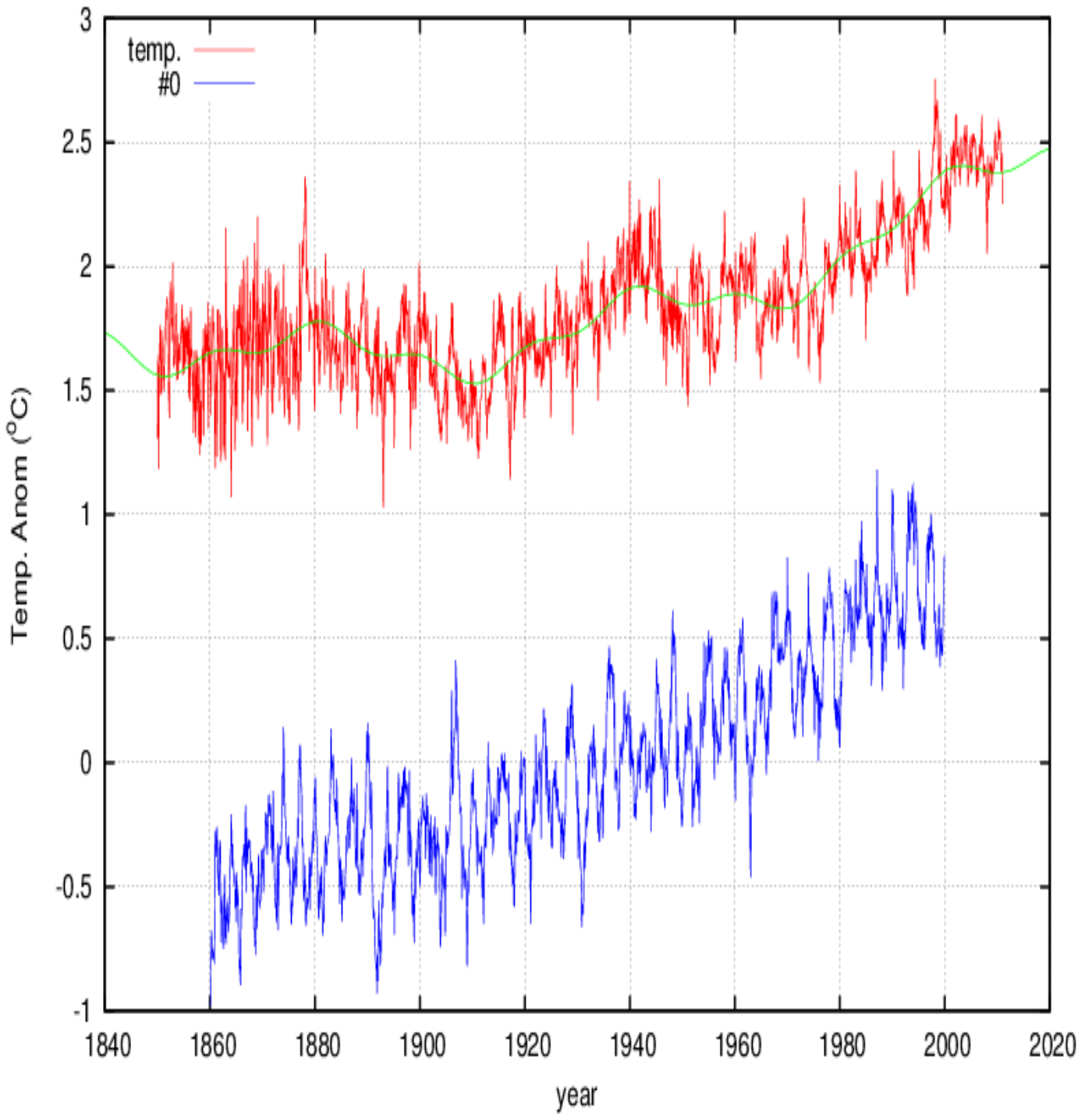
Institution: Météo-France / Centre National de Recherches Météorologiques, France
Note that the simulations increase quite monotonically without any multidecadal dynamics.
The large 3-5 year oscillations appear quite artificial and unrlated to the real ENSO oscillations.

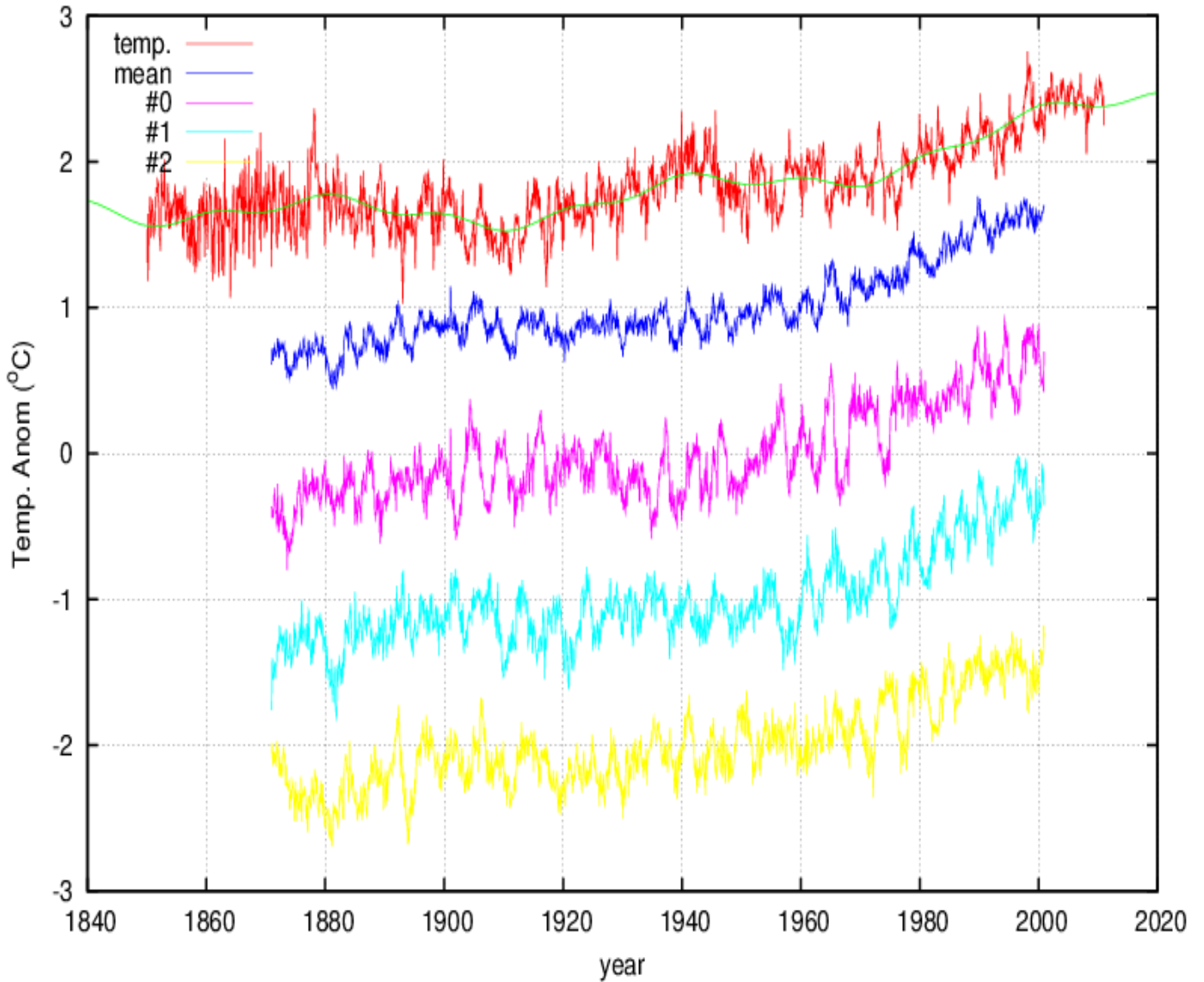| model	n.	a	err	b	err	c	err	d	err	X^2
CNRM CM3	0	-0.01	0.07	-0.27	0.18	2.02	0.03	0.39	0.008	322

7) itas csiro mk3 0 20c3m
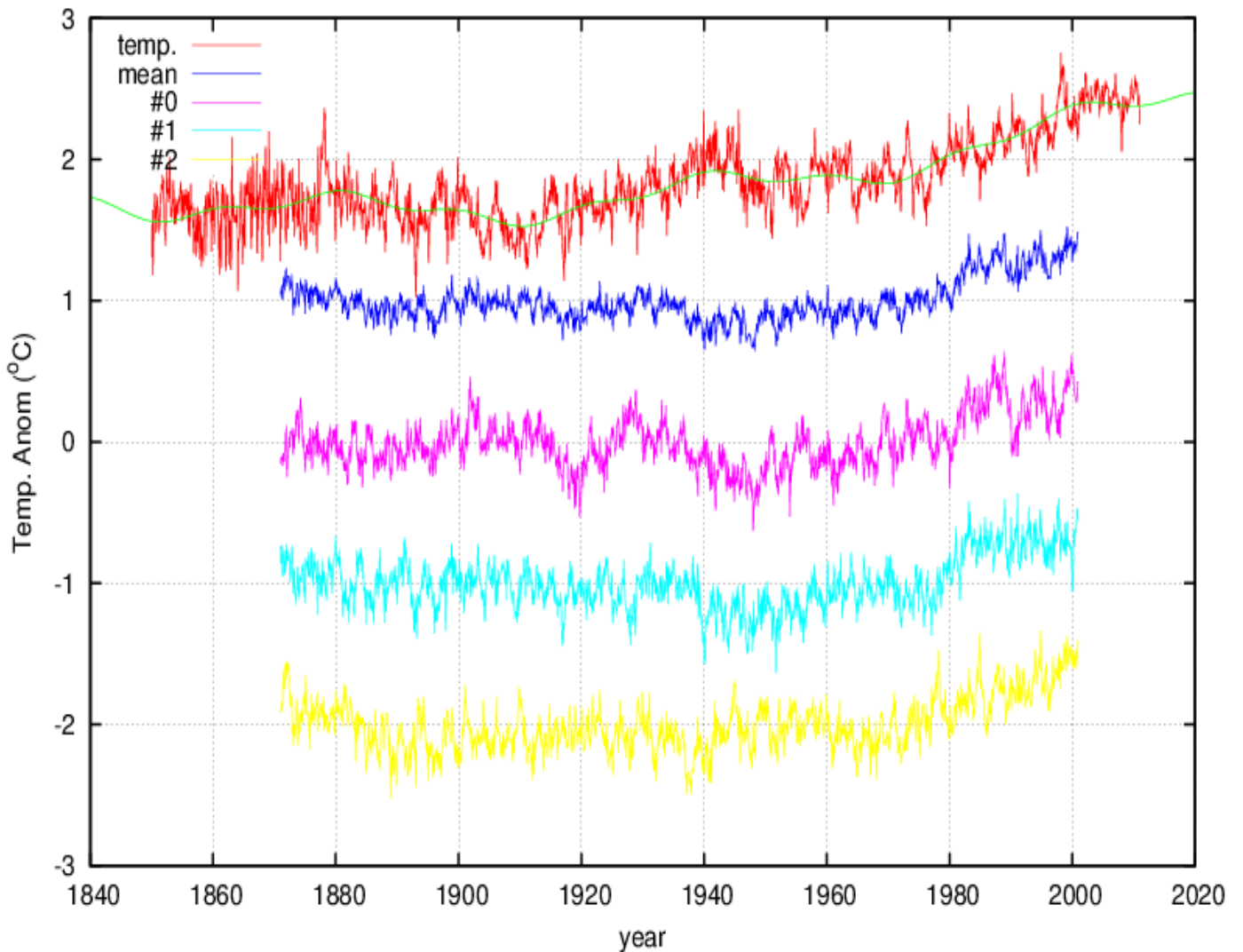
Institution: CSIRO Atmospheric Research, Australia
Note that the simulations increase quite monotonically without any multidecadal dynamics.
The simulations present large multi-decadal oscillations unrelated to the real observations

| model	n.	a	err	b	err	c	err	d	err	X^2
CSIRO MK3.0	mean	0.30	0.04	-0.12	0.11	0.48	0.02	0.08	0.004	176
CSIRO MK3.0	0	0.06	0.06	-0.68	0.15	0.46	0.02	0.08	0.006	203
CSIRO MK3.0	1	0.27	0.06	-0.02	0.15	0.42	0.02	0.07	0.006	186
CSIRO MK3.0	2	0.58	0.05	0.33	0.14	0.57	0.02	0.10	0.005	98

8) itas csiro mk3 5 20c3m

Institution: CSIRO Atmospheric Research, Australia
Note that the simulations increase quite monotonically without any multidecadal dynamics.
The large 3-5 year oscillations appear quite artificial and unrlated to the real ENSO oscillations.

| model	n.	a	err	b	err	c	err	d	err	X^2
CSIRO MK3.5	mean	-0.19	0.04	-0.19	0.10	1.38	0.02	0.25	0.004	197
CSIRO MK3.5	0	-0.51	0.06	0.47	0.16	1.40	0.02	0.26	0.006	195
CSIRO MK3.5	1	0.12	0.06	-0.37	0.16	1.42	0.02	0.25	0.006	131
CSIRO MK3.5	2	-0.18	0.06	-0.69	0.14	1.30	0.02	0.23	0.006	143

9) itas gfdl cm2 0 20c3m
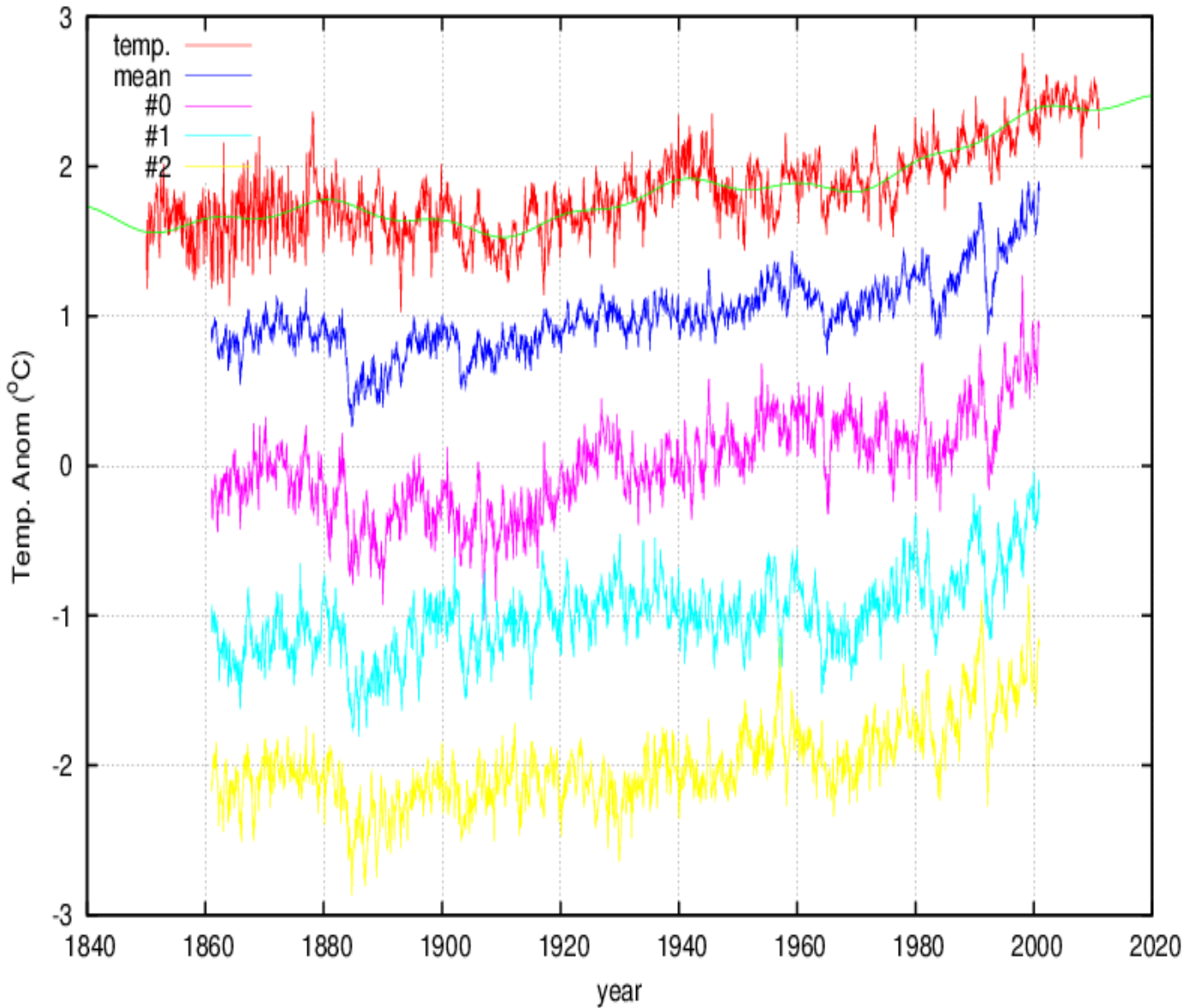
Institution: US Dept. of Commerce / NOAA / Geophysical Fluid Dynamics Laboratory, USA
Note that the simulations present a multidecadal dynamics not related to the observation.
There are very large volcano cooling spikes and signatures not observed in the temperature data.

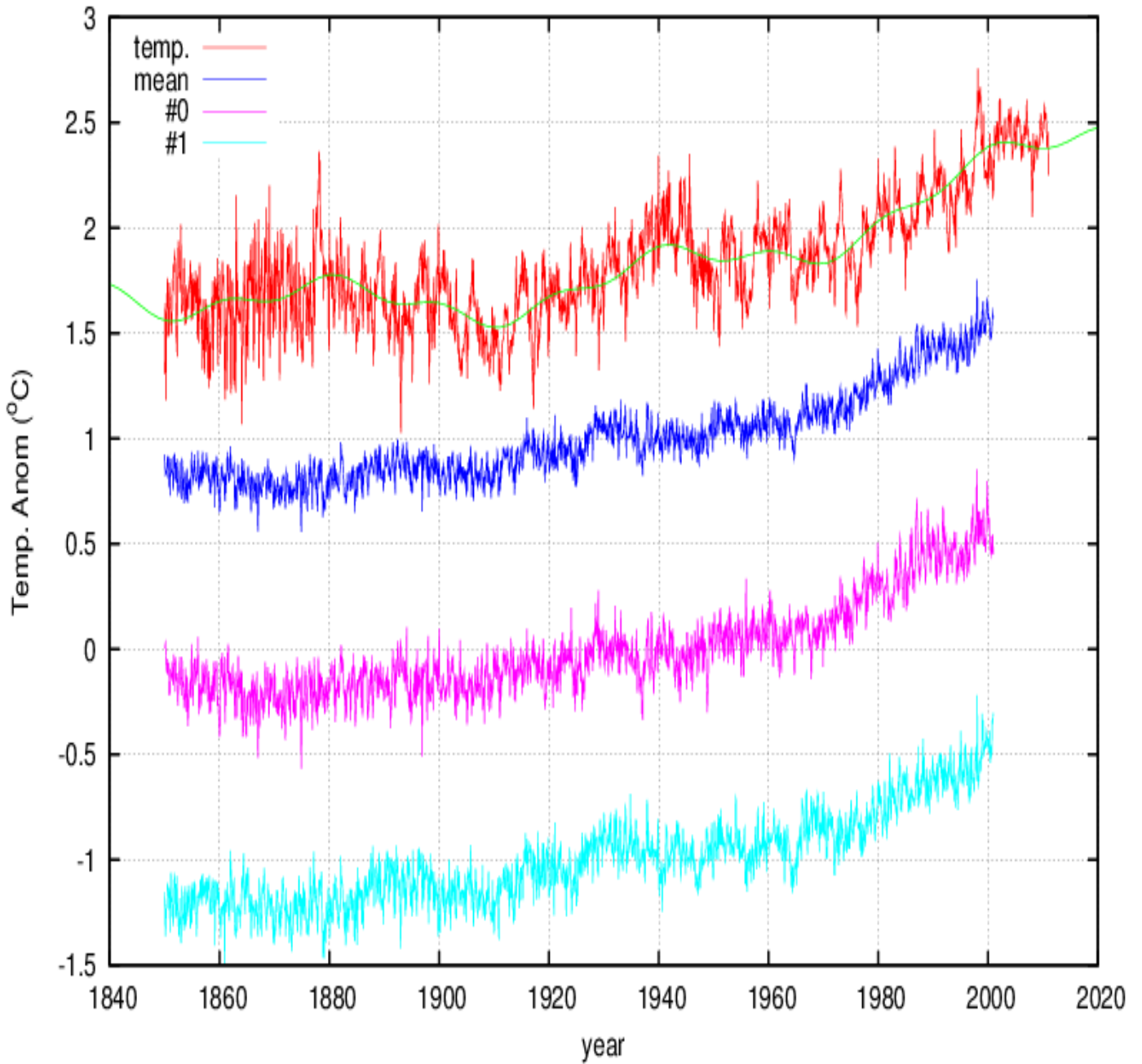| model	n.	a	err	b	err	c	err	d	err	X^2
GFDL CM2.0	mean	0.44	0.05	0.90	0.12	1.12	0.02	0.21	0.005	28
GFDL CM2.0	0	0.70	0.07	0.38	0.18	1.30	0.03	0.24	0.007	29
GFDL CM2.0	1	0.38	0.07	1.53	0.18	0.91	0.03	0.17	0.007	24
GFDL CM2.0	2	0.24	0.06	0.79	0.16	1.16	0.02	0.22	0.006	44

10) itas gfdl cm2 1 20c3m
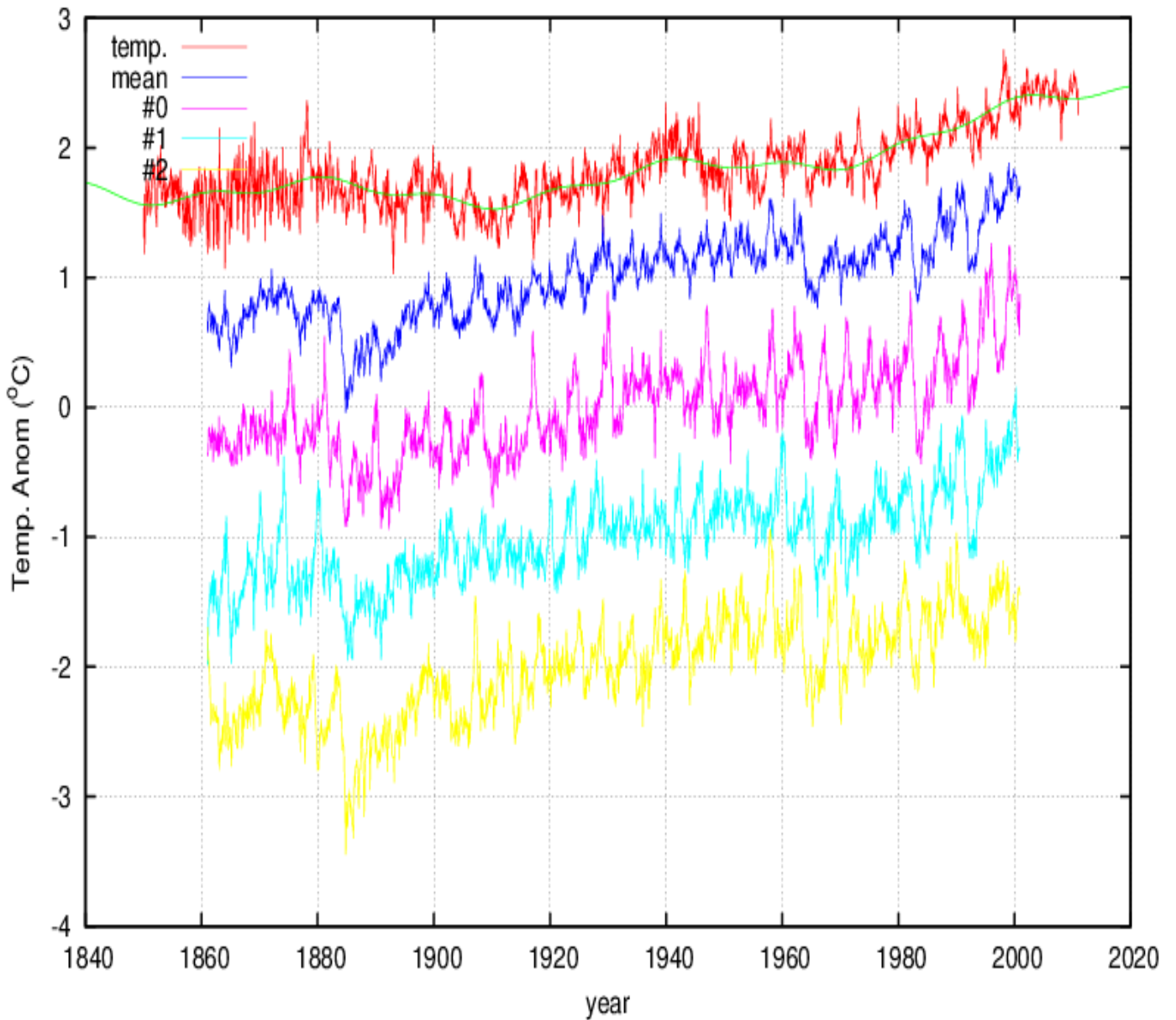
Institution: US Dept. of Commerce / NOAA / Geophysical Fluid Dynamics Laboratory, USA
Note that the simulations present a large 3-5 year oscillations and multidecadal dynamics not related to the observation. There are very large volcano cooling spikes and signatures not observed in the temperature data.

| model	n.	a	err	b	err	c	err	d	err	X^2
GFDL CM2.1	mean	0.37	0.07	0.75	0.17	1.37	0.03	0.26	0.007	53
GFDL CM2.1	0	0.77	0.09	1.19	0.22	1.38	0.03	0.26	0.009	37
GFDL CM2.1	1	0.43	0.09	0.52	0.21	1.29	0.03	0.24	0.009	33
GFDL CM2.1	2	-0.10	0.10	0.53	0.25	1.45	0.04	0.28	0.010	67

11) itas giss aom 20c3m

Institution: NASA / Goddard Institute for Space Studies, USA

Note that the simulations increase quite monotonically without any multidecadal dynamics.

| model	n.	a	err	b	err	c	err	d	err	X^2
GISS AOM	mean	0.22	0.03	-0.14	0.06	1.10	0.01	0.22	0.003	93
GISS AOM	0	0.14	0.03	-0.10	0.08	1.15	0.01	0.23	0.003	110
GISS AOM	1	0.30	0.03	-0.18	0.09	1.05	0.01	0.21	0.004	74

12) itas giss model e h 20c3m
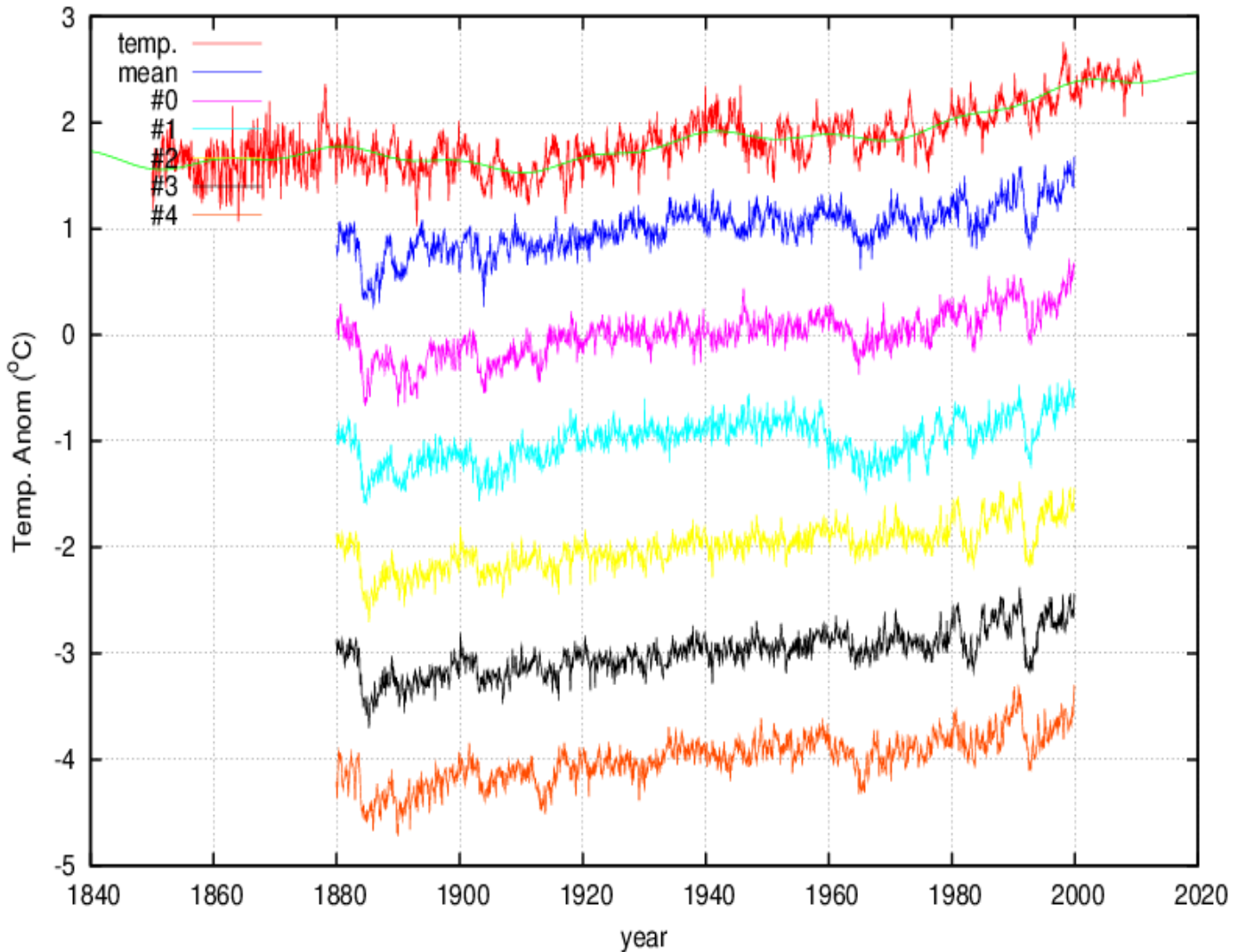
Institution: NASA / Goddard Institute for Space Studies, USA

Note that the simulations increase monotonically with a dynamics not related to the observation. There are very large volcano cooling spikes and signatures not observed in the temperature data.

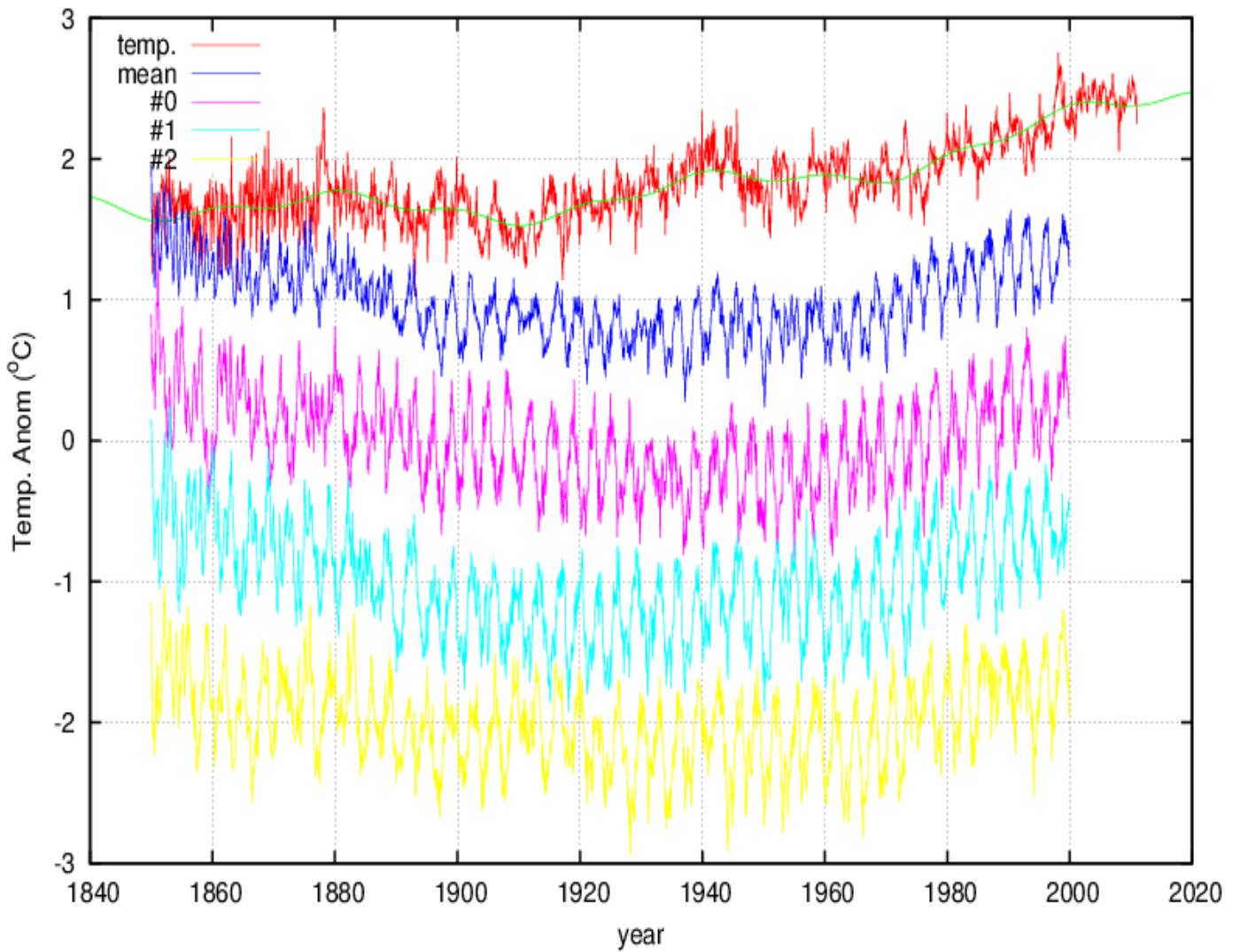| model	n.	a	err	b	err	c	err	d	err	X^2
GISS EH	mean	0.48	0.04	0.96	0.11	0.80	0.02	0.14	0.004	43
GISS EH	0	0.52	0.05	1.19	0.13	0.84	0.02	0.14	0.005	30
GISS EH	1	1.02	0.06	0.99	0.15	0.57	0.02	0.10	0.006	81
GISS EH	2	0.16	0.05	0.96	0.12	0.84	0.02	0.14	0.005	63
GISS EH	3	0.24	0.06	1.01	0.14	0.90	0.02	0.15	0.005	39
GISS EH	4	0.44	0.06	0.65	0.14	0.83	0.02	0.14	0.005	34

13) itas giss model e r 20c3m
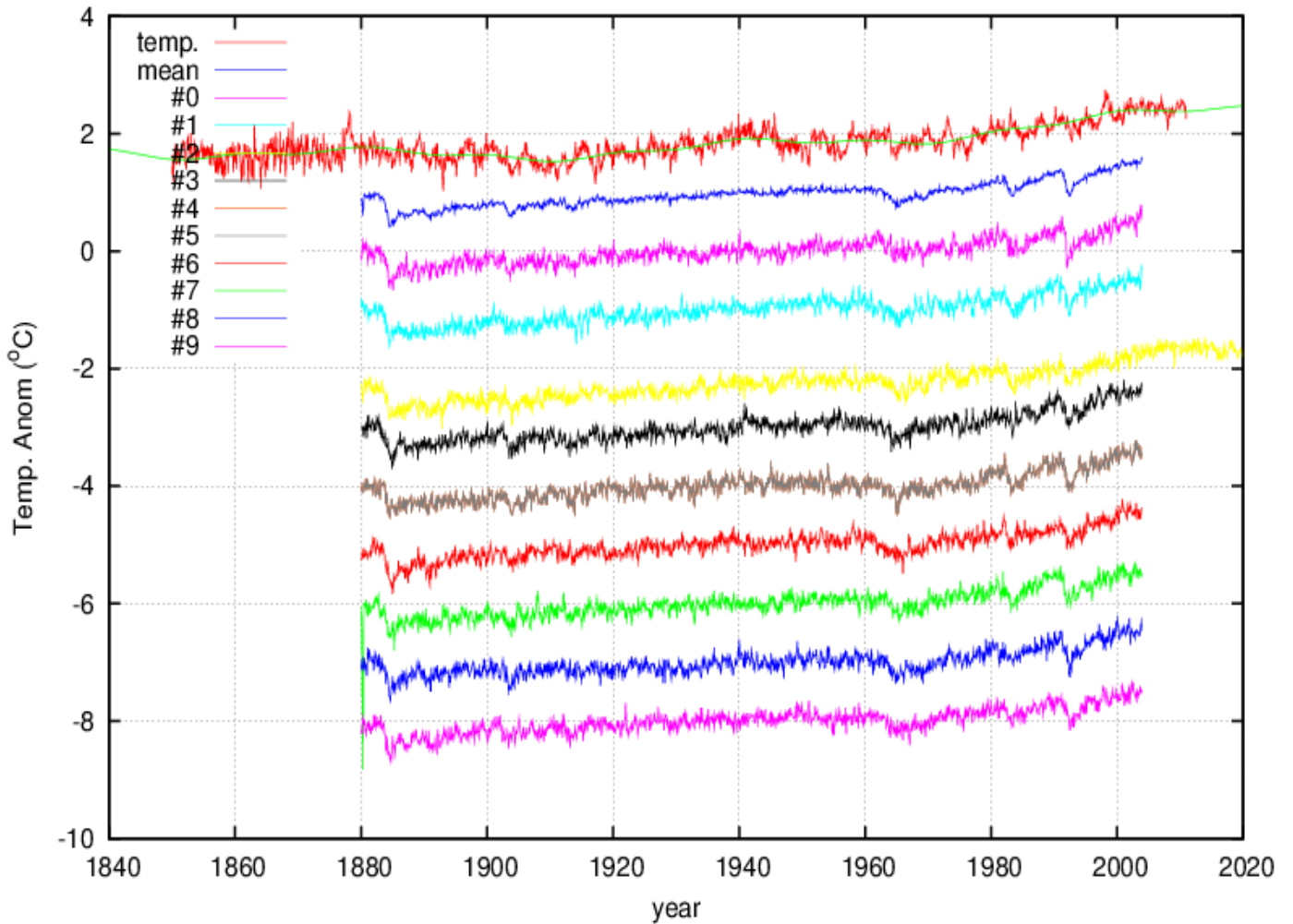
Institution: NASA / Goddard Institute for Space Studies, USA

Note that the simulations increase monotonically with a dynamics not related to the observation. There are very large volcano cooling spikes and signatures not observed in the temperature data.

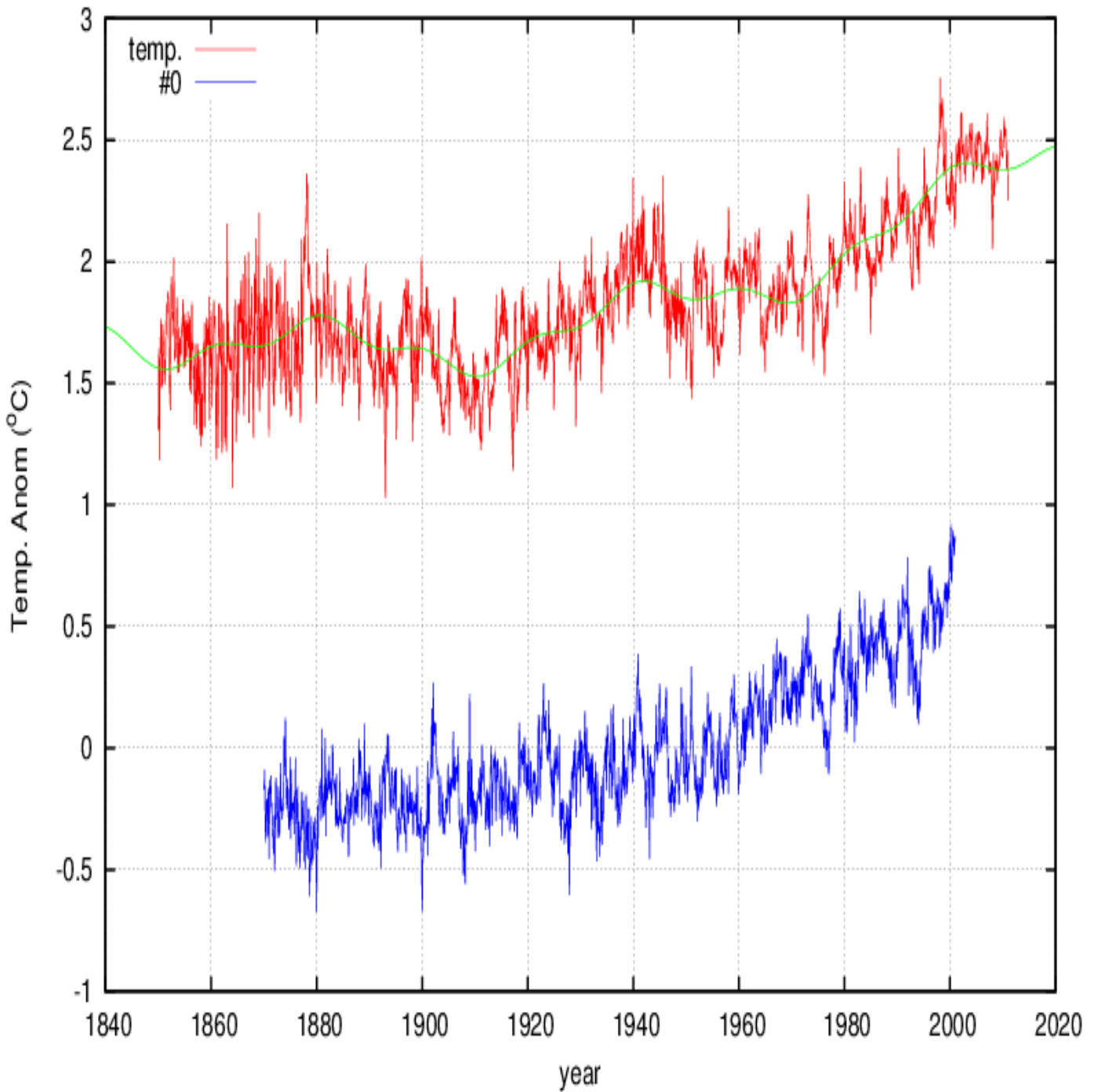| model	n.	a	err	b	err	c	err	d	err	X^2
GISS ER	mean	0.47	0.04	0.80	0.08	0.90	0.02	0.11	0.004	31
GISS ER	0	0.23	0.05	1.22	0.12	0.84	0.02	0.13	0.004	57
GISS ER	1	0.54	0.05	0.69	0.12	0.95	0.02	0.15	0.004	19
GISS ER	2	0.40	0.05	0.21	0.12	0.52	0.01	-0.18	0.004	222
GISS ER	3	0.73	0.05	0.87	0.11	0.99	0.02	0.15	0.004	6
GISS ER	4	0.76	0.05	0.78	0.12	0.88	0.02	0.13	0.004	12
GISS ER	5	0.37	0.05	0.81	0.13	0.89	0.02	0.14	0.005	35
GISS ER	6	0.30	0.06	0.16	0.14	0.99	0.02	0.15	0.005	36
GISS ER	7	0.57	0.05	0.97	0.11	0.80	0.02	0.12	0.004	32
GISS ER	8	0.36	0.05	0.83	0.12	0.82	0.02	0.12	0.004	45

14) itas iap fgoals1 0 g 20c3m

Institution: LASG / Institute of Atmospheric Physics, China

The simulations do not appear to have any similarity with the data at all time scales.

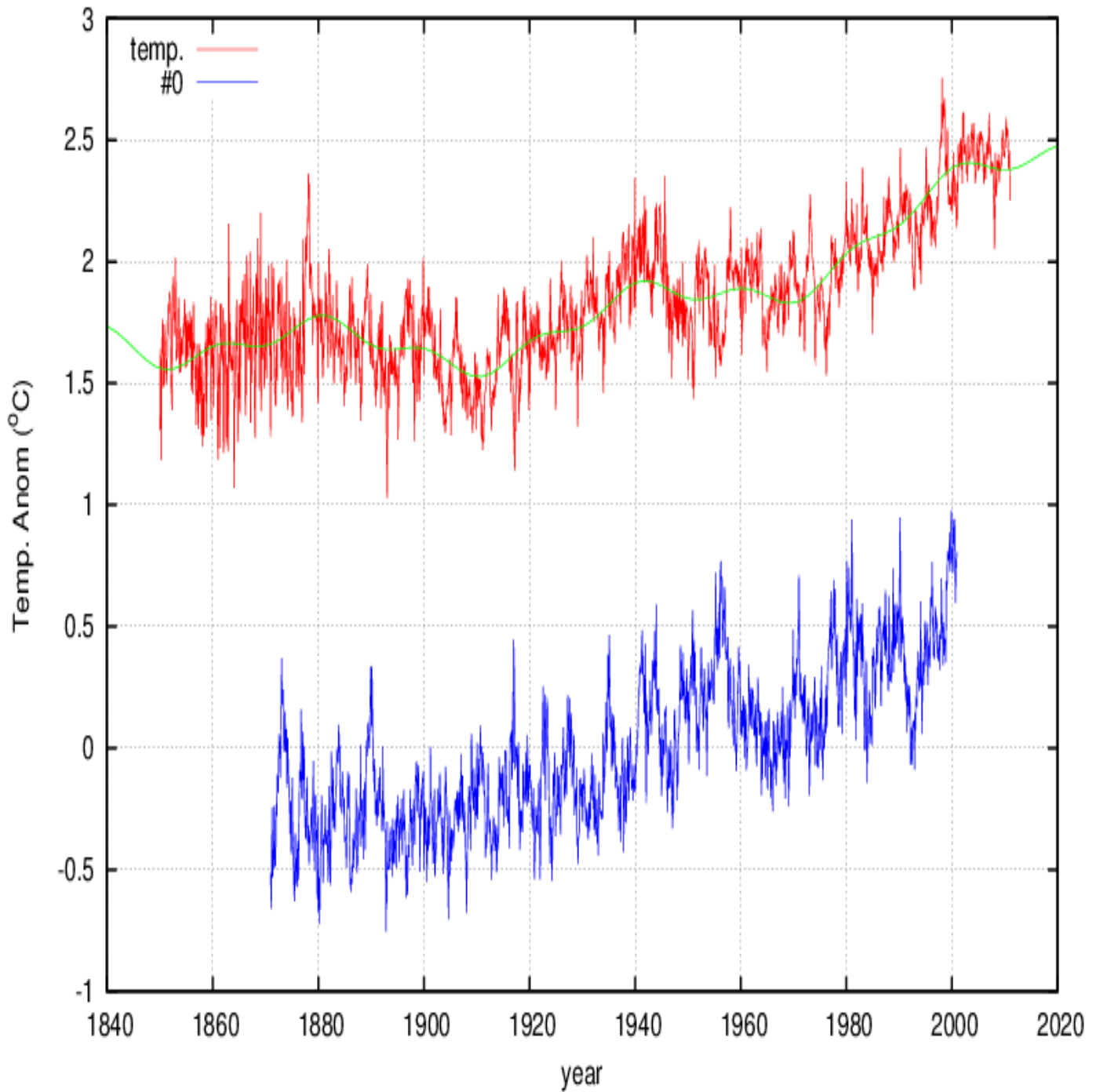| model	n.	a	err	b	err	c	err	d	err	X^2
FGOALS g1.0	mean	0.10	0.09	-0.15	0.21	0.28	0.03	0.06	0.009	171
FGOALS g1.0	0	-0.07	0.11	-0.51	0.27	0.14	0.04	0.03	0.012	162
FGOALS g1.0	1	0.29	0.12	-0.02	0.30	0.40	0.05	0.08	0.013	57
FGOALS g1.0	2	0.08	0.10	0.09	0.26	0.29	0.04	0.06	0.011	114

15) itas ingv echam4 20c3m

Institution: Instituto Nazionale di Geofisica e Vulcanologia, Italy
Note that the simulation increases quite monotonically without any multidecadal dynamics.

model	n.	a	err	b	err	c	err	d	err	X^2
INVG ECHAM4	0	-0.12	0.05	0.37	0.12	1.34	0.02	0.24	0.005	138

16) itas inmcm3 0 20c3m (#0)

Institution: Institute for Numerical Mathematics, Russia
Note that the simulation increases quite monotonically with a decadal and multidecadal dynamics quite unrelated to the observations.

| model	n.	a	err	b	err	c	err	d	err	X^2
INM CM3.0	0	0.30	0.07	0.47	0.18	1.34	0.03	0.24	0.007	54

17) itas ipsl cm4 20c3m
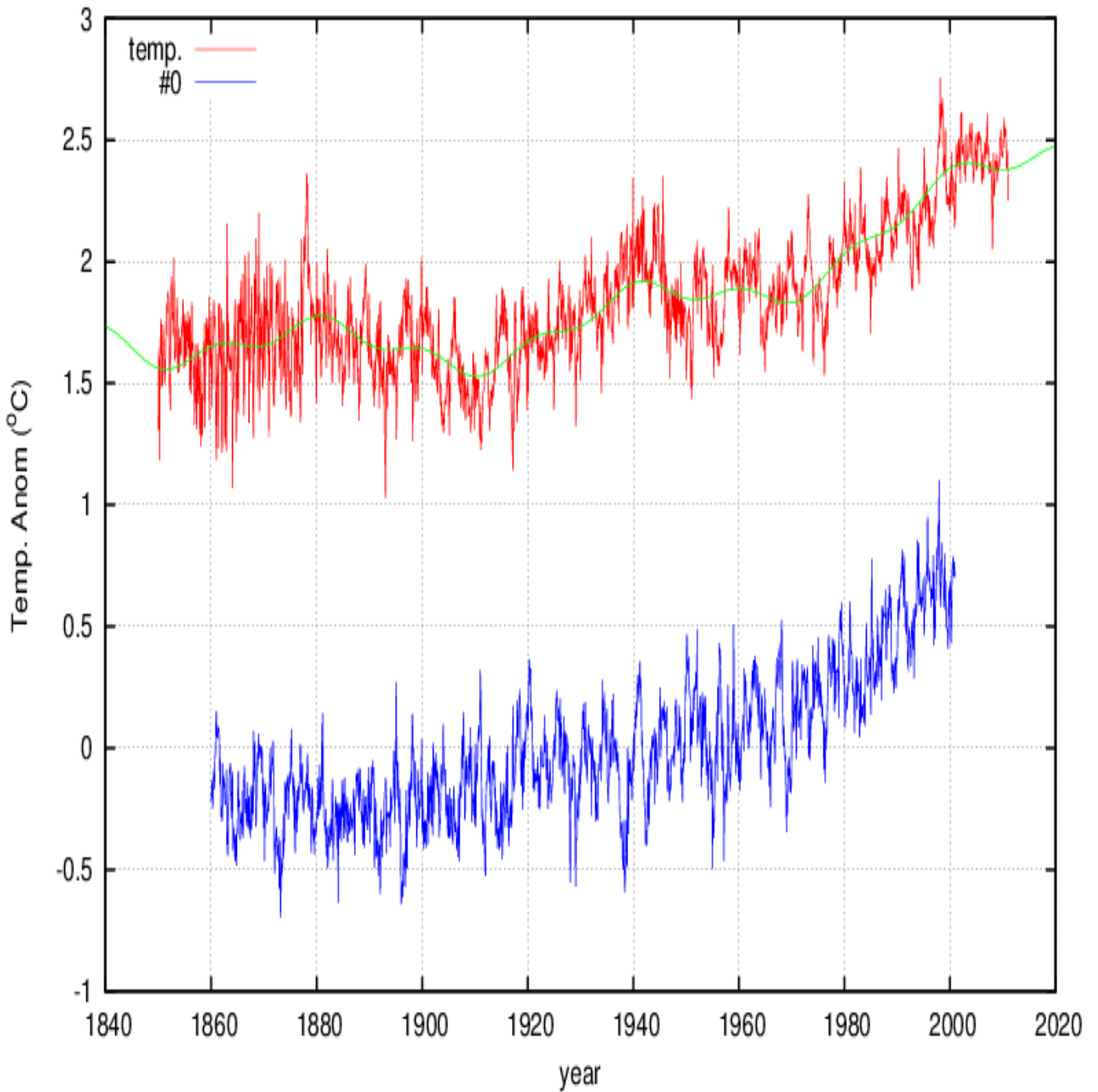
Institution: Institute Simon-Pierre LaPlace, France
Note that the simulation increases quite monotonically with a fluctuating dynamics quite unrelated to the observations.

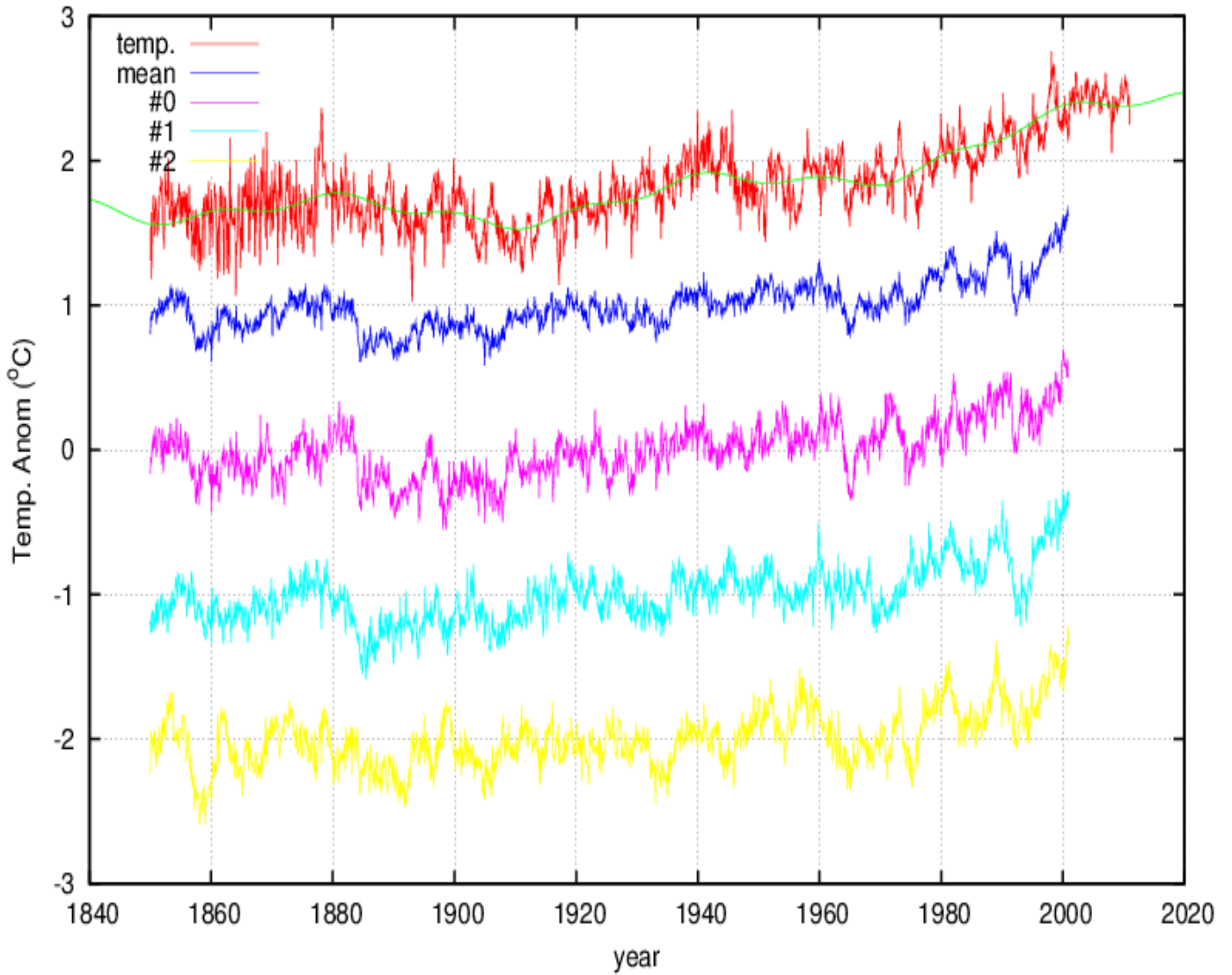| model	n.	a	err	b	err	c	err	d	err	X^2
IPSL CM4	0	0.13	0.06	0.05	0.14	1.37	0.02	0.26	0.006	107

18) itas miroc3 2 hires 20c3m
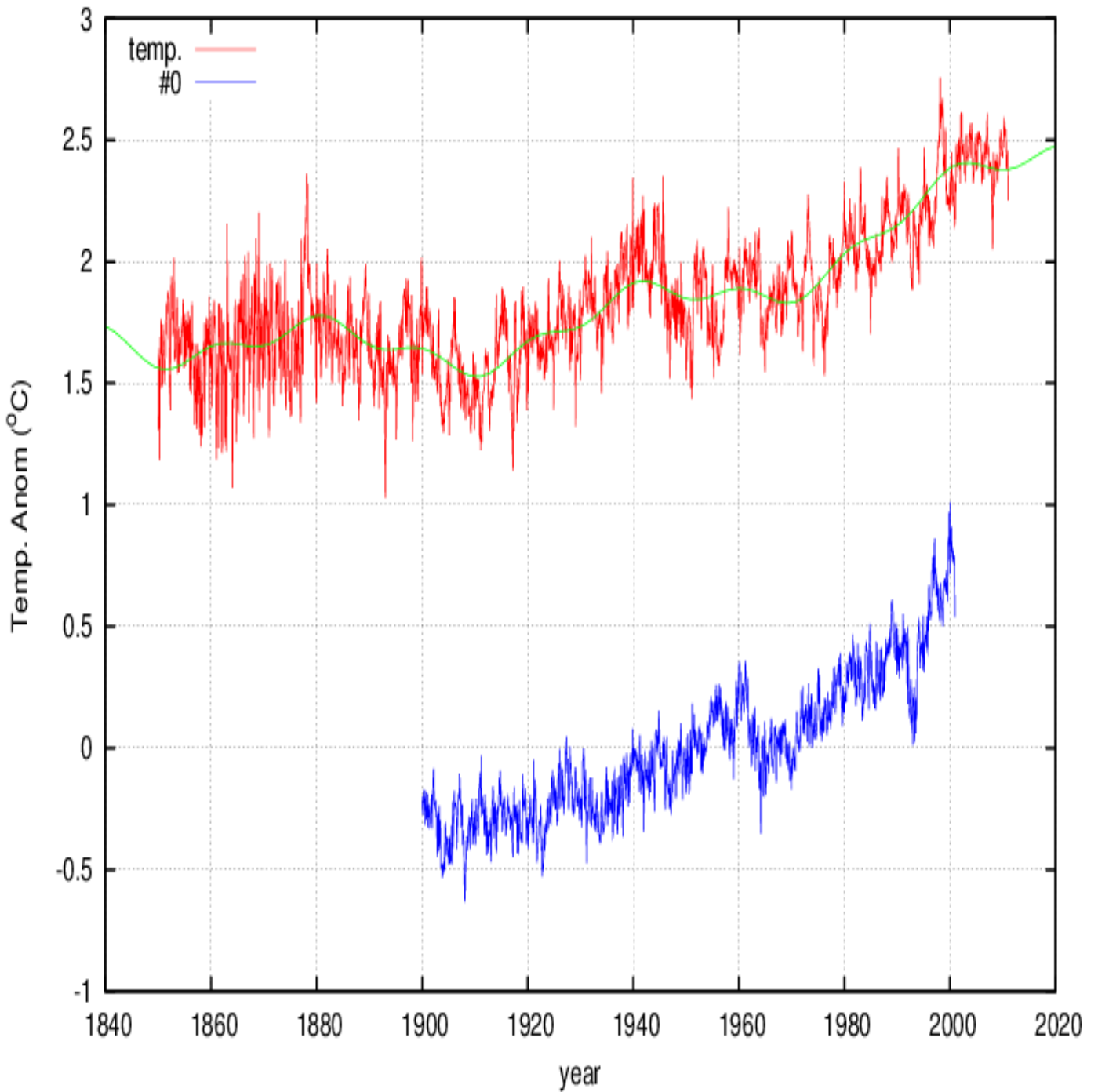
Institution: Center for Climate System Research (The University of Tokyo), Japan
Note that the simulation increases quite monotonically with a fluctuating dynamics quite
unrelated to the observations and large volcano cooling spikes not observed in the temperature.

| model	n.	a	err	b	err	c	err	d	err	X^2
MIROC3. 2 Hires	0	0.35	0.05	0.92	0.12	1.43	0.02	0.19	0.004	104

19) itas miroc3 2 medres 20c3m

Institution: Center for Climate System Research (The University of Tokyo), Japan
Note that the simulations present a decadal and multidecadal dynamics quite unrelated to the observations and some large volcano cooling spikes not observed in the temperature.

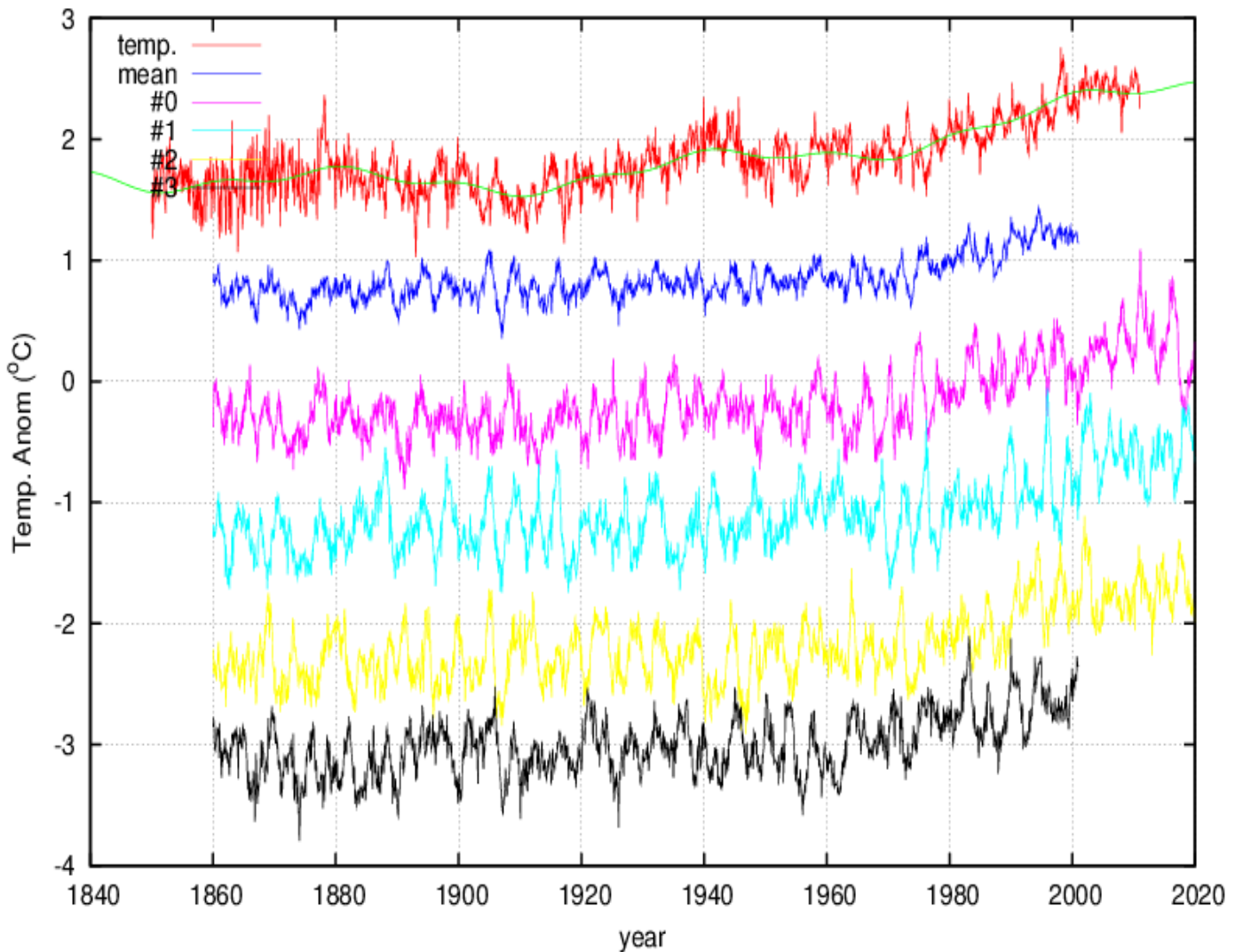| model	n.	a	err	b	err	c	err	d	err	X^2
MIROC3.2 Medres	mean	0.34	0.03	0.76	0.09	0.72	0.01	0.14	0.004	104
MIROC3.2 Medres	0	0.44	0.05	0.49	0.11	0.77	0.02	0.15	0.005	50
MIROC3.2 Medres	1	0.30	0.05	1.40	0.11	0.75	0.02	0.15	0.005	69
MIROC3.2 Medres	2	0.29	0.05	0.40	0.13	0.65	0.02	0.13	0.006	94

20) itas miub echo g 20c3m
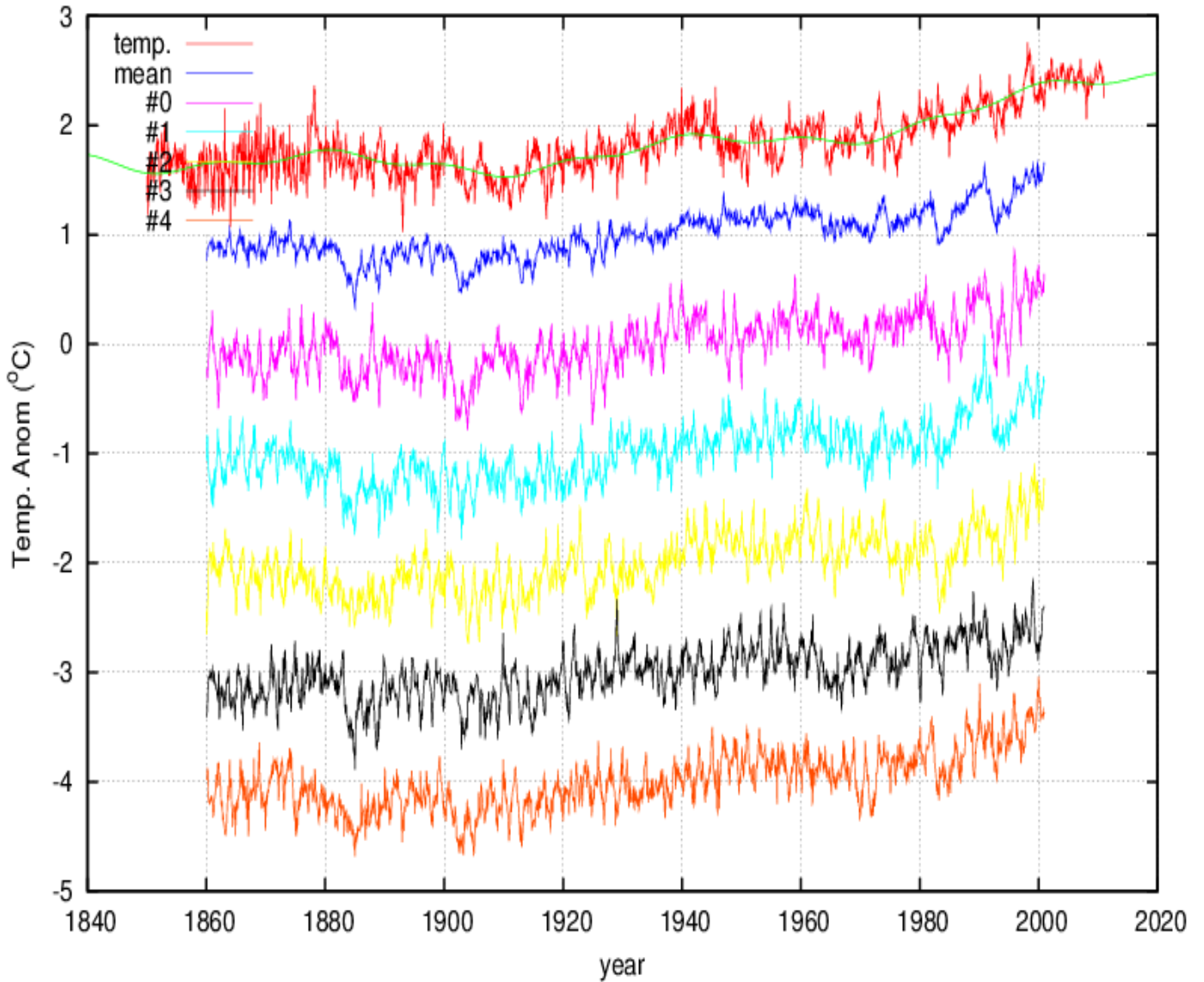
Institution: Meteorological Institute of the University of Bonn, Meteorological Research Institute of KMA, and Model and Data group, Germany / Korea

Note that the simulations present 2-3 year large oscillations, a decadal and multidecadal dynamics and some large volcano spikes unrelated to the observations

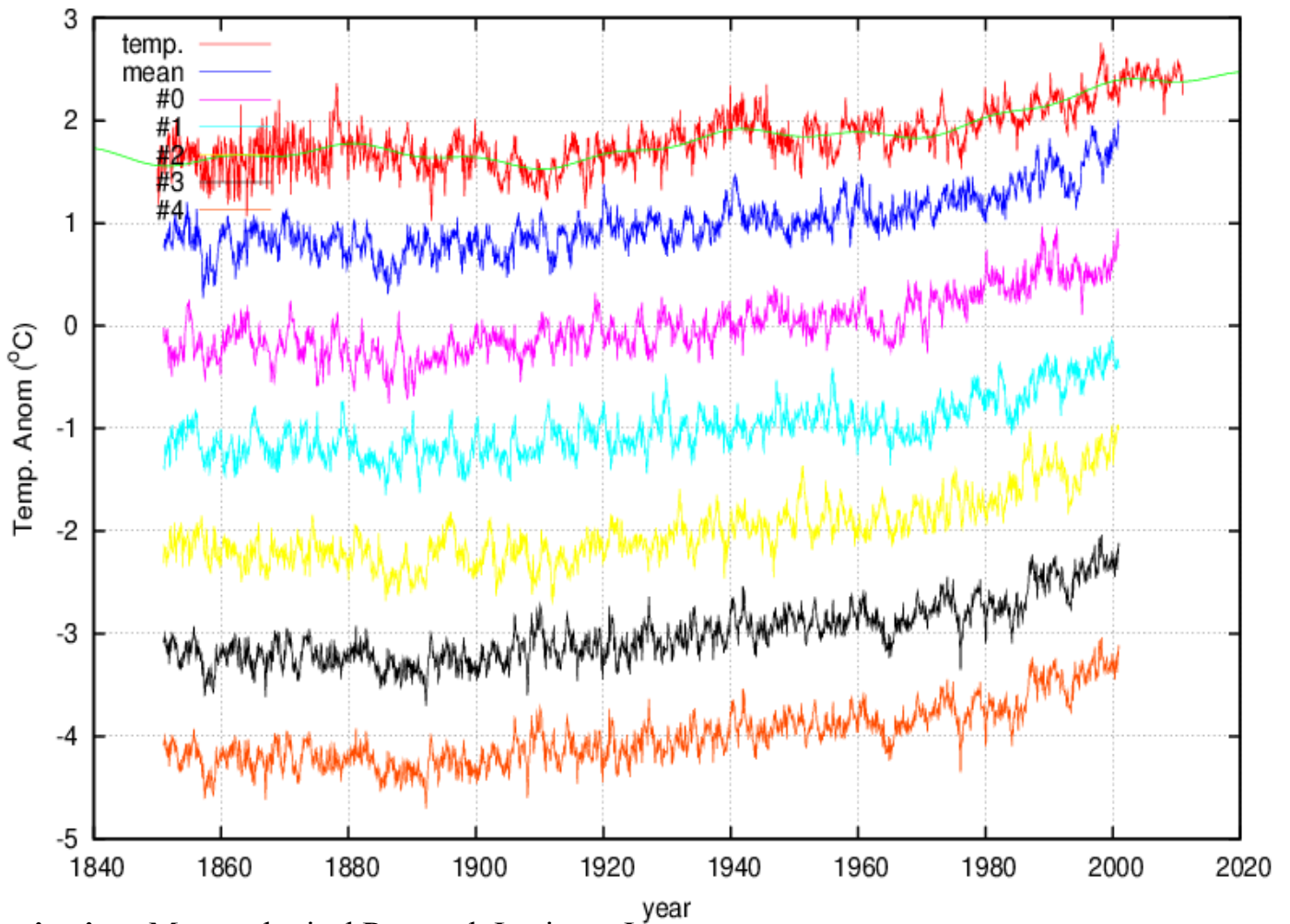| model	n.	a	err	b	err	c	err	d	err	X^2
ECHO G	mean	0.58	0.04	0.16	0.10	0.98	0.02	0.18	0.004	26
ECHO G	0	0.66	0.07	0.87	0.16	0.94	0.03	0.18	0.006	8
ECHO G	1	0.68	0.06	-0.63	0.16	1.07	0.03	0.20	0.006	29
ECHO G	2	0.42	0.07	0.57	0.17	0.96	0.03	0.18	0.007	19
ECHO G	3	0.51	0.06	0.21	0.15	0.89	0.03	0.17	0.006	24
ECHO G	4	0.64	0.06	-0.23	0.15	1.06	0.03	0.20	0.006	22

21) itas mpi echam5 20c3m

Institution: Max Planck Institute for Meteorology, Germany
Note that the simulations are almost flat until 1970. There are large 3-5 year oscillations that appear quite different from the ENSO oscillations.

| model	n.	a	err	b	err	c	err	d	err	X^2
ECHAM5/ MPI-OM	mean	0.19	0.04	0.31	0.09	0.70	0.02	-0.02	0.004	104
ECHAM5/ MPI-OM	0	0.69	0.06	0.32	0.15	0.43	0.01	-0.12	0.005	260
ECHAM5/ MPI-OM	1	0.32	0.07	0.09	0.16	0.43	0.01	-0.12	0.005	279
ECHAM5/ MPI-OM	2	0.32	0.07	0.46	0.17	0.71	0.02	-0.01	0.005	62
ECHAM5/ MPI-OM	3	-0.09	0.07	0.30	0.17	0.78	0.03	0.15	0.007	74

22) itas mri cgcm2 3 2a 20c3m

Institution: Meteorological Research Institute, Japan

Note that the simulations increase quite monotonically without any multidecadal dynamics.

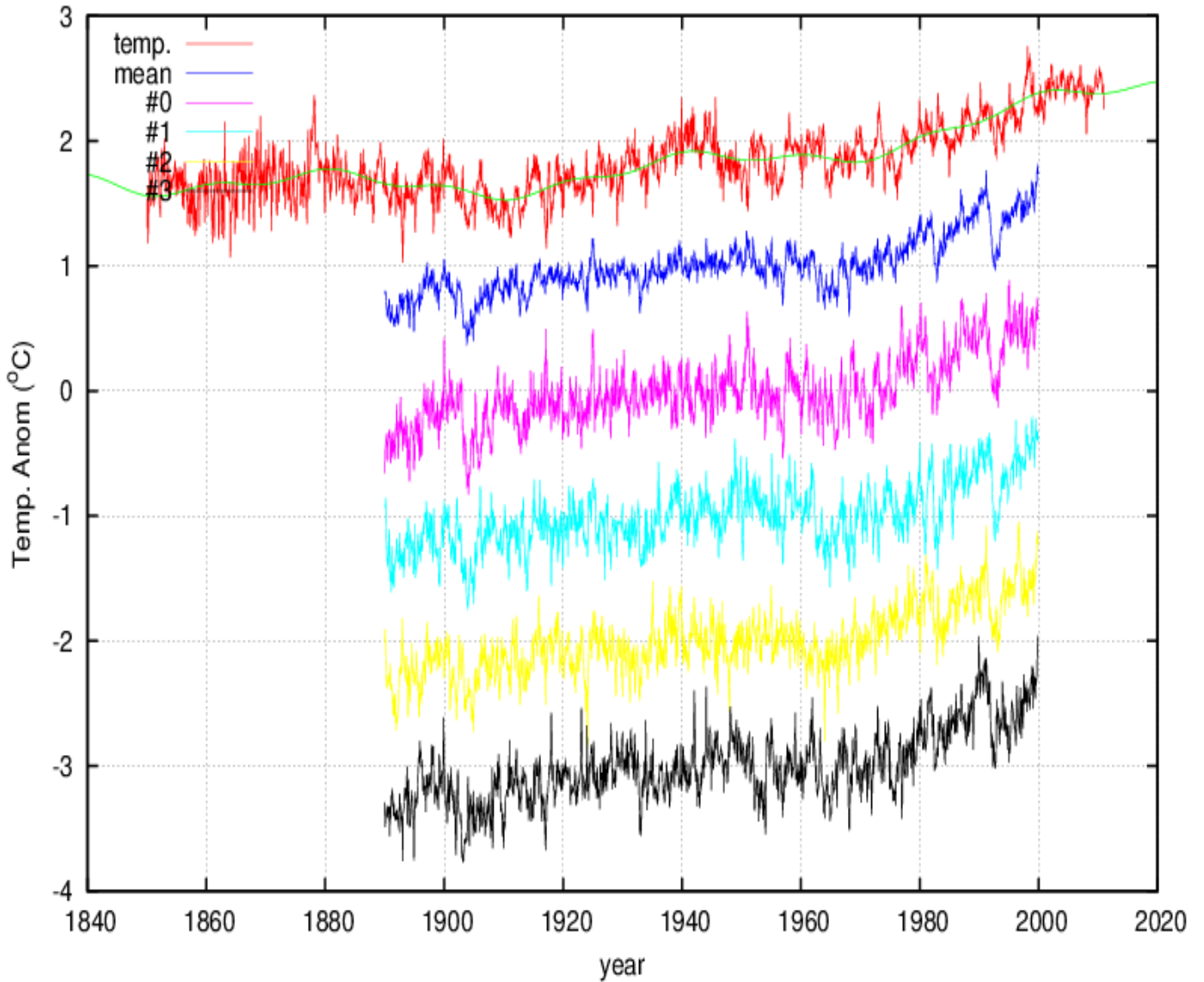| model	n.	a	err	b	err	c	err	d	err	X^2
MRI CGCM 2.3.2	mean	0.31	0.03	0.03	0.07	1.36	0.01	0.27	0.004	149
MRI CGCM 2.3.2	0	0.05	0.05	0.23	0.13	1.37	0.02	0.27	0.005	125
MRI CGCM 2.3.2	1	0.44	0.05	-0.32	0.13	1.21	0.02	0.24	0.005	58
MRI CGCM 2.3.2	2	0.46	0.05	0.34	0.13	1.54	0.02	0.31	0.005	143
MRI CGCM 2.3.2	3	0.31	0.05	-0.43	0.12	0.14	0.02	0.28	0.005	373
MRI CGCM 2.3.2	4	0.29	0.05	0.30	0.12	1.33	0.02	0.26	0.005	85

23) itas ncar ccsm3 0 20c3m
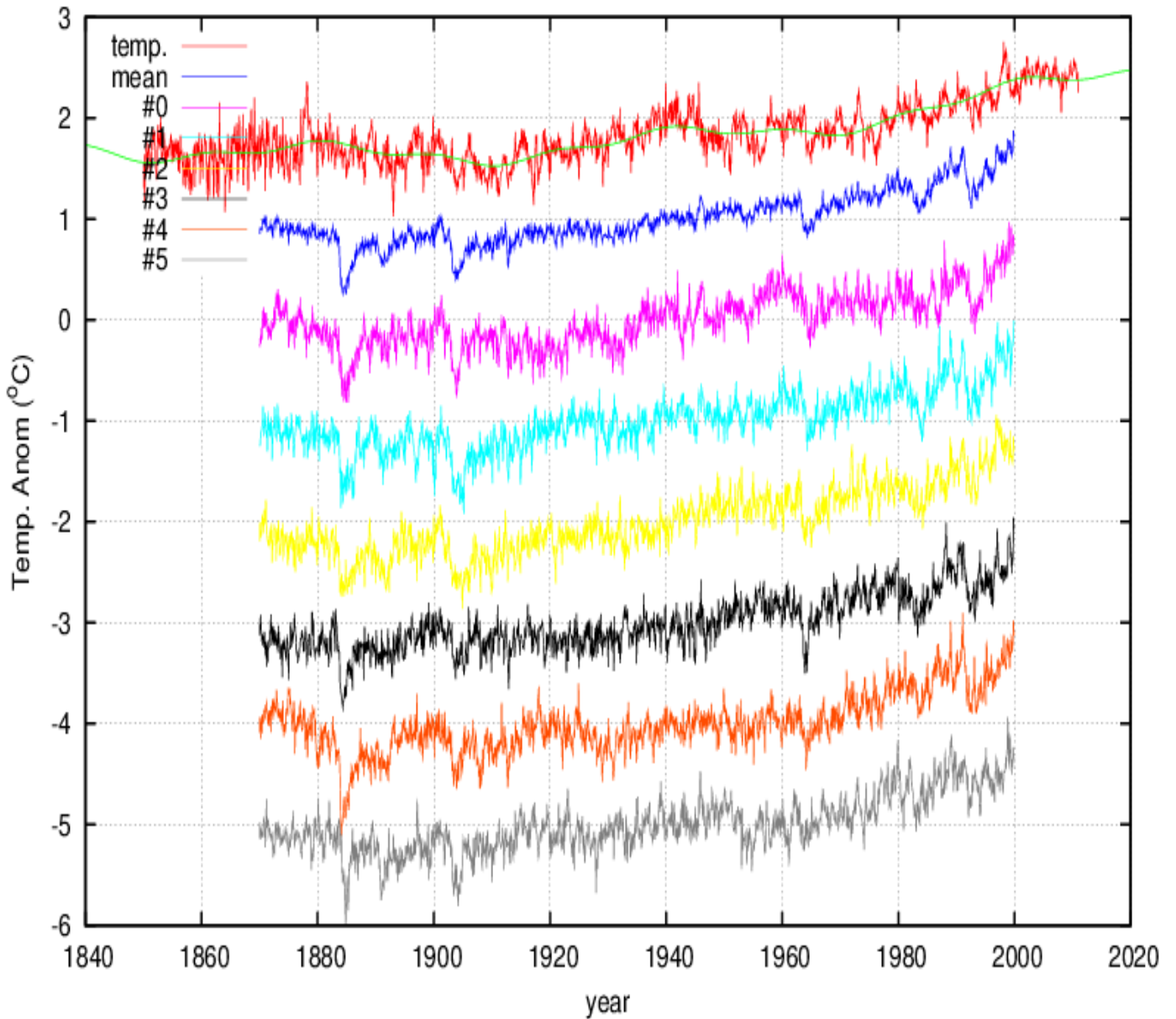
Institution: National Center for Atmospheric Research, USA (NCAR)
Note that the simulations increase monotonically with a dynamics not related to the observation.
There are very large volcano cooling spikes and signatures not observed in the temperature data.

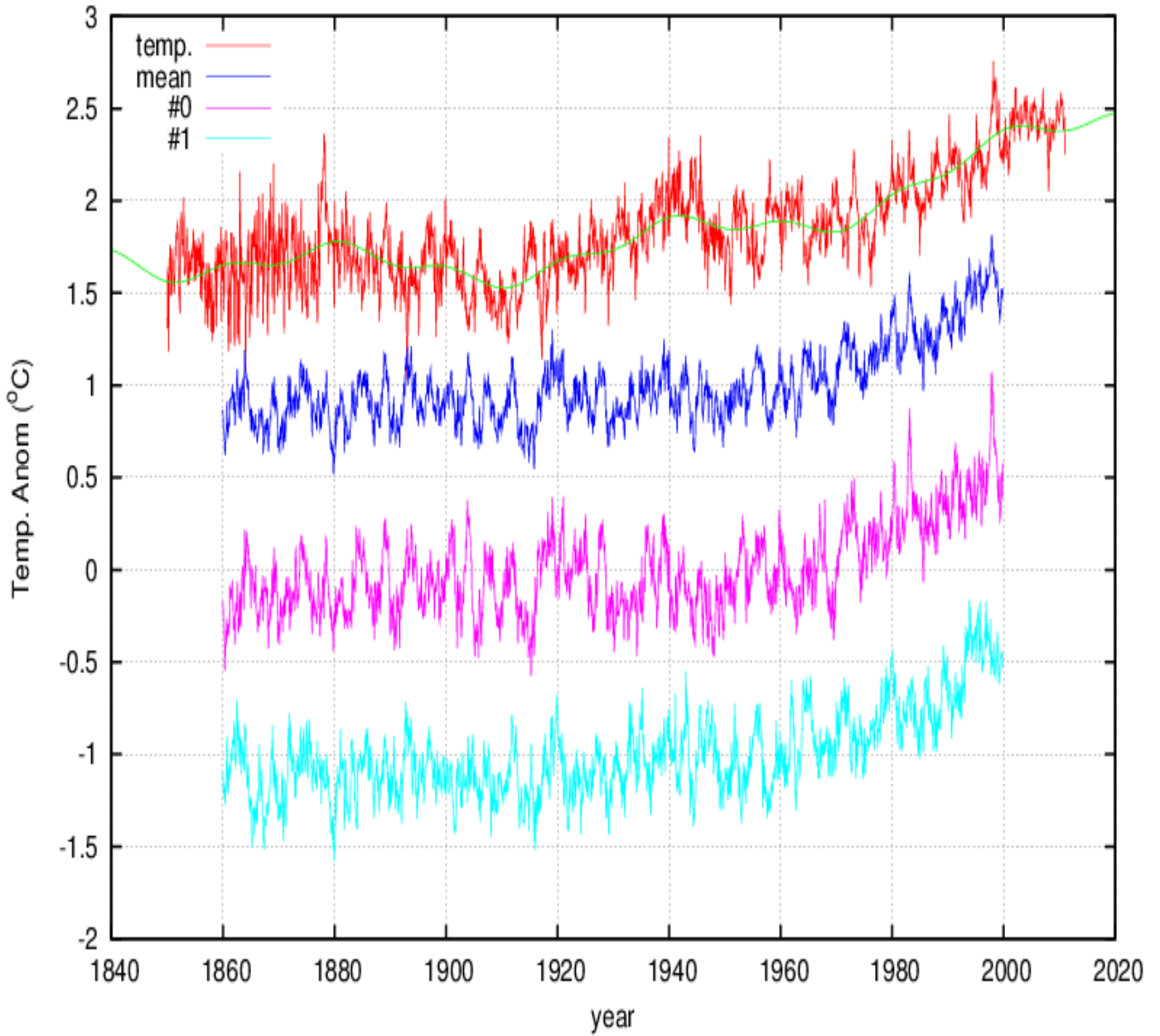| model	n.	a	err	b	err	c	err	d	err	X^2
CCSM3.0	mean	0.34	0.04	0.43	0.10	1.29	0.02	0.24	0.004	76
CCSM3.0	0	0.45	0.06	0.52	0.16	1.14	0.03	0.21	0.006	25
CCSM3.0	1	0.56	0.06	0.63	0.16	1.28	0.02	0.23	0.006	44
CCSM3.0	2	0.40	0.06	0.14	0.15	1.59	0.02	0.29	0.006	149
CCSM3.0	3	-0.10	0.06	0.02	0.14	1.28	0.02	0.24	0.006	109
CCSM3.0	4	0.28	0.07	0.84	0.17	1.24	0.03	0.23	0.007	39
CCSM3.0	5	0.45	0.06	0.46	0.15	1.24	0.03	0.22	0.006	34

24) itas ncar pcm1 20c3m

Institution: National Center for Atmospheric Research, USA (NCAR)
The simulations present a multidecadal dynamics and some large volcano spikes not observed in the data

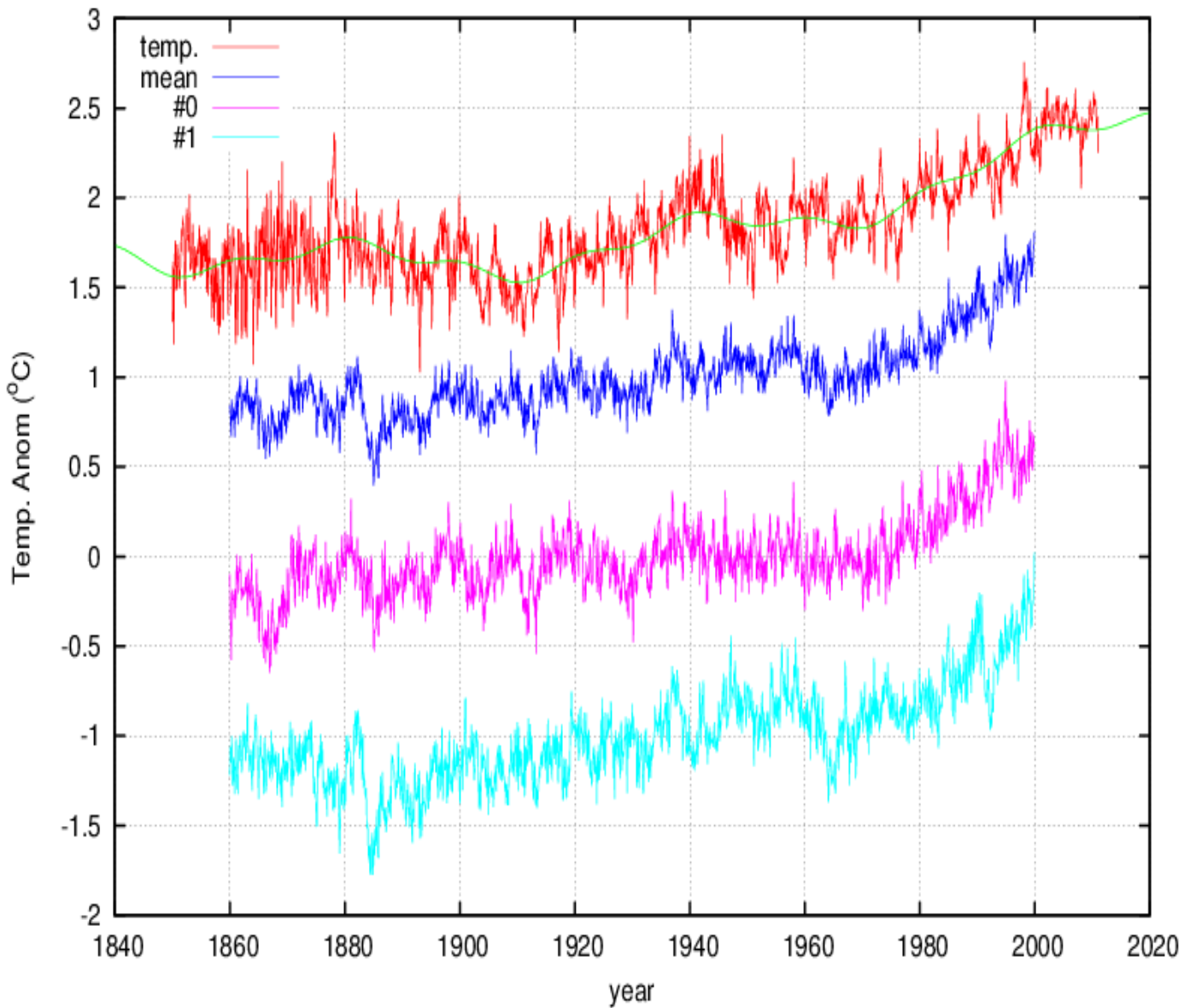| model	n.	a	err	b	err	c	err	d	err	X^2
PCM	mean	0.77	0.05	0.49	0.12	1.00	0.02	0.16	0.004	7
PCM	0	0.71	0.08	0.45	0.19	1.02	0.03	0.16	0.007	6
PCM	1	0.86	0.08	0.57	0.18	0.86	0.03	0.14	0.007	8
PCM	2	0.57	0.07	0.85	0.17	1.02	0.03	0.16	0.006	10
PCM	3	0.94	0.08	0.10	0.19	1.10	0.03	0.17	0.007	7

25) itas ukmo hadcm3 20c3m

Institution: Hadley Centre for Climate Prediction and Research / Met Office, UK
Note that the simulations are almost flat until1970.

model	n.	a	err	b	err	c	err	d	err	X^2
UKMO HADCM3	mean	0.28	0.05	0.56	0.11	0.94	0.02	0.18	0.005	42
UKMO HADCM3	0	0.13	0.06	0.75	0.15	0.90	0.03	0.18	0.006	47
UKMO HADCM3	1	0.42	0.06	0.36	0.13	0.97	0.02	0.19	0.006	25

26) itas ukmo hadgem1 20c3m

Institution: Hadley Centre for Climate Prediction and Research / Met Office, UK.
The simulations show some multidecadal dynamics not related to the observations and some too large volcano spikes.

model	n.	a	err	b	err	c	err	d	err	X^2
UKMO HADGE M1	mean	0.52	0.04	0.63	0.10	1.05	0.02	0.20	0.004	24
UKMO HADGE M1	0	0.61	0.05	0.80	0.13	0.91	0.02	0.17	0.005	16
UKMO HADGE M1	1	0.44	0.06	0.45	0.14	1.18	0.02	0.23	0.005	35

Section 3: page 29-31
Testing the Maximum Entropy Method

In Figure 3 in the paper and in the previous Section 1, we have used Maximum Entropy Method (MEM) power spectrum estimates to determine that the global surface temperature record presents major cycles at about 9.1, 10-10.5, 20, 60 year periodicities. These estimates were performed in Scafetta (2010b).

MEM is a peculiar methodology whose output strongly depends on a free parameter called *pole order M* (Priestley, 1981; Press et al., 2004). In Scafetta (2010b) the calculations are done with a pole number M equal to half of the length N of the monthly data points since 1850. Thus, I used a value of $M \approx 1000$ because $N \approx 2000$.

My choice of using $M \approx 1000$ may surprise some readers because in the textbooks for N = 1000 or 10000 it is usually advised to use from $M = 20$ to $M = 50$. The claim is that using a larger number of poles would produce spurious galore of peaks. Thus, a reader may seriously question my choice of using a so large value of poles, $M \approx 1000$, for my analysis. So, I believe that this issue needs to be clarified for those readers who do not have a practical expertise with MEM.

First, a reader needs to realize that, as I explained in the Introduction, the frequencies that I found have been approximately found also by numerous other authors by using numerous methodologies of data analysis and also different climate records. Moreover, in Scafetta (2010b), MEM has also been applied to study the frequencies of an astronomical planetary record whose frequencies can be directly deduced from the orbits of the planets. So, the accuracy of the results of MEM could be directly evaluated. So, my estimates cannot be lightly questioned because they are supported by numerous other studies and by celestial mechanics as I also explain in the Introduction.

About the MEM pole order M, it is important to well understand its mathematical meaning and the mathematical advantage of the MEM methodology against other power spectrum techniques of analysis such as the Lomb periodogram or Fourier transforms. To address the latter issue it is important to realize that it is no true that MEM produces a spurious peak galore, while the other methods do not. All techniques produce the same numerous peaks which include a strong galore at all frequencies because all techniques attempt to give an estimate of the power associated at each frequency. The major advantage of MEM is that it produces much sharper peaks that allow a more detailed analysis of the *low-frequency band* of the spectrum. The MEM peaks are also higher in the presence of a small true ciclicity, and MEM also reduces the frequency leakage that may corrupt the periodogram estimates.

The maximum number of theoretically possible poles is $M = N/2$. This parameter measures the order of the autoregressive model used to evaluate the MEM power spectrum. Larger values of M allow the technique to detect a larger number of peaks which are always *true* relative to the geometry of the time series, although the smallest galore peak might not have a physical meaning. The detection of a higher density of peaks also implies that the resolution of the methodology increases with M.

Indeed, the choice of M depends on the application. In a few words, if somebody suspects that a signal is made of two very close frequencies, closer the two frequencies are and larger the pole order M must be to properly separate them. This same property also implies that if somebody is interested in resolving frequencies in the very-low frequency band, for example $0 < f < 0.01$, one also needs to use an appropriate large pole order.

The typical advised $M = 20$ or 50 poles for $N = 1000$ or 10000 data points may be appropriate only if somebody is interested in resolving the high frequency band of the spectrum $0.1 < f < 0.5$, as done in Numerical Recipes (Press et al., 2004). But such a choice would be severely inappropriate for resolving the very-low frequency band of the spectrum $0 < f < 0.01$, which in our case is the frequency band that contains the decadal and multidecadal periodicities.

Because I have about 160 years of data that contain about 2000 data points, if I want to properly detect the largest possible multidecadal cycles I need to use a very high pole order M up to half of the length of the sequence (that is 1000 poles), which would make the technique accurate up to frequencies corresponding to a 100-year period, which is approximately half of the about 160-year period covered by the data.

To prove the above claim, the simplest way is to generate 2000 artificial data made of four cycles at 9, 10.5, 20 and 60 years periodicity plus some random noise. The four frequencies and their relative amplitude approximately correspond to the four major frequencies detected in the temperature record, and the 2000 data correspond to the about 2000 monthly data points of the temperature record since 1850.

Figure A shows these data. Figure B shows the MEM analysis of the data using $M = 1000$ poles (red curve) against the MEM evaluation with $M = 300$, $M = 250$ and $M = 50$. It is evident from the figure that only with M larger than 300 the four peaks are sufficiently well detected. Using just the advised $M = 50$ poles is totally inefficient, no peak at all is detected.

However, the temperature data are not stationary, and an additional upward trend is present. To simulate this situation I add an opportune upward linear trend to the data depicted in Figure A and plot the result in Figure C. Figure D shows the MEM analysis of the data using $M = 1000$ poles (red curve) against the MEM evaluation with $M = 500$ and $M = 300$. It is evident from the figure that now only with M larger than 500 the four peaks are sufficiently well detected. In fact, to separate the trending from the cycles there is the need to use a larger pole number than in the previous case.

Figures B and D clearly show that when MEM is used with 1000 poles, as I did, it detects extremely well the four cycles at 9, 10.5, 20 and 60 years within a 3% error. However, when MEM is used with the advised $M = 50$ poles, as done in Numerical Recipes, it does not detect anything.

The minimum number of poles in my second example is M = 500, but as Figure D shows the largest frequency at 60-year is poorly detected because the width of the peak is very large. If I would not know already that a 60-year frequency is present and I wanted to look for periodicities up to 100 years, I would have to use a larger value of M that would have made the peak sharper. Thus, I needed to use a value of M significantly larger than 500.

In conclusion, the above simple experiment confirms that my choice of using $M = N/2 \approx 1000$ to study the monthly temperature data since 1850 cannot be considered erroneous, but it is very likely the best choice for addressing my specific case. In general, it is in solving these specific cases that MEM performs better than more traditional techniques such as Fast Fourier Transforms and the periodograms.
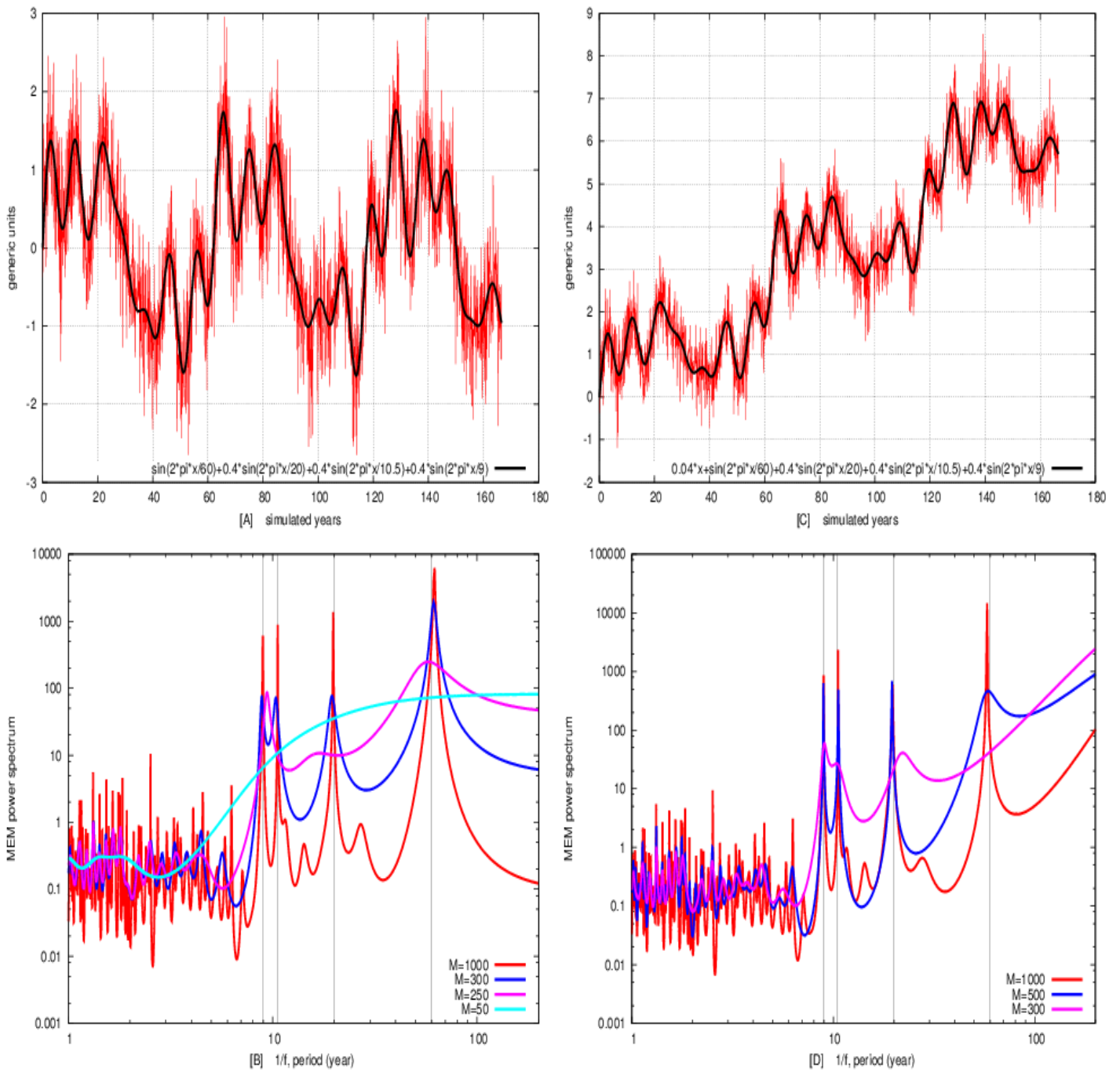
Figure S3: [A] 2000 monthly syntectic data made of four periodicities plus Gaussian noise as depicted in the figure. [B] MEM estimates of [A] using $M = 1000$, $M = 300$, $M = 250$ and $M = 50$: note that M must be larger than 300 to detect the four peaks. [C] 2000 monthly syntectic data made of four periodicities plus Gaussian noise plus a linear trend. [D] MEM estimates of [C] using $M = 1000$, $M = 500$, $M = 300$: note that M must be larger than 500 to detect well the four peaks.

References:

Press W. H., S. A. Teukolsky, W. T. Vetterling and B. P. Flannery. Numerical Recipes, Third Edition. (Cambridge University Press, 2007).

Priestley M. B., 1981. Spectral Analysis and time series. (Academic Press.)

IPCC 2007 mean anthropogenic net warming trend from 1970 to 2050
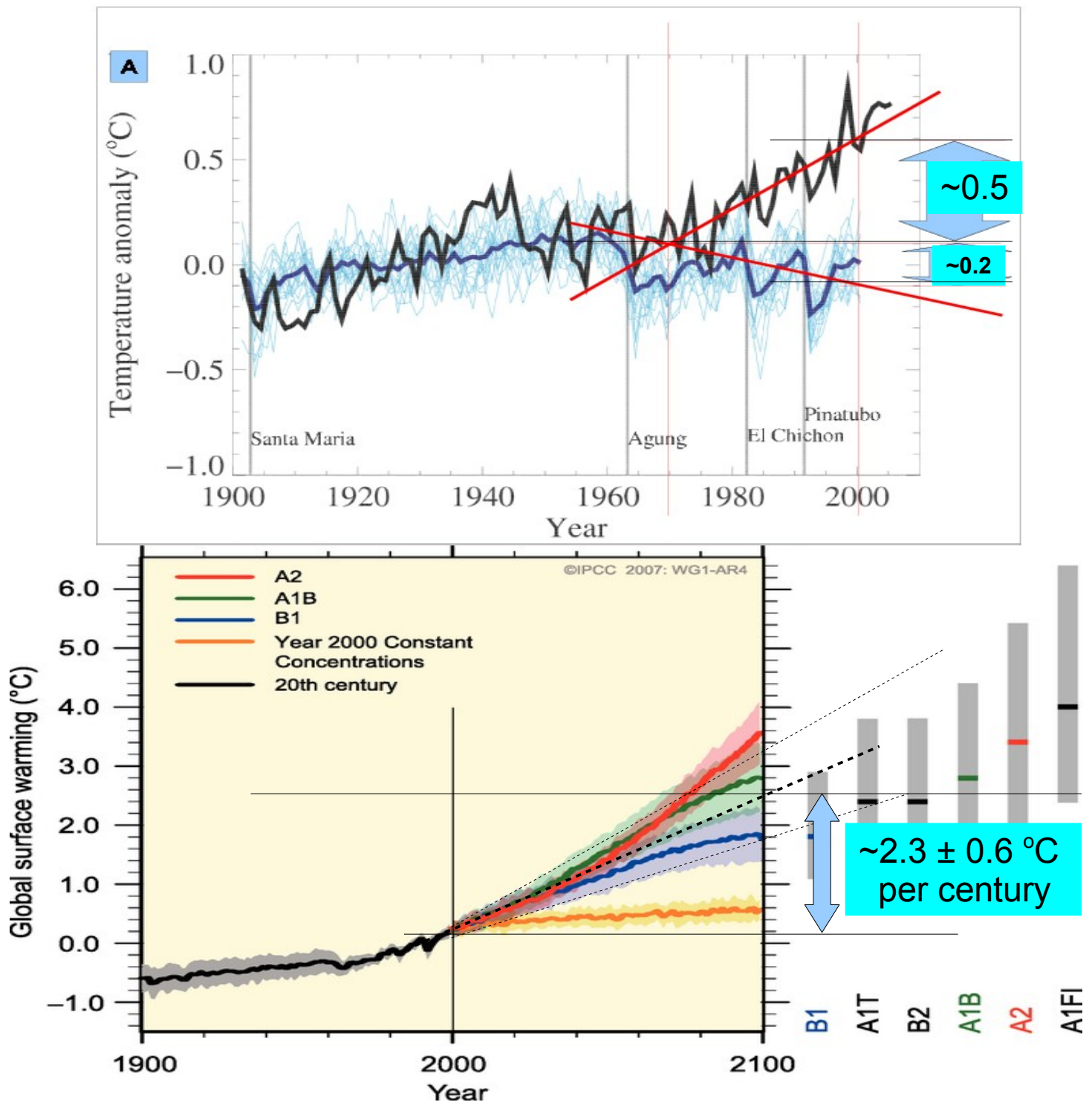
Figure S4. The figure reproduces figure 9.5b [A] and figure SPM.5 [B] of the IPCC 2007 report. [A] The black curve is the global surface temperature, the blue curves are the outputs of general circulation models forced with natural (solar plus volcano) forcing alone as claimed by the IPCC. The red lines are added by me to evaluate that according the IPCC the net anthropogenic forcings have induced a warming of about 0.7 °C from 1970 to 2000, which corresponds to a rate of 2.3 °C/century. [B] The figure shows the average outputs of computer climate models. Note that the black curve from 1900 to 2000 represents the average computer model reconstruction of the 20th century warming. Note that the 10, 20 and 60-year oscillations are not reproduced, only some volcano cooling spikes are visible. The average projections proposed by the IPCC present a warming rate of about 2.3 ± 0.6 °C/century from 2000 to 2050 as shown by the black dot lines added by me plus a vertical error of ± 0.1 °C due to the thickness of the curves.

IPCC 2007 figure 9.5 with its original caption that proves that the IPCC models have interpreted the warming trending observed since 1970 as 100% due "only" to anthropogenic forcings. Note also the discrepancy between the data (my blue lines in (a)) and the models (red) before 1960.
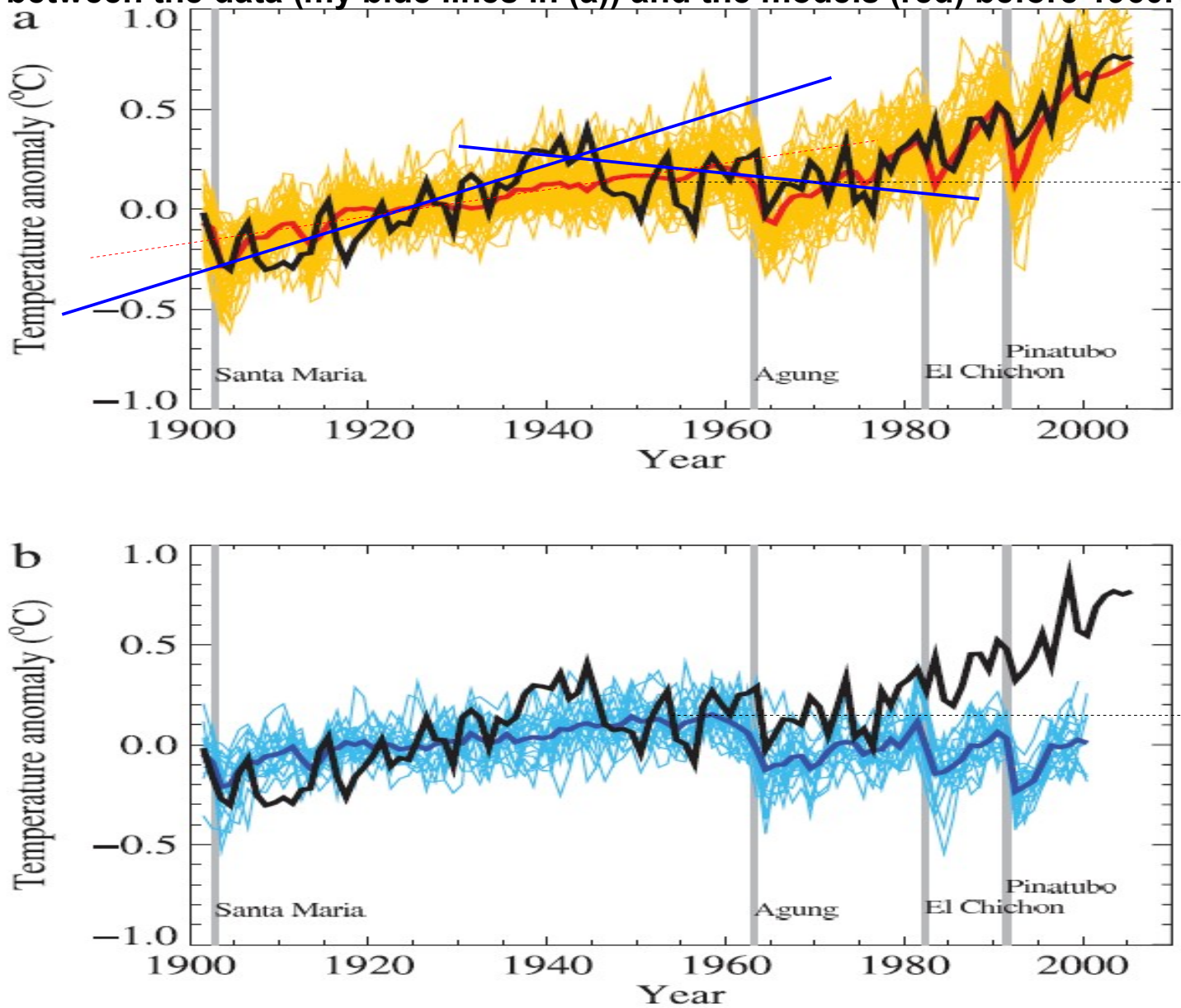

Figure 9.5. Comparison between global mean surface temperature anomalies (°C) from observations (black) and AOGCM simulations forced with (a) both anthropogenic and natural forcings and (b) natural forcings only. All data are shown as global mean temperature anomalies relative to the period 1901 to 1950, as observed (black, Hadley Centre/Climatic Research Unit gridded surface temperature data set (HadCRUT3); Brohan et al., 2006) and, in (a) as obtained from 58 simulations produced by 14 models with both anthropogenic and natural forcings. The multimodel ensemble mean is shown as a thick red curve and individual simulations are shown as thin yellow curves. Vertical grey lines indicate the timing of major volcanic events. Those simulations that ended before 2005 were extended to 2005 by using the fi rst few years of the IPCC Special Report on Emission Scenarios (SRES) A1B scenario simulations that continued from the respective 20th-century simulations, where available. The simulated global mean temperature anomalies in (b) are from 19 simulations produced by five models with natural forcings only. The multi-model ensemble mean is shown as a thick blue curve and individual simulations are shown as thin blue curves. Simulations are selected that do not exhibit excessive drift in their control simulations (no more than 0.2°C per century). Each simulation was sampled so that coverage corresponds to that of the observations. Further details of the models included and the methodology for producing this figure are given in the Supplementary Material, Appendix 9.C. After Stott et al. (2006b).

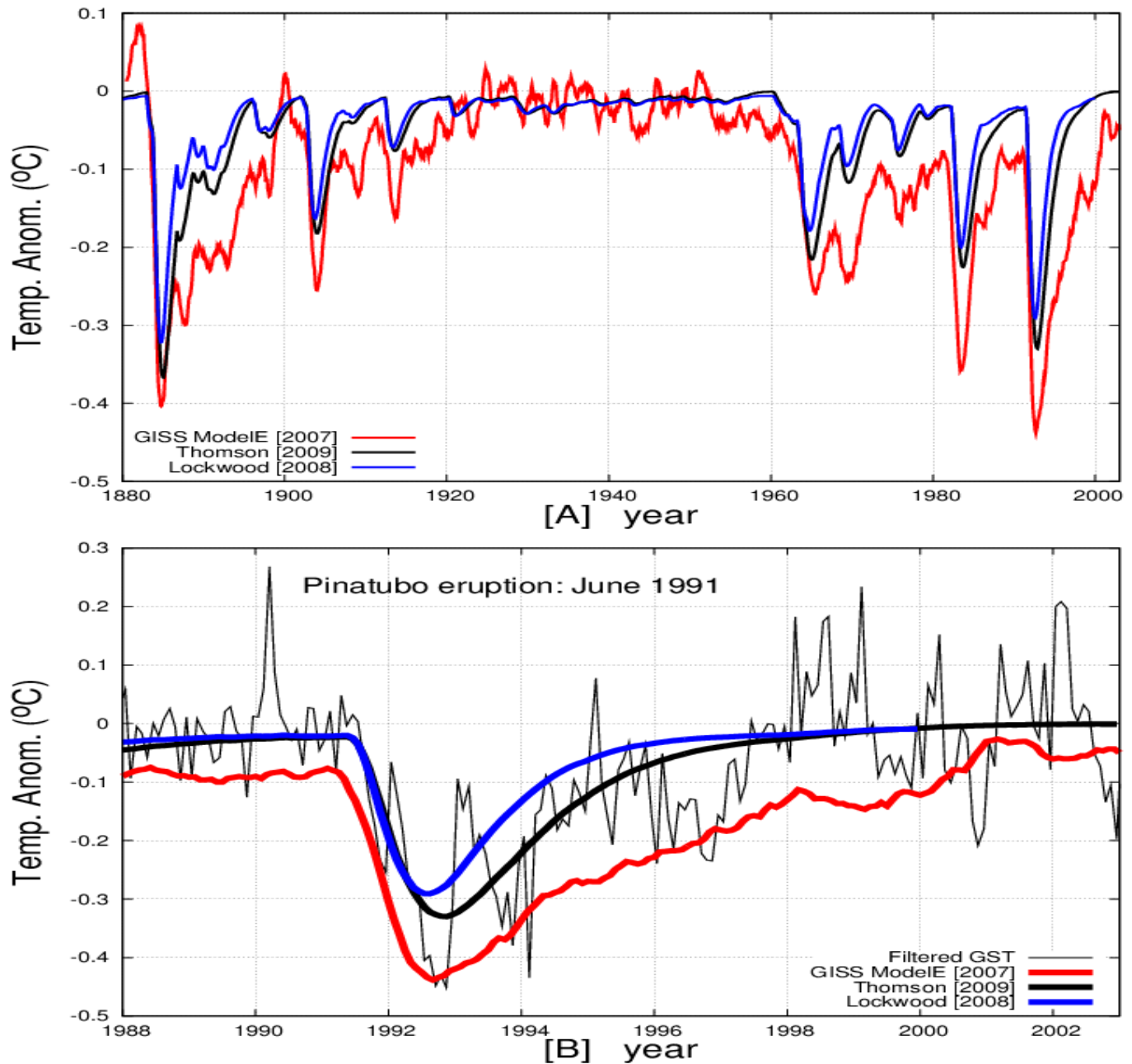Overestimation of the GISS ModelE reconstruction of the volcano signature

Figure S5. The figure shows that the volcano signature reconstructed by the GCM is 2-3 times larger than what can be empirically found. In particular the log-time range effect of the volcano aerosols appears grossly overestimated. [A] Lockwood (2008) (blue) and Thompson et al. (2009) (black) empirical analyses of the volcano signature on global surface temperature against the GISS ModelE estimates (red) by (Hansen et al., 2007). [B] Filtered temperature (thin gray) vs. the three model reconstructions of the Pinatubo eruption in 1991. The figure clearly suggests that GISS ModelE overestimates the volcano signal both in amplitude and long-range duration as determined by the empirical filtering. By 2000 the volcano signature in the empirical studies vanishes.
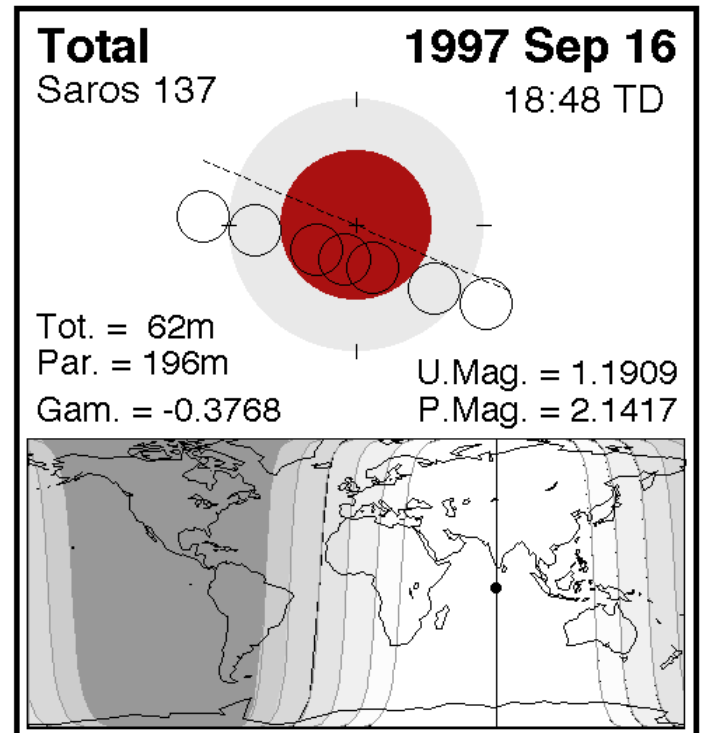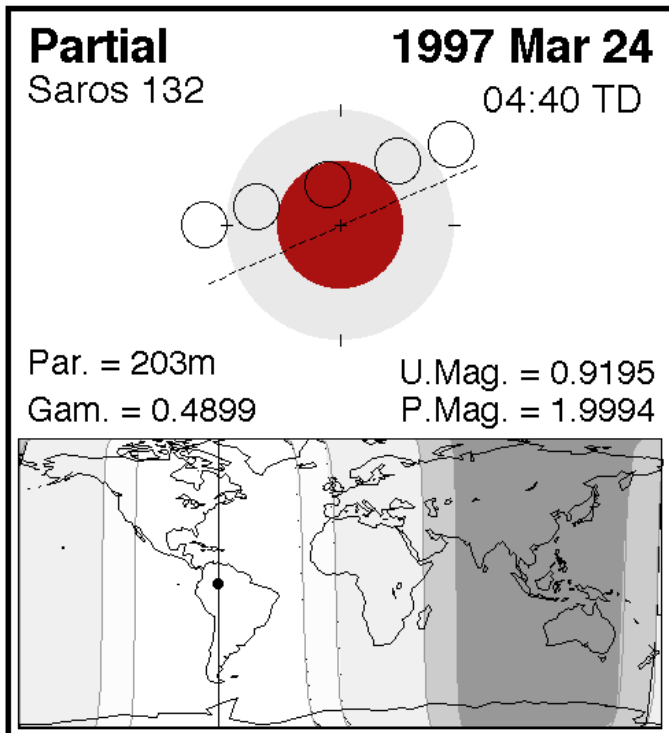
The 9-year cycle of the Lunar (top) and Solar (bottom) eclipses at the equinoxes in 1997-2006

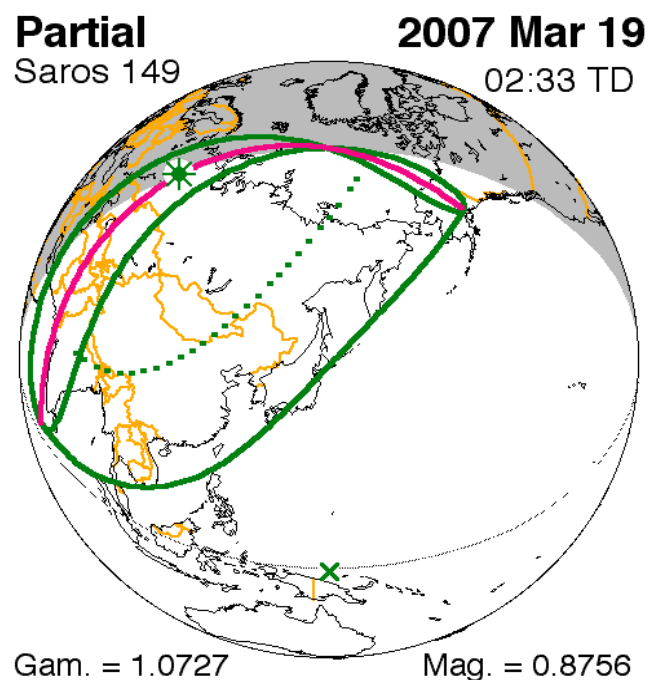http://eclipse.gsfc.nasa.gov/eclipse.html

Partial   **1997 Mar 24**
Saros 132   04:40 TD

Par. = 203m   U.Mag. = 0.9195
Gam. = 0.4899   P.Mag. = 1.9994

Five Millennium Canon of Lunar Eclipses (Espenak & Meeus)
NASA TP-2009-214172

Total   **1997 Sep 16**
Saros 137   18:48 TD

Tot. = 62m
Par. = 196m   U.Mag. = 1.1909
Gam. = -0.3768   P.Mag. = 2.1417

Five Millennium Canon of Lunar Eclipses (Espenak & Meeus)
NASA TP-2009-214172

Annular   **2006 Sep 22**
Saros 144   11:41 TD

Alt. = 66°
Gam. = -0.4062   Dur. = 07m09s

Five Millennium Canon of Solar Eclipses (Espenak & Meeus)

Partial   **2007 Mar 19**
Saros 149   02:33 TD

Gam. = 1.0727   Mag. = 0.8756
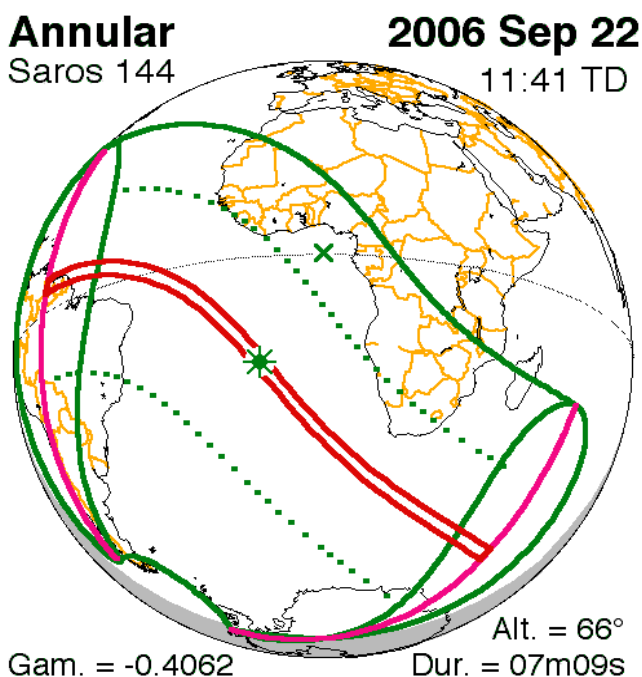
Five Millennium Canon of Solar Eclipses (Espenak & Meeus)

Solar Eclipses			Lunar Eclipses		
1988	Mar	18	1988	Mar	3
1988	Sep	11	1988	Aug	27
1989	Mar	7	1989	Feb	20
1989	Aug	31	1989	Aug	17
1990	Jan	26	1990	Feb	9
1990	Jul	22	1990	Aug	6
1991	Jan	15	1991	Jan	30
1991	Jul	11	1991	Jun	27
			1991	Jul	26
1992	Jan	4	1991	Dec	21
1992	Jun	30	1992	Jun	15
1992	Dec	24	1992	Dec	9
1993	May	21	1993	Jun	4
1993	Nov	13	1993	Nov	29
1994	May	10	1994	May	25
1994	Nov	3	1994	Nov	18
1995	Apr	29	1995	Apr	15
1995	Oct	24	1995	Oct	8
1996	Apr	17	1996	Apr	4
1996	Oct	12	1996	Sep	27
1997	Mar	9	1997	Mar	24
1997	Sep	2	1997	Sep	16
1998	Feb	26	1998	Mar	13
1998	Aug	22	1998	Aug	8
			1998	Sep	6
1999	Feb	16	1999	Jan	31
1999	Aug	11	1999	Jul	28
2000	Feb	5	2000	Jan	21
2000	Jul	1	2000	Jul	16
2000	Jul	31			
2000	Dec	25	2001	Jan	9
2001	Jun	21	2001	Jul	5
2001	Dec	14	2001	Dec	30
2002	Jun	10	2002	May	26
			2002	Jun	24
2002	Dec	4	2002	Nov	20
2003	May	31	2003	May	16
2003	Nov	23	2003	Nov	9
2004	Apr	19	2004	May	4
2004	Oct	14	2004	Oct	28
2005	Apr	8	2005	Apr	24
2005	Oct	3	2005	Oct	17
2006	Mar	29	2006	Mar	14
2006	Sep	22	2006	Sep	7
2007	Mar	19	2007	Mar	3
2007	Sep	11	2007	Aug	28
2008	Feb	7	2008	Feb	21
2008	Aug	1	2008	Aug	16
2009	Jan	26	2009	Feb	9
2009	Jul	22	2009	Jul	7
			2009	Aug	6
			2009	Dec	31
2010	Jan	15	2010	Jun	26
2010	Jul	11			

9-year cycle

9-year cycle

9.07-year Temperature Cycle

Temp. Anom. (C)

-0.06 -0.04 -0.02 0 0.02 0.04 0.06

1988 1990 1992 1994 1996 1998 2000 2002 2004 2006 2008
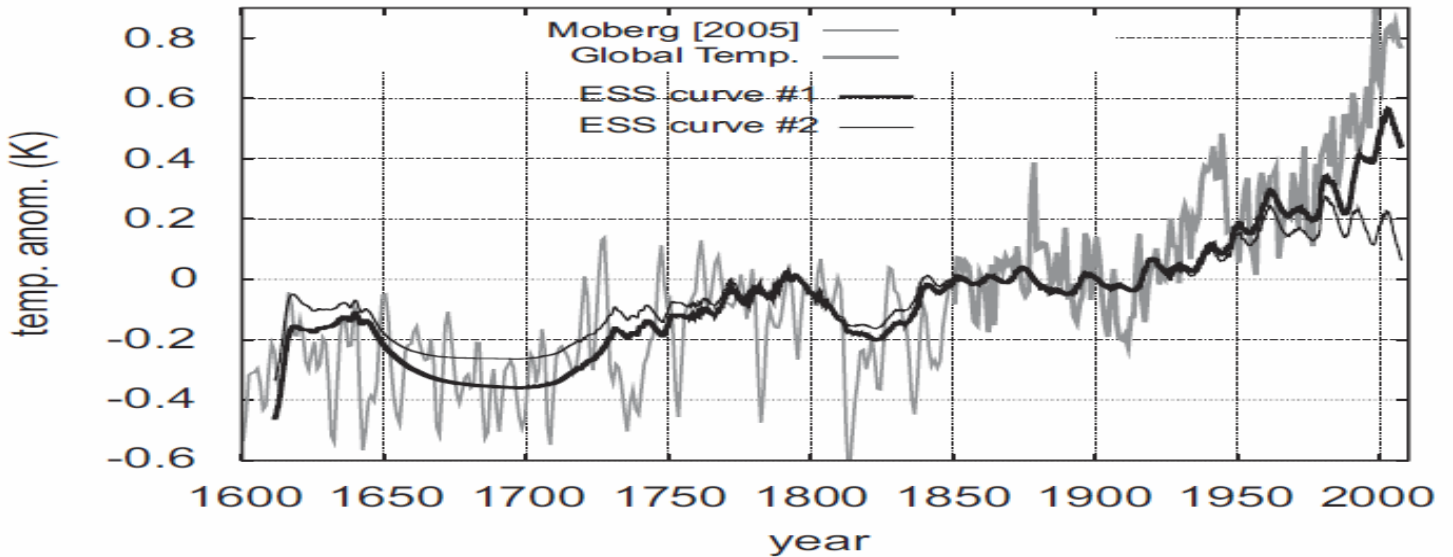
year
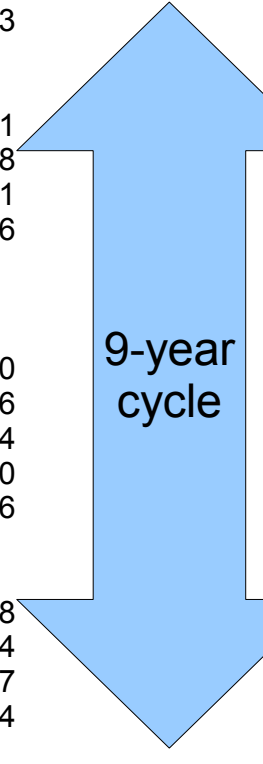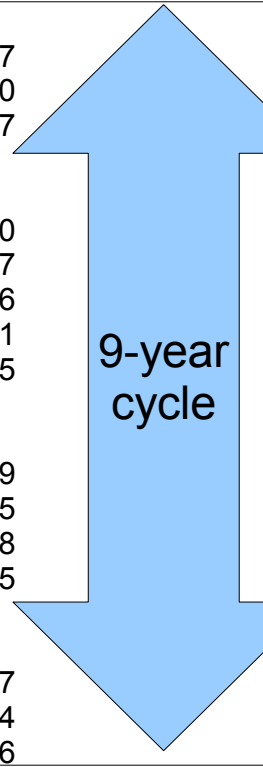
temperature cycle at 9.07-year
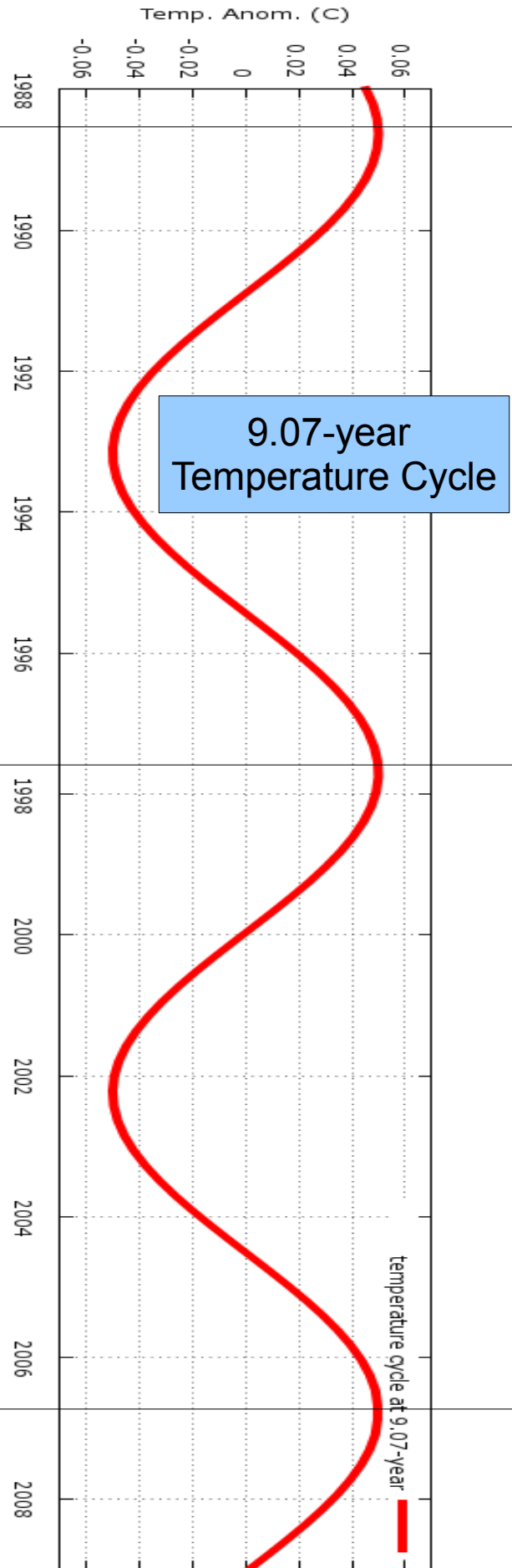
Section 7: page 37

Preliminary attempts to interpret the warming since 1850 as partially due to multisecular and millennial cycles

1) Scafetta, N., 2009. Empirical analysis of the solar contribution to global mean air surface temperature change. J. Atm. and Solar-Terr. Phys. 71, 1916-1923.


Empirical solar signature curves (black) curves against a paleoclimate temperature reconstruction (Moberg et al., 2005) from 1600 to 1850 (thin gray line) and global surface temperature record since 1950 (Brohan et al., 2006) (thick black line).

2) Humlum, O., Solheim, J.-K. and Stordahl, K. 2011. Identifying natural contributions to late Holocene climate change. *Global and Planetary Change* **79**: 145-156.
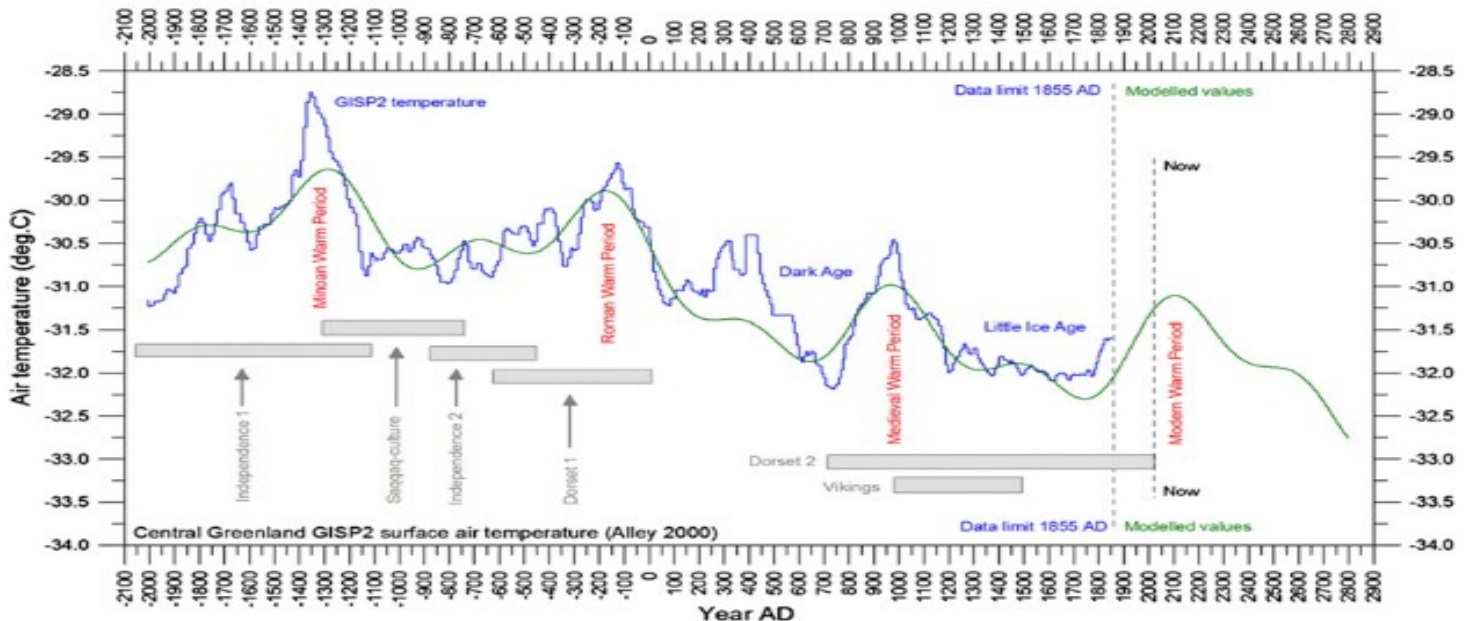

The Central Greenland surface temperature from GISP2 project for the past 4000 years (blue line) and the modeled temperature adopting only 3 periods at 2804-year, 1186-year and 556-year. The 3-period model was able to replicate most of the observed changes (with one major exception at around the warming peak of 3 to 400 AD) and forecasted a large cooling trend in contrast to the IPCC-predicted rising atmospheric CO2 scenario from computer climate models.
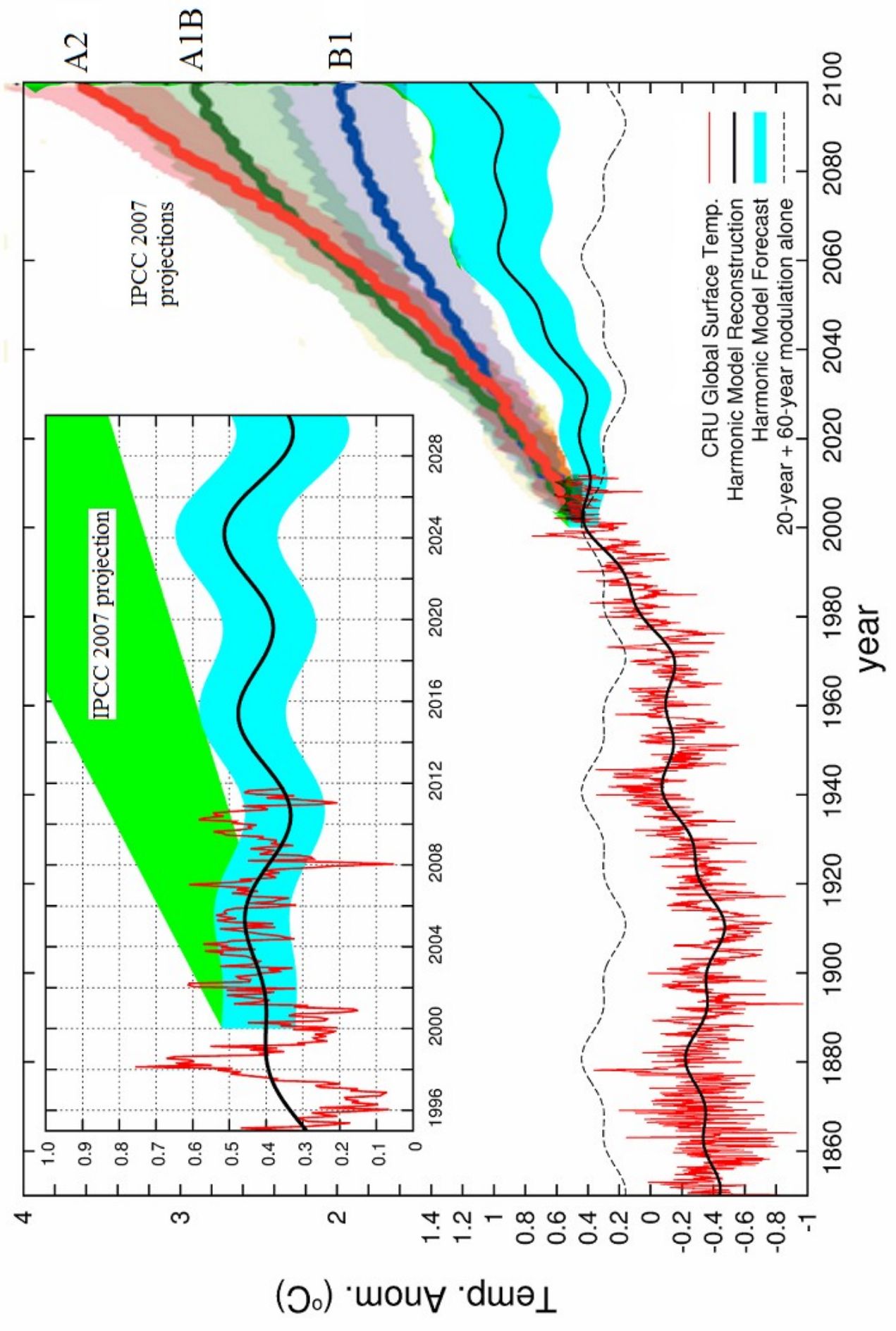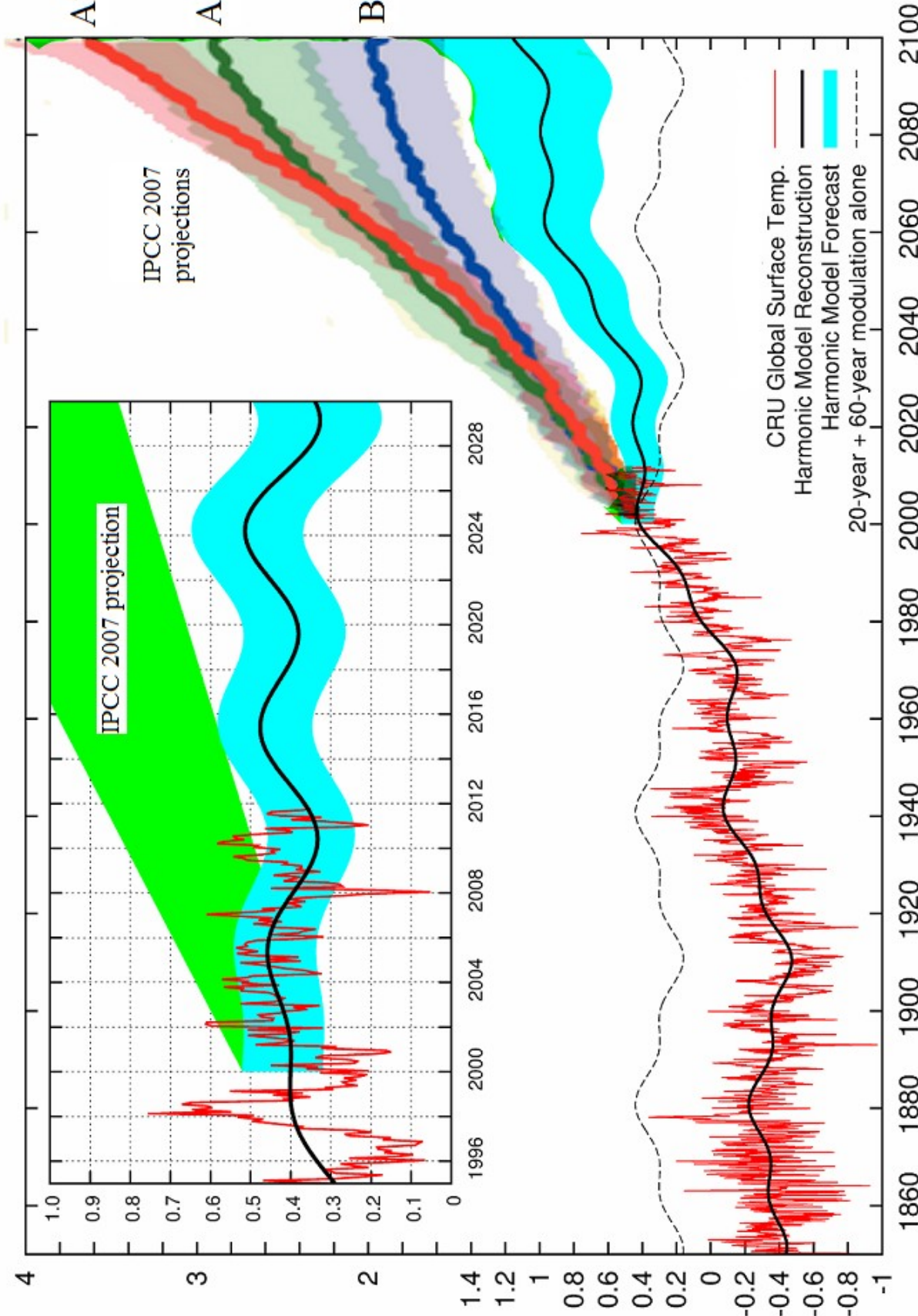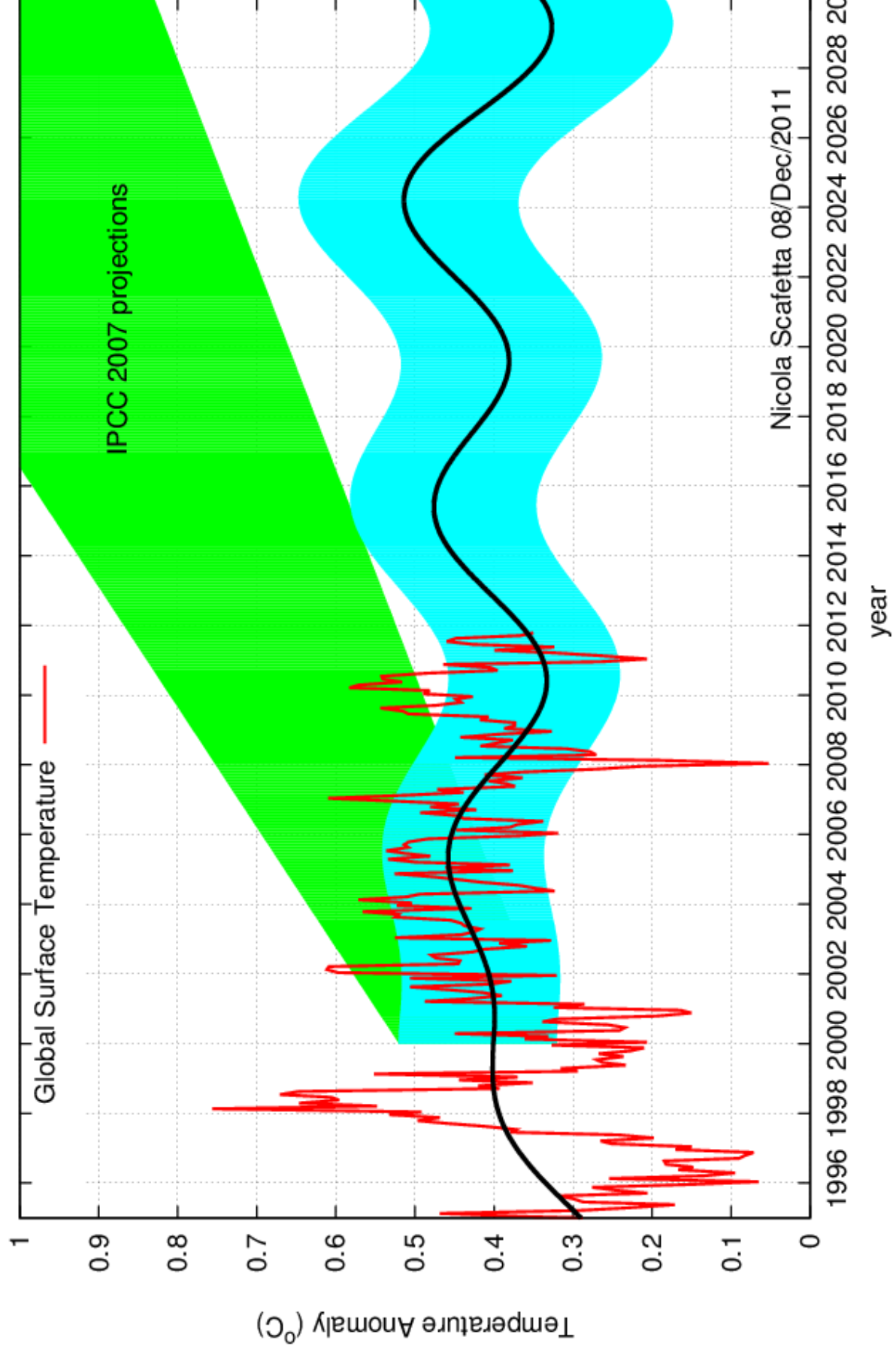
Harmonic model (9.07,10.44,20,60-yr + anthropogenic trend) forecast VS. IPCC 2007 projections

IPCC 2007 projections

IPCC 2007 projections

Global Surface Temperature

Nicola Scafetta 08/Dec/2011

Temperature Anomaly (°C)

year